

Pseudo-spectra of multivariate inhomogeneous spatial point processes

Qi-Wen Ding* ¹, Junho Yang ¹, and Joonho Shin[†] ²

¹Institute of Statistical Science, Academia Sinica

²School of Mathematics, Statistics and Data Science, Sungshin Women's University

February 17, 2025

Abstract

In this article, we propose a spectral method for multivariate inhomogeneous spatial point processes. A key ingredient is utilizing the asymptotic behavior of the periodogram. The periodogram is an asymptotically unbiased estimator of the spectrum of a second-order stationary point process. By extending this property, we show that under inhomogeneity, the expectation of the periodogram also converges to a matrix-valued function, which we refer to as the pseudo-spectrum. The pseudo-spectrum shares similar properties with the spectrum of stationary processes and can be interpreted using local parameters. We derive a consistent estimator of the pseudo-spectrum through kernel smoothing and propose two bandwidth selection methods. The performance and utility of our frequency domain methods are illustrated through simulation studies and a real data analysis of rainforest data.

Keywords and phrases: Bandwidth selection method, BCI data, intensity reweighted processes, local spectrum

1 Introduction

As an alternative to time and spatial domain approaches, frequency domain methods have been extensively studied in time series and random fields. For point pattern data, the spectral analysis of spatial point processes has a history dating back to the work by Bartlett in the 1960s

*The first two authors are ordered alphabetically.

[†]*Emails:* {qwding, junhoyang}@stat.sinica.edu.tw, joonho.shin@sungshin.ac.kr

(Bartlett (1964)), who defined the spectrum of two-dimensional point processes and proposed to use periodogram to estimate the spectrum. Nevertheless, analogous frequency domain tools for spatial point processes are largely unexplored due to the technical difficulties in handling point data that are scattered irregularly in space. In recent years, with advancements in techniques for analyzing irregularly spaced data (e.g., Matsuda and Yajima (2009)), some theoretical developments in the discrete Fourier transforms (DFTs) and periodograms of spatial point patterns have been established. For example, Rajala et al. (2023) calculated the moments of the DFTs and periodograms at fixed frequencies, and Yang and Guan (2024) extended these results by considering frequencies that can vary with n and proved new α -mixing CLT for the integrated periodogram.

The aforementioned approaches assume that the data-generating process is second-order stationary (SOS), where the spectrum is well-defined through the inverse Fourier transform of the reduced covariance intensity function. However, in real-life applications, it is more realistic to assume that the true data-generating process is inhomogeneous over the domain. This violates the SOS condition, in turn, the spectrum is not well-defined. This issue also arises in other types of spatial data. A widely used approach for geostatistical data is to remove the mean field using appropriate de-trending techniques, such as universal kriging (cf. Cressie (2015)), and then apply SOS models to the residuals. However, such techniques are not feasible for presence-only data, necessitating the development of unique (frequency domain) tools to analyze inhomogeneous spatial point pattern data.

Therefore, to keep pace with the increasing demand for analyzing inhomogeneous point pattern data, we aim to extend the concept of the spectrum for SOS point processes to multivariate inhomogeneous point processes. Specifically, by utilizing the asymptotic behavior of the periodogram, we define the so-called pseudo-spectrum of inhomogeneous processes (Section 2). The pseudo-spectrum possesses properties similar to those of the spectrum for SOS processes. More intriguingly, the pseudo-spectrum can be represented as an integral of the spectra of certain SOS processes with a localization factor, enabling the extraction of frequency domain features for inhomogeneous point processes (Section 3).

In Section 4, we investigate the joint asymptotic behaviors of the DFTs and periodograms under inhomogeneity. In Section 5, we propose a consistent estimator of the pseudo-spectrum using a kernel smoothing method. In Section 6, we propose two kernel bandwidth selection methods, namely the optimal mean squared error criterion and the frequency domain cross-validation criterion. We illustrate our proposed methods through simulations (Section 7) and a real-data application of five-variate rainforest point pattern data (Section 8). Lastly, technical details, proofs of the results, and details on the simulation settings and data analysis can be found in the Supplement Material (Appendix, hereafter).

2 Pseudo-spectrum of inhomogeneous point process

2.1 Preliminaries

Throughout this article, for a vector $\mathbf{v} = (v_1, \dots, v_d)^\top \in \mathbb{C}^d$, let $|\mathbf{v}| = \sum_{j=1}^d |v_j|$, $\|\mathbf{v}\| = \{\sum_{j=1}^d |v_j|^2\}^{1/2}$, and $\|\mathbf{v}\|_\infty = \max_{1 \leq j \leq d} |v_j|$. For vectors $\mathbf{u} = (u_1, \dots, u_d)^\top$ and $\mathbf{v} = (v_1, \dots, v_d)^\top$ in \mathbb{R}^d , we define $\mathbf{u} \cdot \mathbf{v} = (u_1 v_1, \dots, u_d v_d)^\top$ and $\mathbf{u}/\mathbf{v} = (u_1/v_1, \dots, u_d/v_d)^\top$, provided $v_1, \dots, v_d \neq 0$. For a matrix $A \in \mathbb{C}^{m \times n}$, $|A| = \sum_{i,j} |A^{(i,j)}|$ denotes the entrywise sum. For $p \in [1, \infty)$, $L_p(\mathbb{R}^d)$ denotes the set of all measurable functions $g : \mathbb{R}^d \rightarrow \mathbb{C}$ such that $\int_{\mathbb{R}^d} |g|^p < \infty$. Let $L_p^{m \times n}(\mathbb{R}^d)$ be the set of all $m \times n$ matrix valued function on \mathbb{R}^d such that each element belongs to $L_p(\mathbb{R}^d)$. For G belongs to either $L_1^{m \times n}(\mathbb{R}^d)$ or $L_2^{m \times n}(\mathbb{R}^d)$, the Fourier transform and inverse Fourier transform are respectively defined as $\mathcal{F}(G)(\cdot) = \int_{\mathbb{R}^d} G(\mathbf{x}) \exp(i\mathbf{x}^\top \cdot) d\mathbf{x}$ and $\mathcal{F}^{-1}(G)(\cdot) = (2\pi)^{-d} \int_{\mathbb{R}^d} G(\mathbf{x}) \exp(-i\mathbf{x}^\top \cdot) d\mathbf{x}$.

Now, let $\underline{X} = (X_1, \dots, X_m)$ be an m -variate simple spatial point process defined on \mathbb{R}^d . Let $N_i(\cdot)$ be the counting measure induced by X_i and let $\underline{N}(\cdot) = (N_1(\cdot), \dots, N_m(\cdot))^\top$. Then, the vector-valued first-order intensity function and matrix-valued covariance intensity function of \underline{X} , denoted as $\underline{\lambda}_1(\cdot) = (\lambda_1^{(1)}(\cdot), \dots, \lambda_1^{(m)}(\cdot))^\top : \mathbb{R}^d \rightarrow \mathbb{R}^m$ and $\Gamma_2(\cdot, \cdot) = (\gamma_2^{(i,j)}(\cdot, \cdot))_{1 \leq i, j \leq m} : \mathbb{R}^d \times \mathbb{R}^d \rightarrow \mathbb{R}^{m \times m}$, satisfy for any disjoint Borel measurable sets A, B on \mathbb{R}^d ,

$$\mathbb{E}[\underline{N}(A)] = \int_A \underline{\lambda}_1(\mathbf{x}) d\mathbf{x} \quad \text{and} \quad \text{cov}(\underline{N}(A), \underline{N}(B)) = \iint_{A \times B} \Gamma_2(\mathbf{x}, \mathbf{y}) d\mathbf{x} d\mathbf{y}. \quad (2.1)$$

By using the above notation, we define the ‘‘complete’’ covariance intensity function of \underline{X} in the sense of Bartlett (1964) by

$$\tilde{C}(\mathbf{x}, \mathbf{y}) = (\tilde{C}^{(i,j)}(\mathbf{x}, \mathbf{y}))_{1 \leq i, j \leq m} = \text{diag}(\underline{\lambda}_1(\mathbf{x})) \delta(\mathbf{x} - \mathbf{y}) + \Gamma_2(\mathbf{x}, \mathbf{y}), \quad (2.2)$$

where diag denotes the diagonal matrix and $\delta(\cdot)$ denotes the Dirac delta function.

2.2 A working example: second-order stationary case

In this section, we first assume that \underline{X} is an SOS process and review the frequency domain representation of (2.2). Under the SOS framework, there exists $\underline{\lambda}_1 = (\lambda_1^{(1)}, \dots, \lambda_1^{(m)})^\top$ and $\Gamma_{2,\text{red}}(\cdot) = (\gamma_{2,\text{red}}^{(i,j)}(\cdot))_{1 \leq i, j \leq m}$ such that

$$\underline{\lambda}_1(\mathbf{x}) = \underline{\lambda}_1 \quad \text{and} \quad \Gamma_2(\mathbf{x}, \mathbf{y}) = \Gamma_{2,\text{red}}(\mathbf{x} - \mathbf{y}).$$

We refer to $\Gamma_{2,\text{red}}(\cdot)$ as the reduced covariance intensity function of \underline{X} . Then, the complete covariance intensity in (2.2) also has the following reduced form:

$$\tilde{C}(\mathbf{x}, \mathbf{y}) = \text{diag}(\underline{\lambda}_1) \delta(\mathbf{x} - \mathbf{y}) + \Gamma_{2,\text{red}}(\mathbf{x} - \mathbf{y}) =: C(\mathbf{x} - \mathbf{y}). \quad (2.3)$$

Provided that $\Gamma_{2,\text{red}} \in L_1^{m \times m}(\mathbb{R}^d)$, the matrix-valued spectrum of \underline{X} is defined as the inverse Fourier transform of C :

$$F(\boldsymbol{\omega}) = \mathcal{F}^{-1}(C)(\boldsymbol{\omega}) = (2\pi)^{-d} \text{diag}(\underline{\lambda}_1) + \mathcal{F}^{-1}(\Gamma_{2,\text{red}})(\boldsymbol{\omega}), \quad \boldsymbol{\omega} \in \mathbb{R}^d. \quad (2.4)$$

Then, $F(\cdot)$ satisfies the usual conditions for the spectrum of multivariate time series or random fields, such as $F(\cdot)$ being conjugate symmetric and positive definite (see, Daley and Vere-Jones (2003), Chapter 8.6).

To estimate the spectrum of \underline{X} , we consider the DFT of the observed point pattern. Let $\{D_n\}$ be a sequence of common windows of X_1, \dots, X_m of the form:

$$D_n = [-A_1/2, A_1/2] \times \dots \times [-A_d/2, A_d/2], \quad n \in \mathbb{N}. \quad (2.5)$$

Here, for each i , $\{A_i = A_i(n)\}_{n=1}^\infty$ denotes an increasing sequence of positive numbers. Let $h(\mathbf{x})$, $\mathbf{x} \in \mathbb{R}^d$, be a non-negative data taper with a support $[-1/2, 1/2]^d$, and let $H_{h,k} = \int_{[-1/2, 1/2]^d} h(\mathbf{x})^k d\mathbf{x}$. Using this notation, the DFT of \underline{X} with data taper h is defined as $\underline{\mathcal{J}}_{h,n}(\boldsymbol{\omega}) = (\mathcal{J}_{h,n}^{(1)}(\boldsymbol{\omega}), \dots, \mathcal{J}_{h,n}^{(m)}(\boldsymbol{\omega}))^\top$, $\boldsymbol{\omega} \in \mathbb{R}^d$, where

$$\mathcal{J}_{h,n}^{(j)}(\boldsymbol{\omega}) = (2\pi)^{-d/2} H_{h,2}^{-1/2} |D_n|^{-1/2} \sum_{\mathbf{x} \in X_j \cap D_n} h(\mathbf{x}/\mathbf{A}) \exp(-i\mathbf{x}^\top \boldsymbol{\omega}). \quad (2.6)$$

Lastly, the periodogram, a raw estimator of the spectrum, is defined as

$$I_{h,n}(\boldsymbol{\omega}) = \underline{J}_{h,n}(\boldsymbol{\omega}) \underline{J}_{h,n}(\boldsymbol{\omega})^*, \quad (2.7)$$

where $\underline{J}_{h,n}(\cdot) = (J_{h,n}^{(1)}(\cdot), \dots, J_{h,n}^{(m)}(\cdot))^\top = \underline{\mathcal{J}}_{h,n}(\cdot) - \mathbb{E}[\underline{\mathcal{J}}_{h,n}(\cdot)]$ is the centered DFT (we will elaborate on the expression of $\mathbb{E}[\underline{\mathcal{J}}_{h,n}(\boldsymbol{\omega})]$ in Section 4.1).

2.3 The pseudo-spectrum under a new asymptotic framework

Now, we extend the frequency domain representation of SOS processes to inhomogeneous point processes. We use the term ‘‘inhomogeneous’’ to indicate that the first-order intensity function $\underline{\lambda}_1(\cdot)$ may vary with location. Thus, the complete covariance intensity does not admit the reduced form described in (2.3). If, however, there is no structure imposed on the intensity functions, it remains unclear what the periodogram estimates in the inhomogeneous case. In this context, we confine our attention to a class of second-order intensity reweighted stationary processes (SOIRS; Baddeley et al. (2000)). Specifically, we say that \underline{X} is an m -variate SOIRS process if there exists $L_2(\cdot) = (\ell_2^{(i,j)}(\cdot))_{1 \leq i,j \leq m}$ such that the covariance intensity function of \underline{X} can be written as

$$\Gamma_2(\mathbf{x}, \mathbf{y}) = \text{diag}(\lambda_1(\mathbf{x})) L_2^{(i,j)}(\mathbf{x} - \mathbf{y}) \text{diag}(\lambda_1(\mathbf{y})). \quad (2.8)$$

An equivalent definition is that there exists an m -variate SOS process \tilde{X} whose first-order intensity and reduced covariance intensity are respectively given by $(1, \dots, 1)^\top$ and $L_2(\cdot)$ (see Appendix A for a detailed construction). Here, we refer to \tilde{X} as the intensity reweighted process of X .

Now, we propose an analogous concept of the spectrum for SOIRS processes. A key idea is to leverage the asymptotic behavior of the periodogram. In Yang and Guan (2024) (hereafter, YG24), we showed that under the increasing domain framework, the periodogram of a univariate SOS process satisfies

$$\lim_{n \rightarrow \infty} \mathbb{E}[I_{h,n}(\boldsymbol{\omega})] = F(\boldsymbol{\omega}), \quad \boldsymbol{\omega} \in \mathbb{R}^d. \quad (2.9)$$

That is, under stationarity, the periodogram is an asymptotically unbiased estimator of the spectrum. Therefore, by investigating the limiting behavior of the expectation of the periodogram under the SOIRS framework, we can extend the concept of the spectrum. To achieve this, we introduce a new asymptotic framework, which is motivated by the local stationarity in time series (cf. Dahlhaus (1997)). In particular, let $\{\underline{X}_{D_n}\}$ be a doubly-indexed sequence of m -variate processes, where for each $n \in \mathbb{N}$, \underline{X}_{D_n} denotes the SOIRS process observed on the window D_n of form (2.5). Then, we impose the following structural assumptions on \underline{X}_{D_n} .

Assumption 2.1. *For $n \in \mathbb{N}$, let $\underline{\lambda}_{1,n}(\cdot)$ and $\Gamma_{2,n}(\cdot, \cdot)$ be the first-order and covariance intensity function of \underline{X}_{D_n} . Then, the following two conditions hold:*

- (i) *There exists a reduced covariance intensity function $L_2(\cdot) = (\ell_2^{(i,j)}(\cdot))_{1 \leq i, j \leq m} : \mathbb{R}^d \rightarrow \mathbb{R}^{m \times m}$ that does not depend on $n \in \mathbb{N}$ and satisfies*

$$\Gamma_{2,n}(\mathbf{x}, \mathbf{y}) = \text{diag}(\lambda_{1,n}(\mathbf{x}))L_2(\mathbf{x} - \mathbf{y})\text{diag}(\lambda_{1,n}(\mathbf{y})), \quad n \in \mathbb{N}, \quad \mathbf{x}, \mathbf{y} \in D_n.$$

- (ii) *There exists a non-negative function $\underline{\lambda}(\mathbf{x}) = (\lambda^{(1)}(\mathbf{x}), \dots, \lambda^{(m)}(\mathbf{x}))^\top$, $\mathbf{x} \in \mathbb{R}^d$, which is continuous on its support $[-1/2, 1/2]^d$ and satisfies*

$$\underline{\lambda}_{1,n}(\mathbf{x}) = \underline{\lambda}(\mathbf{x}/\mathbf{A}), \quad n \in \mathbb{N}, \quad \mathbf{x} \in D_n. \quad (2.10)$$

The Assumption 2.1(i) states that the intensity reweighted process \tilde{X}_{D_n} of \underline{X}_{D_n} can be viewed as an n th-section of certain SOS process observed on the increasing domains. Assumption 2.1(ii) concerns the infill asymptotic behavior for the sequence of first-order intensity functions ensuring that we gain information about the spatially varying first-order intensity function as the domain increases. Both assumptions are required to guarantee that the moments of the DFT converge as $|D_n| \rightarrow \infty$.

Let $H_{h^2\lambda} = (H_{h^2\lambda^{(1)},1}, \dots, H_{h^2\lambda^{(m)},1})^\top$ and $H_{h^2\lambda, \lambda^\top} = (H_{h^2\lambda^{(i)}\lambda^{(j)},1})_{1 \leq i, j \leq m}$. Then, in Theorem 4.1 below, we show that under the above asymptotic framework,

$$\lim_{n \rightarrow \infty} \mathbb{E}[I_{h,n}(\boldsymbol{\omega})] = (2\pi)^{-d} H_{h,2}^{-1} \text{diag}(H_{h^2\lambda}) + H_{h,2}^{-1} (H_{h^2\lambda, \lambda^\top} \odot \mathcal{F}^{-1}(L_2)(\boldsymbol{\omega})).$$

Here, $A \odot B = (A^{(i,j)} B^{(i,j)})$ denotes the Hadamard product (entrywise product) of two matrices A and B . This indicates that even though the spectrum is not well-defined for an SOIRS process, the expectation of the periodogram still converges to a function with a closed-form expression. Therefore, using the above result in conjunction with (2.9), we now define the pseudo-spectrum.

Definition 2.1 (Pseudo-spectrum of a multivariate SOIRS process). *Let \underline{X}_{D_n} ($n \in \mathbb{N}$) be a sequence of m -variate SOIRS processes that satisfies Assumption 2.1. Suppose further that $L_2(\cdot)$ in Assumption 2.1(i) belongs to $L_1^{m \times m}(\mathbb{R}^d)$. Then, the pseudo-spectrum of $\{\underline{X}_{D_n}\}$ corresponding to the data taper h is defined as*

$$F_h(\boldsymbol{\omega}) = (2\pi)^{-d} H_{h,2}^{-1} \text{diag}(H_{h^2 \underline{\lambda}}) + H_{h,2}^{-1} (H_{h^2 \underline{\lambda}, \underline{\lambda}^\top} \odot \mathcal{F}^{-1}(L_2)(\boldsymbol{\omega})). \quad (2.11)$$

In Proposition B.1 in the Appendix, we show that the pseudo-spectrum shares similar properties to the spectrum of an SOS process, such as conjugate symmetry and positive definiteness.

3 Interpretation of the pseudo-spectrum using the local parameters

Although we have an exact expression, the proposed pseudo-spectrum lacks interpretation. In this section, we provide alternative expressions for F_h with some intuition.

3.1 The local representation

To develop the ideas, we first focus on the univariate complete covariance intensity function $\tilde{C}_n(\mathbf{x}, \mathbf{y})$ of X_{D_n} . By using a reparametrization $(\mathbf{u}, \mathbf{r}) = (\mathbf{x}/\mathbf{A}, \mathbf{x} - \mathbf{y})$, we obtain

$$\begin{aligned} \tilde{C}_n(\mathbf{x}, \mathbf{y}) &= \lambda_{1,n}(\mathbf{x})\delta(\mathbf{r}) + \gamma_{2,n}(\mathbf{x}, \mathbf{x} - \mathbf{r}) \\ &= \lambda(\mathbf{u})\delta(\mathbf{r}) + \lambda(\mathbf{u})\lambda(\mathbf{u} - (\mathbf{r}/\mathbf{A}))\ell_2(\mathbf{r}) =: \tilde{C}_n^{\mathbf{u}}(\mathbf{r}). \end{aligned}$$

Here, the second identity above is due to Assumption 2.1 and (2.8). Then, for a fixed $\mathbf{u} \in [-1/2, 1/2]^d$, as $n \rightarrow \infty$, $\tilde{C}_n^{\mathbf{u}}(\cdot)$ can be closely approximated by $\lambda(\mathbf{u})\delta(\cdot) + \{\lambda(\mathbf{u})\}^2 \ell_2(\cdot)$. A similar argument can also be applied to the multivariate case. That is, for large enough $n \in \mathbb{N}$,

$$(\tilde{C}_n^{\mathbf{u}})^{(i,j)}(\cdot) \approx \lambda^{(i)}(\mathbf{u})\delta(\cdot)\delta_{i,j} + \lambda^{(i)}(\mathbf{u})\lambda^{(j)}(\mathbf{u})\ell_2^{(i,j)}(\cdot), \quad i, j \in \{1, \dots, m\},$$

where $\delta_{i,j} = 1$ if $i = j$ and zero otherwise. Intriguingly, the right-hand side above is indeed an (i, j) th component of a valid complete covariance intensity function of some SOS process indexed by a localization factor $\mathbf{u} \in [-1/2, 1/2]^d$. This leads to the use of the ‘‘local’’ version of the complete covariance intensity function and spectrum.

Definition 3.1 (Local complete covariance intensity function and local spectrum). *Let \underline{X}_{D_n} ($n \in \mathbb{N}$) be a sequence of m -variate SOIRS processes that satisfies Assumption 2.1. Then, the local complete covariance intensity function at the location $\mathbf{u} \in [-1/2, 1/2]^d$ is defined as*

$$C^{\mathbf{u}}(\mathbf{x}) = \text{diag}(\underline{\lambda}(\mathbf{u}))\delta(\mathbf{x}) + (\underline{\lambda}(\mathbf{u})\underline{\lambda}(\mathbf{u})^\top) \odot L_2(\mathbf{x}). \quad (3.1)$$

Suppose further $L_2 \in L_1^{m \times m}(\mathbb{R}^d)$. Then, local spectrum is defined as

$$F^{\mathbf{u}}(\boldsymbol{\omega}) = \mathcal{F}^{-1}(C^{\mathbf{u}})(\boldsymbol{\omega}) = (2\pi)^{-d} \text{diag}(\underline{\lambda}(\mathbf{u})) + (\underline{\lambda}(\mathbf{u})\underline{\lambda}(\mathbf{u})^\top) \odot \mathcal{F}^{-1}(L_2)(\boldsymbol{\omega}). \quad (3.2)$$

Below, we show that $C^{\mathbf{u}}(\cdot)$ and $F^{\mathbf{u}}(\cdot)$ are valid complete covariance matrix and spectrum for some SOS process.

Theorem 3.1. *Let \underline{X}_{D_n} ($n \in \mathbb{N}$) be a sequence of m -variate point processes that satisfies Assumption 2.1. Suppose further $L_2 \in L_1^{m \times m}(\mathbb{R}^d)$. Then, for every $\mathbf{u} \in [-1/2, 1/2]^d$, there exists an m -variate SOS process $\underline{X}^{\mathbf{u}}$ on \mathbb{R}^d such that the complete covariance intensity function and the spectrum of $\underline{X}^{\mathbf{u}}$ are given by $C^{\mathbf{u}}(\cdot)$ and $F^{\mathbf{u}}(\cdot)$, respectively. Here, $\underline{X}^{\mathbf{u}}$ approximates the local behavior of \underline{X}_{D_n} around the neighborhood of $\mathbf{x} = \mathbf{u} \cdot \mathbf{A}$.*

Proof. See Appendix C.1. □

The next theorem shows that the pseudo-spectrum F_h can be written in terms of the weighted integral of the local spectra.

Theorem 3.2. *Let \underline{X}_{D_n} ($n \in \mathbb{N}$) be a sequence of m -variate SOIRS processes that satisfies Assumption 2.1. Suppose further that $L_2(\cdot) \in L_1^{m \times m}(\mathbb{R}^d)$. Then,*

$$F_h(\boldsymbol{\omega}) = \frac{1}{H_{h,2}} \int_{[-1/2, 1/2]^d} h(\mathbf{u})^2 F^{\mathbf{u}}(\boldsymbol{\omega}) d\mathbf{u}.$$

Proof. See Appendix C.2. □

3.2 Frequency domain features for inhomogeneous processes

In YG24, Section 2.3, we showed that the spectrum of an SOS process contains some global features of the point process, such as the value of the first-order intensity, overall clustering/repulsive behavior, and the amount of clustering/repulsiveness. By using Theorem 3.2, we can also extract some features of the inhomogeneous point process from the pseudo-spectrum.

Specifically, let $f^{\mathbf{u}}$ be the frequency domain feature of $\underline{X}^{\mathbf{u}}$ (as in Theorem 3.1) that can be obtained from the local spectrum, $F^{\mathbf{u}}$. Since $\underline{X}^{\mathbf{u}}$ characterizes the behavior of the point pattern in the neighborhood of $\mathbf{x} = \mathbf{u} \cdot \mathbf{A}$, Theorem 3.2 yields that the pseudo-spectrum F_h has a feature of the SOIRS processes $\{\underline{X}_{D_n}\}$ on the entire domain, which can be quantified as an averaged

effect of all features $f^{\mathbf{u}}$ on $\mathbf{u} \in [-1/2, 1/2]^d$, with weights proportional to $h^2(\mathbf{u})$. For example, by applying Theorem 3.2 with $h \equiv 1$ in $[-1/2, 1/2]^d$ and using (2.11), we obtain

$$F_0^{(i,i)}(\boldsymbol{\omega}) - (2\pi)^{-d} H_{\lambda^{(i)},1} = \int_{[-1/2, 1/2]^d} \{ (F^{\mathbf{u}})^{(i,i)}(\boldsymbol{\omega}) - (2\pi)^{-d} \lambda^{(i)}(\mathbf{u}) \} d\mathbf{u}.$$

Here, F_0 denotes the pseudo-spectrum for a unit taper function. Following the interpretation in YG24, $(F^{\mathbf{u}})^{(i,i)}(\boldsymbol{\omega}) - (2\pi)^{-d} \lambda^{(i)}(\mathbf{u}) > 0$ (resp., < 0) around the frequencies $\boldsymbol{\omega}$ near the origin indicates that X_i exhibits clustering (resp., repulsive) behavior in the local area near $\mathbf{x} = \mathbf{u} \cdot \mathbf{A}$. Therefore, $F_0^{(i,i)}(\boldsymbol{\omega}) - (2\pi)^{-d} H_{\lambda^{(i)},1} > 0$ (resp., < 0) at low frequencies implies that X_i is ‘‘overall’’ clustered (resp., repelled) across the entire domain. We refer the reader to Section 8 for the additional frequency domain features through the real data example.

4 Sampling properties of the DFTs and periodograms

4.1 The feasible criteria

Let $\underline{\lambda}(\mathbf{x}) = (\lambda^{(1)}(\mathbf{x}), \dots, \lambda^{(m)}(\mathbf{x}))^\top$ be the scaled first-order intensity function as in Assumption 2.1(ii). For the function h with support $[-1/2, 1/2]^d$ and for $k \in \mathbb{N}$, let

$$H_{h,k}^{(n)}(\boldsymbol{\omega}) = \int_{D_n} h(\mathbf{x}/\mathbf{A})^k \exp(-i\mathbf{x}^\top \boldsymbol{\omega}) d\mathbf{x}. \quad (4.1)$$

Then, using Campbell’s formula (see (A.1) in the Appendix), the expectation of the DFT under Assumption 2.1 is given by

$$\mathbb{E}[\underline{\mathcal{J}}_{h,n}(\boldsymbol{\omega})] = (2\pi)^{-d/2} H_{h,2}^{-1/2} |D_n|^{-1/2} H_{h,\underline{\lambda}}^{(n)}(\boldsymbol{\omega}), \quad (4.2)$$

where $H_{h,\underline{\lambda}}^{(n)}(\boldsymbol{\omega}) = (H_{h\lambda^{(1)},1}^{(n)}(\boldsymbol{\omega}), \dots, H_{h\lambda^{(m)},1}^{(n)}(\boldsymbol{\omega}))^\top$. Therefore, the centered DFT and the periodogram for SOIRS process are respectively defined as

$$\begin{aligned} \underline{J}_{h,n}(\boldsymbol{\omega}) &= \underline{\mathcal{J}}_{h,n}(\boldsymbol{\omega}) - (2\pi)^{-d/2} H_{h,2}^{-1/2} |D_n|^{-1/2} H_{h,\underline{\lambda}}^{(n)}(\boldsymbol{\omega}) \quad \text{and} \\ I_{h,n}(\boldsymbol{\omega}) &= (I_{h,n}^{(i,j)}(\boldsymbol{\omega}))_{1 \leq i,j \leq m} = \underline{J}_{h,n}(\boldsymbol{\omega}) \underline{J}_{h,n}(\boldsymbol{\omega})^*. \end{aligned} \quad (4.3)$$

Since $H_{h,\underline{\lambda}}^{(n)}(\cdot)$ depends on the unknown first-order intensities, the theoretical DFTs and periodograms need to be estimated. To do so, we first consider the estimation of the first-order intensity function. In particular, we assume the parametric model $\underline{\lambda}(\cdot) = \underline{\lambda}(\cdot; \boldsymbol{\beta}) = (\lambda^{(1)}(\cdot; \boldsymbol{\beta}), \dots, \lambda^{(m)}(\cdot; \boldsymbol{\beta}))^\top$ for $\boldsymbol{\beta} \in \Theta \subset \mathbb{R}^p$. Let $\boldsymbol{\beta}_0 \in \Theta$ be the true parameter, and let $\widehat{\boldsymbol{\beta}}_n$ be an estimator of $\boldsymbol{\beta}_0$ based on the n th observational window D_n . Then, the natural estimator of $H_{h,\underline{\lambda}}^{(n)}(\boldsymbol{\omega})$ is given by $\widehat{H}_{h,\underline{\lambda}}^{(n)}(\boldsymbol{\omega}) = (H_{h\widehat{\lambda}^{(1)},1}^{(n)}(\boldsymbol{\omega}), \dots, H_{h\widehat{\lambda}^{(m)},1}^{(n)}(\boldsymbol{\omega}))^\top$, where $\widehat{\lambda}^{(j)}(\cdot) = \lambda^{(j)}(\cdot; \widehat{\boldsymbol{\beta}}_n)$ is the estimator of the j th intensity function. Finally, our feasible criteria of $\underline{J}_{h,n}(\boldsymbol{\omega})$ and $\underline{I}_{h,n}(\boldsymbol{\omega})$,

denoted as $\widehat{J}_{h,n}(\boldsymbol{\omega})$ and $\widehat{I}_{h,n}(\boldsymbol{\omega})$, are defined similarly to (4.3), but with $\widehat{H}_{h\lambda}^{(n)}(\boldsymbol{\omega})$ replacing $H_{h\lambda}^{(n)}(\cdot)$ in the equation.

Below, we assume some mild conditions on the parametric form of $\underline{\lambda}$ and $\widehat{\boldsymbol{\beta}}_n$.

Assumption 4.1. *The first-order intensity has a parametric form $\{\underline{\lambda}(\cdot; \boldsymbol{\beta}) : \boldsymbol{\beta} \in \Theta\}$, where the parameter space $\Theta \subset \mathbb{R}^p$ is compact and the true parameter $\boldsymbol{\beta}_0$ lies in the interior of Θ . For any j , $\lambda^{(j)}(\cdot; \boldsymbol{\beta})$ is infinitely differentiable with respect to $\boldsymbol{\beta} \in \Theta$ and it holds that $\inf_{\mathbf{x} \in [-1/2, 1/2]^d} \lambda^{(j)}(\mathbf{x}; \boldsymbol{\beta}_0) > 0$.*

Assumption 4.2. *The estimator $\widehat{\boldsymbol{\beta}}_n$ of the true parameter $\boldsymbol{\beta}_0 \in \Theta$ lies in the interior of Θ and satisfies one of the following two conditions:*

$$(i) \quad |D_n|^{1/2} |\widehat{\boldsymbol{\beta}}_n - \boldsymbol{\beta}_0| = O_p(1), \quad n \rightarrow \infty.$$

$$(ii) \quad \text{There exists } r \in (1, \infty) \text{ such that } \mathbb{E}\{|D_n|^{1/2} |\widehat{\boldsymbol{\beta}}_n - \boldsymbol{\beta}_0|\}^r = O(1), \quad n \rightarrow \infty.$$

Under some mild conditions, the pseudo maximum likelihood estimator $\widehat{\boldsymbol{\beta}}_n$ using the log-linear first-order intensity model considered in Guan and Loh (2007) satisfies Assumptions 4.1 and 4.2(i,ii).

4.2 The joint asymptotic behavior of the DFTs and periodograms

From now on, we assume that \underline{X}_{D_n} ($n \in \mathbb{N}$) is a sequence of m -variate SOIRS processes that satisfies Assumption 2.1. To derive the sampling properties of the DFTs and periodograms, we require the following sets of assumptions.

The first assumption is on the observational windows.

Assumption 4.3. *The sequence of observation windows $\{D_n\}$ has the form as in (2.5). Moreover, it holds that $\lim_{n \rightarrow \infty} A_i(n) = \infty$, $i \in \{1, \dots, d\}$.*

The next assumption is on the integrability of the higher-order joint cumulant intensity functions of \underline{X}_{D_n} . For $\boldsymbol{\alpha} = (\alpha_1, \dots, \alpha_d) \in \{0, 1, \dots\}^d$, let $\gamma_n^\alpha : D_n^{d \times |\boldsymbol{\alpha}|} \rightarrow \mathbb{R}$ be the $\boldsymbol{\alpha}$ th-order joint cumulant intensity function of \underline{X}_{D_n} , defined as in (A.2) in the Appendix.

Assumption 4.4. *Let $k \in \{2, 3, \dots\}$ be fixed. Then, for any $\boldsymbol{\alpha} \in \{0, 1, \dots\}^m$ with $|\boldsymbol{\alpha}| \in \{1, \dots, k\}$, γ_n^α is well-defined and for $|\boldsymbol{\alpha}| \in \{2, \dots, k\}$,*

$$\sup_{n \in \mathbb{N}} \sup_{\mathbf{x}_{|\boldsymbol{\alpha}|} \in D_n} \int_{D_n^{|\boldsymbol{\alpha}|-1}} |\gamma_n^\alpha(\mathbf{x}_1, \dots, \mathbf{x}_{|\boldsymbol{\alpha}|-1}, \mathbf{x}_{|\boldsymbol{\alpha}|})| d\mathbf{x}_1 \cdots d\mathbf{x}_{|\boldsymbol{\alpha}|-1} < \infty.$$

The last assumption is on the data taper.

Assumption 4.5. *The data taper $h(\cdot)$ is non-negative, has support in $[-1/2, 1/2]^d$, and is continuous on $[-1/2, 1/2]^d$.*

Next, for two sequences of frequencies $\{\boldsymbol{\omega}_{1,n}\}_{n=1}^\infty$ and $\{\boldsymbol{\omega}_{2,n}\}_{n=1}^\infty$ on \mathbb{R}^d , we say $\{\boldsymbol{\omega}_{1,n}\}$ and $\{\boldsymbol{\omega}_{2,n}\}$ are asymptotically distant if $\lim_{n \rightarrow \infty} |D_n|^{1/d} \|\boldsymbol{\omega}_{1,n} - \boldsymbol{\omega}_{2,n}\| = \infty$.

Below theorem states that the DFTs and periodograms are asymptotically uncorrelated for two asymptotically distant frequencies and that the periodogram is an asymptotically unbiased estimator (except for the origin) of the pseudo-spectrum.

Theorem 4.1. *Suppose that Assumptions 4.1, 4.2(ii) (for $r > 2$), 4.3, 4.4 (for $k = 2$), and 4.5 hold. Let $\{\boldsymbol{\omega}_{1,n}\}$ and $\{\boldsymbol{\omega}_{2,n}\}$ be two frequencies in \mathbb{R}^d such that $\{\boldsymbol{\omega}_{1,n}\}$, $\{\boldsymbol{\omega}_{2,n}\}$, and $\{\mathbf{0}\}$ are pairwise asymptotically distant. Moreover, let $\{\boldsymbol{\omega}_n\}$ be a sequence that is asymptotically distant from $\{\mathbf{0}\}$ and satisfies $\lim_{n \rightarrow \infty} \boldsymbol{\omega}_n = \boldsymbol{\omega} \in \mathbb{R}^d$. Then,*

$$\lim_{n \rightarrow \infty} \text{cov}(\widehat{J}_{h,n}(\boldsymbol{\omega}_{1,n}), \widehat{J}_{h,n}(\boldsymbol{\omega}_{2,n})) = O_m \quad \text{and} \quad (4.4)$$

$$\lim_{n \rightarrow \infty} \text{var}(\widehat{J}_{h,n}(\boldsymbol{\omega}_n)) = \lim_{n \rightarrow \infty} \mathbb{E}[\widehat{J}_{h,n}(\boldsymbol{\omega}_n)] = F_h(\boldsymbol{\omega}), \quad (4.5)$$

where O_m denotes the $m \times m$ zero matrix.

Suppose further that Assumptions 4.2(ii) (for $r > 4$) and 4.4 (for $k = 4$) hold and that $\{\boldsymbol{\omega}_{1,n}\}$ and $\{-\boldsymbol{\omega}_{2,n}\}$ are asymptotically distant. Then, for $i_1, i_2, j_1, j_2 \in \{1, \dots, m\}$,

$$\lim_{n \rightarrow \infty} \text{cov}(\widehat{I}_{h,n}^{(i_1, j_1)}(\boldsymbol{\omega}_{1,n}), \widehat{I}_{h,n}^{(i_2, j_2)}(\boldsymbol{\omega}_{2,n})) = 0 \quad \text{and} \quad (4.6)$$

$$\lim_{n \rightarrow \infty} \text{cov}(\widehat{I}_{h,n}^{(i_1, j_1)}(\boldsymbol{\omega}_n), \widehat{I}_{h,n}^{(i_2, j_2)}(\boldsymbol{\omega}_n)) = F_h^{(i_1, i_2)}(\boldsymbol{\omega}) F_h^{(j_1, j_2)}(-\boldsymbol{\omega}). \quad (4.7)$$

Proof. See Appendix C.3. □

Remark 4.1 (Asymptotic joint normality). *Under the additional α -mixing conditions on \underline{X} , we can show the central limit theorem for the joint distribution of the DFTs and periodograms. Please refer to Theorem B.1 in the Appendix for the details.*

5 Nonparametric estimation of the pseudo-spectrum

We note from Theorem 4.1 that the periodogram does not consistently estimate the pseudo-spectrum. In this section, we provide a consistent estimator of the pseudo-spectrum via kernel smoothing of the periodogram in time series.

Let $K : \mathbb{R}^d \rightarrow \mathbb{R}$ be a non-negative symmetric kernel function that satisfies (i) $K(\mathbf{x})$ has support on $\mathbf{x} \in [-1, 1]^d$ and is continuous on \mathbb{R}^d , (ii) $\int_{\mathbb{R}^d} K(\mathbf{x}) d\mathbf{x} = 1$, and (iii) $\int_{\mathbb{R}^d} |K(\mathbf{x})|^2 d\mathbf{x} < \infty$. Let $\mathbf{b} = (b_1, \dots, b_d)^\top \in (0, \infty)^d$ be the bandwidth, and let $K_{\mathbf{b}}(\cdot) = (b_1 \cdots b_d)^{-1} K(\cdot/\mathbf{b})$. Then, the nonparametric estimator of the pseudo-spectrum is defined as

$$\widehat{F}_{n, \mathbf{b}}(\boldsymbol{\omega}) = \int_{\mathbb{R}^d} K_{\mathbf{b}}(\boldsymbol{\omega} - \mathbf{x}) \widehat{I}_{h,n}(\mathbf{x}) d\mathbf{x}. \quad (5.1)$$

To derive the asymptotic properties of $\widehat{F}_{n,\mathbf{b}}(\boldsymbol{\omega})$, we assume that the bandwidth $\mathbf{b} = \mathbf{b}(n) = (b_1(n), \dots, b_d(n))^\top$ depends only on $n \in \mathbb{N}$ and satisfies

$$\lim_{n \rightarrow \infty} \{\|\mathbf{b}(n)\|_\infty + \|1/(\mathbf{A}(n) \cdot \mathbf{b}(n))\|_\infty\} = 0, \quad (\text{B})$$

where $\mathbf{A}(n) = (A_1(n), \dots, A_d(n))^\top$ are the side lengths of D_n as in (2.5).

In the theorem below, we show that $\widehat{F}_{n,\mathbf{b}}(\boldsymbol{\omega})$ converges to the pseudo-spectrum in two different modes of convergence.

Theorem 5.1. *Suppose that Assumptions 4.1, 4.2(i), 4.3, 4.4 (for $k = 4$), and 4.5 hold. Moreover, the bandwidth $\mathbf{b} = \mathbf{b}(n)$ satisfies condition (B). Then, for $\boldsymbol{\omega} \in \mathbb{R}^d$,*

$$\widehat{F}_{n,\mathbf{b}}(\boldsymbol{\omega}) \xrightarrow{\mathcal{P}} F_h(\boldsymbol{\omega}), \quad (5.2)$$

where $\xrightarrow{\mathcal{P}}$ denotes convergence in probability. If we further assume Assumption 4.2(ii) for $r > 4$, then

$$\lim_{n \rightarrow \infty} \mathbb{E} |\widehat{F}_{n,\mathbf{b}}(\boldsymbol{\omega}) - F_h(\boldsymbol{\omega})|^2 = 0. \quad (5.3)$$

Proof. See Appendix C.4. □

In practice, we compute $\widehat{F}_{n,\mathbf{b}}(\boldsymbol{\omega})$ using the Riemann sum approximation:

$$\widehat{F}_{n,\mathbf{b}}^{(R)}(\boldsymbol{\omega}) = \frac{\sum_{\mathbf{k} \in \mathbb{Z}^d} K_{\mathbf{b}}(\boldsymbol{\omega} - \mathbf{x}_{\mathbf{k},\boldsymbol{\Omega}}) \widehat{I}_{h,n}(\mathbf{x}_{\mathbf{k},\boldsymbol{\Omega}})}{\sum_{\mathbf{k} \in \mathbb{Z}^d} K_{\mathbf{b}}(\boldsymbol{\omega} - \mathbf{x}_{\mathbf{k},\boldsymbol{\Omega}})}. \quad (5.4)$$

Here, $\mathbf{x}_{\mathbf{k},\boldsymbol{\Omega}} = (2\pi k_1/\Omega_1, \dots, 2\pi k_d/\Omega_d)^\top$ for some grid vector $\boldsymbol{\Omega} = (\Omega_1, \dots, \Omega_d)^\top$. We note that since $K_{\mathbf{b}}(\cdot)$ has finite support, the summations in (5.4) are finite sums. For theoretical justification, by using similar techniques to prove Theorem 5.1, one can also show the consistency and L_2 -convergence of $\widehat{F}_{n,\mathbf{b}}^{(R)}(\boldsymbol{\omega})$, provided the grid $\boldsymbol{\Omega}$ increases with n and has the form $c\mathbf{A}(n)$ for some constant $c \in (0, \infty)$.

6 Bandwidth selection methods

Although our kernel spectral density estimator $\widehat{F}_{n,\mathbf{b}}(\cdot)$ consistently estimates the pseudo-spectrum for any bandwidth \mathbf{b} satisfying condition (B), a poorly chosen bandwidth will result in an underperforming estimation. In this section, we propose two different approaches to select the bandwidth of $\widehat{F}_{n,\mathbf{b}}(\cdot)$. For the sake of parsimony, we set $b_1 = \dots = b_d = b$ for some $b \in (0, \infty)$.

6.1 Method I: The optimal MSE criterion

The first approach is based on the optimal mean squared error (MSE) criterion. Let

$$\text{MSE}(b) = \sup_{\boldsymbol{\omega} \in \mathbb{R}^d} \mathbb{E} |\widehat{F}_{n,b}(\boldsymbol{\omega}) - F_h(\boldsymbol{\omega})|^2, \quad (6.1)$$

where $\widehat{F}_{n,b}(\boldsymbol{\omega})$ is the kernel spectral density estimator using the common bandwidth b in all coordinates. To obtain the rate of convergence of $\text{MSE}(b)$, we require the following two additional assumptions.

First, we assume that the side lengths $\mathbf{A}(n)$ of D_n grow regularly in all coordinates:

$$A_i(n) \propto A_j(n), \quad i, j \in \{1, \dots, d\}, \quad (\text{SL})$$

where for two positive sequences $\{a_n\}$ and $\{b_n\}$, $a_n \propto b_n$ means $0 < \inf_n (a_n/b_n) \leq \sup_n (a_n/b_n) < \infty$. The next assumption is on the pseudo-spectrum. For $\boldsymbol{\alpha} = (\alpha_1, \dots, \alpha_d) \in \{0, 1, \dots\}^d$, let $\partial^\alpha = (\partial/\partial\omega_1)^{\alpha_1} \dots (\partial/\partial\omega_d)^{\alpha_d}$.

Assumption 6.1. *The pseudo-spectrum $F_h(\boldsymbol{\omega})$ satisfies the following conditions:*

(i) $F_h(\boldsymbol{\omega}) - (2\pi)^{-d} H_{h,2}^{-1} \text{diag}(H_{h^2\lambda}) \in L_1^{m \times m}(\mathbb{R}^d)$.

(ii) For $\boldsymbol{\alpha} \in \{0, 1, \dots\}^d$ with $|\boldsymbol{\alpha}| = 2$, $\partial^\alpha F_h(\boldsymbol{\omega})$ exists and is continuous on \mathbb{R}^d . Moreover, it holds that $\sup_{\boldsymbol{\omega}} |\partial^\alpha F_h(\boldsymbol{\omega})| < \infty$.

By using (2.11), it can be easily seen that Assumption 6.1(i) yields $\mathcal{F}^{-1}(L_2) \in L_1^{m \times m}(\mathbb{R}^d)$. Then, thanks to Theorem D.2 in the Appendix, we have

$$\text{MSE}(b) = O(b^4 + |D_n|^{-2/d} + |D_n|^{-1} b^{-d}), \quad (6.2)$$

provided $r \in (0, \infty)$ in Assumption 4.2(ii) is sufficiently large. Therefore, we choose $b = b_{\text{opt}}$ which minimizes the asymptotic order of the right-hand side above. In the theorem below, we provide the rates of convergence of b_{opt} and $\text{MSE}(b_{\text{opt}})$ to zero for multivariate inhomogeneous spatial point processes (the proof immediately follows from Theorem D.2, so we omit the details).

Theorem 6.1. *Suppose that Assumptions 4.1, 4.2(ii) (for $r = 6$), 4.3, 4.4 (for $k = 4$), 4.5, and 6.1 hold. Moreover, we assume that the data taper h is Lipschitz continuous on $[-1/2, 1/2]^d$, the side lengths $\mathbf{A}(n)$ satisfy (SL), and the bandwidth $b = b(n)$ satisfies (B). Let $d \in \{1, 2, 3, 4\}$. Then,*

$$b_{\text{opt}} \propto |D_n|^{-1/(d+4)} \quad \text{and} \quad \text{MSE}(b_{\text{opt}}) \propto |D_n|^{-4/(d+4)}.$$

6.2 Method II: Cross-validation

From our simulation results in Section 7 below, the pseudo-spectrum estimator based on the optimal bandwidth still suffers from large MSE for small sampling windows. Therefore, our second bandwidth selection criterion is based on the data-driven cross-validation method motivated by Beltrão and Bloomfield (1987) in the time series literature. Let $\boldsymbol{\Omega} = (\Omega_1, \dots, \Omega_d)^\top \in (0, \infty)^d$ be the grid vector and let

$$\widehat{F}_{n,b}^{(-1)}(\boldsymbol{\omega}_{t,\boldsymbol{\Omega}}) = \frac{\sum_{\mathbf{k} \in \mathbb{Z}^d \setminus \{t\}} K_b(\boldsymbol{\omega}_{t,\boldsymbol{\Omega}} - \boldsymbol{\omega}_{\mathbf{k},\boldsymbol{\Omega}}) \widehat{I}_{h,n}(\boldsymbol{\omega}_{\mathbf{k},\boldsymbol{\Omega}})}{\sum_{\mathbf{k} \in \mathbb{Z}^d \setminus \{t\}} K_b(\boldsymbol{\omega}_{t,\boldsymbol{\Omega}} - \boldsymbol{\omega}_{\mathbf{k},\boldsymbol{\Omega}})}, \quad (6.3)$$

where for $\mathbf{t} \in \mathbb{Z}^d$, $\boldsymbol{\omega}_{t,\boldsymbol{\Omega}} = 2\pi\mathbf{t}/\boldsymbol{\Omega}$. In the above, $K_b(\cdot) = b^{-d}K(b^{-1}\cdot)$ denotes the scaled kernel function using the univariate bandwidth b . Since $\widehat{F}_{n,b}^{(-1)}(\cdot)$ excludes the center point $\boldsymbol{\omega}_{t,\boldsymbol{\Omega}}$ in the calculation of the local average of the periodograms, $\widehat{F}_{n,b}^{(-1)}(\cdot)$ can be viewed as a leave-one-out estimator of the spectrum $F_h(\cdot)$. To select the appropriate bandwidth $b \in (0, \infty)$, we consider the following cross-validated spectral divergence between $\widehat{F}_{n,b}^{(-1)}$ and the periodogram $\widehat{I}_{h,n}$:

$$L(b) = \sum_{\boldsymbol{\omega}_{t,\boldsymbol{\Omega}} \in W} \left[\text{Tr}\{\widehat{I}_{h,n}(\boldsymbol{\omega}_{t,\boldsymbol{\Omega}}) \widehat{F}_{n,b}^{(-1)}(\boldsymbol{\omega}_{t,\boldsymbol{\Omega}})^{-1}\} + \log \det \widehat{F}_{n,b}^{(-1)}(\boldsymbol{\omega}_{t,\boldsymbol{\Omega}}) \right]. \quad (6.4)$$

Here, $W \subset \mathbb{R}^d$ denotes the prespecified compact domain on \mathbb{R}^d . Then, our second proposed bandwidth selection criterion is based on minimizing the cross-validated spectral divergence:

$$b_{\text{CV}} = \arg \min_{b \in (0, \infty)} L(b). \quad (6.5)$$

Heuristically, the selected b_{CV} minimizes the Kullback–Leibler divergence between $\widehat{F}_{n,b}^{(-1)}$ and $\widehat{I}_{h,n}$, where both are the estimators of the pseudo-spectrum using non-overlapping frequencies. In our simulation study, we observe that the kernel spectral density estimator based on b_{CV} outperforms to that based on b_{opt} . However, we will not investigate the mathematical properties of b_{CV} and $L(b_{\text{CV}})$ in this article.

7 Empirical study

To verify our theoretical findings, we conduct some simulations. For the data-generating process, we use a bi-variate product-shot-noise Cox process considered in Jalilian et al. (2015), but with a modification of their model.

7.1 The data-generating processes

Let $\underline{X} = (X_1, X_2)$ be a bi-variate Cox process on $D = [-A/2, A/2]^2$, where the corresponding latent intensity field $(\Lambda_1(\mathbf{x}), \Lambda_2(\mathbf{x}))^\top$ of \underline{X} is given by

$$\Lambda_i(\mathbf{x}) = \lambda^{(i)}(\mathbf{x}/A)S_i(\mathbf{x})Y_i(\mathbf{x}), \quad \mathbf{x} \in D.$$

Here, $\lambda^{(i)}(\mathbf{x}/A) = \mathbb{E}[\Lambda_i(\mathbf{x})]$ denotes the scaled first-order intensity of X_i , in alignment with the asymptotic framework in Assumption 2.1(ii).

Let Φ_1, Φ_2, Φ_3 be independent homogeneous Poisson point processes on \mathbb{R}^2 . In our bi-variate model, Φ_1 influences X_1 through the shot-noise field $S_1(\cdot)$, with a Gaussian kernel function as its dispersal kernel. The same Φ_1 also contributes to the compound field Y_2 , which influences the second process, X_2 . Similarly, Φ_2 affects X_2 directly through the shot-noise field S_2 and influences X_1 indirectly through the compound field Y_1 .

What distinguishes our model from that of Jalilian et al. (2015) is the inclusion of the third latent parent process, Φ_3 . In our model, Φ_3 affects both X_1 and X_2 indirectly through their compound fields (which is a more realistic scenario for real-life applications). See Figure 1(a) for the schematic diagram of our model.

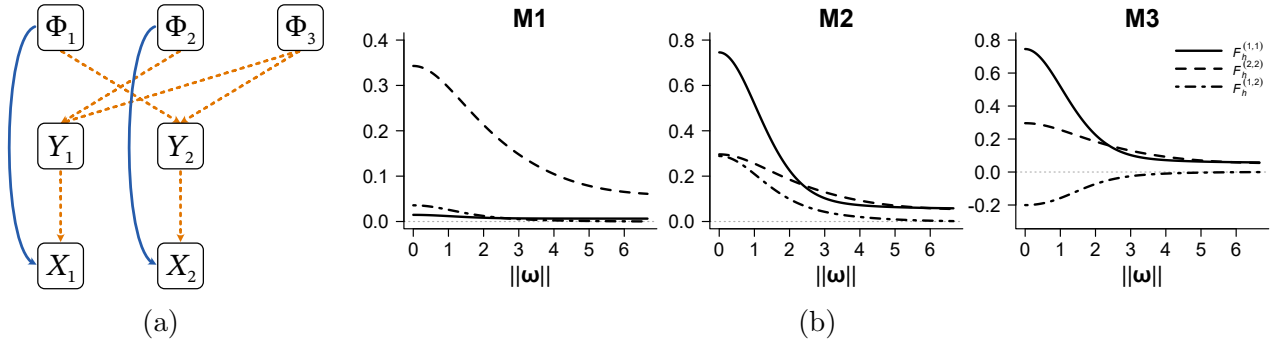


Figure 1: (a) A schematic diagram of our models. The solid lines refer to the direct effects through the shot-noise fields, and the dashed lines refer to the indirect effects through the compound fields. (b) The marginal (solid and dashed lines) and cross (dot-dashed line) spectrum (for M1) and pseudo-spectrum (for M2 and M3) plotted against $\|\omega\|$. Here, we use the data taper in Section 7.2 below to compute the pseudo-spectrum of M2 and M3.

For simulations, we consider the following three possible scenarios, namely M1–M3, based on the intensity functions and the sign of interaction. Due to space constraints, we only depict their main features, and the detailed parameter settings can be found in Appendix F.1.

- M1: Homogeneous isotropic process that exhibits inter-species clustering.
- M2: Inhomogeneous isotropic process that exhibits inter-species clustering.
- M3: Inhomogeneous isotropic process that exhibits inter-species repulsion.

Figure 1(b) plots the marginal and cross spectrum (for M1) and pseudo-spectrum (for M2 and M3). For convenience, we also refer to the spectrum of M1 as the pseudo-spectrum. Note that since all three models above are isotropic, $F_h^{(i,j)}(\boldsymbol{\omega})$ are all real-valued and depend only on the Euclidean norm of $\boldsymbol{\omega} \in \mathbb{R}^2$. In Figure 1(b), we see that the marginal pseudo-spectra $F^{(1,1)}$ and $F^{(2,2)}$ of all three models are all above the asymptote line, indicating that all three models are marginally clustered (see Section 3.2 for the interpretation). However, the cross pseudo-spectrum $F^{(1,2)}(\boldsymbol{\omega})$ is positive for M1 and M2, and negative for M3, yielding that the bi-variate processes cluster each other for M1 and M2, but repel each other for M3.

7.2 Pseudo-spectrum estimators

For each model, we generate 500 replications of the bi-variate spatial point patterns within the observation windows $D = [-A/2, A/2]^2$ for varying side lengths $A \in \{10, 20, 40\}$. To compare the various estimation approaches, for each replication, we evaluate the three different pseudo-spectrum estimators: (i) the raw periodogram ($=\widehat{I}_{h,n}$), (ii) the kernel spectral density estimator using the optimal bandwidth ($=\widehat{F}_{\text{opt}}$), and (iii) the kernel spectral density estimator using the cross-validation method ($=\widehat{F}_{\text{CV}}$). Below, we discuss some computational issues that arise when calculating our estimators.

Firstly, when computing the DFT $\mathcal{J}_{h,n}(\boldsymbol{\omega})$ as in (2.6), we use the separable data taper $h(\mathbf{x}) = h_a(x_1)h_a(x_2)$ with $a = 0.025$, where $h_a(\cdot)$ is as in (F.2) in the Appendix. Here, $a \in (0, 0.5)$ denotes the amount of data taper at each edge. In our simulation, the choice of a does not seem to affect the overall performance of the estimators. Next, when calculating $\widehat{I}_{h,n}$, the first-order intensities $\lambda^{(i)}$ ($i \in \{1, 2\}$) of Models M2 and M3 are estimated by fitting the log-linear first-order intensity model (Waagepetersen (2007)). For M1, since the model is homogeneous, we fit the intercept-only model (see, Appendix F.1 for the detailed procedure).

Next, for both kernel estimators, we implement the Riemann sum approximation version as in (5.4) with the triangular kernel $K(\mathbf{x}) = K_{\text{tri}}(x_1)K_{\text{tri}}(x_2)$, where $K_{\text{tri}}(x) = \max\{1 - |x|, 0\}$. To compute \widehat{F}_{opt} , we use the optimal bandwidth $b_{\text{opt}} = |D|^{-1/6} = A^{-1/3}$ for $A \in \{20, 40\}$ as described in Theorem 6.1. However, for the smallest side length $A = 10$, since the optimal bandwidth $b_{\text{opt}} = 10^{-1/3} \approx 0.46$ is smaller than the computational grid size (we will elaborate on this below), we set $b_{\text{opt}} = 0.5$ for $A = 10$.

Lastly, to compute \widehat{F}_{CV} , we need to determine the prespecified domain W and the computational grid $\boldsymbol{\Omega}$ as in (6.4). Observe from Figure 1(b) that, for all three models, when the frequency $\|\boldsymbol{\omega}\|_{\infty} > 1.5\pi \approx 4.71$, $F_h^{(i,j)}(\boldsymbol{\omega})$ is close to its constant asymptote value. This indicates that there is no additional gain in information about the pseudo-spectrum in the range $\|\boldsymbol{\omega}\|_{\infty} > 1.5\pi$. Therefore, we choose $W = [-1.5\pi, 1.5\pi]^2$ for all three models, ensuring robust results without adding additional computational costs. For a computational grid, we set $\boldsymbol{\Omega} = (\frac{4}{3}A, \frac{4}{3}A)^{\top}$, thus we evaluate $L(b)$ in (6.4) on the grids $\boldsymbol{\omega}_{t,\boldsymbol{\Omega}} = (\frac{1.5\pi t_1}{A}, \frac{1.5\pi t_2}{A})^{\top}$ for $t_1, t_2 \in \{-A, -A+1, \dots, A\}$.

7.3 Simulation results

7.3.1 The bandwidth selection methods

Table 1 below shows the summary statistics (three quartile values and the average) of the selected bandwidth values from 500 replications based on the cross-validation criterion. For reference, on the first row, we also provide the optimal bandwidth b_{opt} . We note that since b_{opt} depends only on the observational window, the selected optimal bandwidths are identical across all models with the same D .

	$D = [-5, 5]^2$			$D = [-10, 10]^2$			$D = [-20, 20]^2$		
	M1	M2	M3	M1	M2	M3	M1	M2	M3
b_{opt}		0.5			0.37			0.29	
Q1	1.13	1.10	1.10	0.59	0.58	0.58	0.32	0.28	0.30
Q2	1.41	1.25	1.25	0.74	0.60	0.60	0.40	0.30	0.30
Q3	1.66	1.58	1.58	0.79	0.78	0.78	0.40	0.38	0.30
Mean	1.45	1.39	1.36	0.71	0.68	0.66	0.37	0.32	0.31

Table 1: Quartiles (second to fourth row) and the average (fifth row) of b_{CV} from 500 replications for each region and model. The first row indicates the optimal bandwidth.

For b_{CV} , we observe that the bandwidth value and the interquartile range both decrease as the window size increases. Moreover, the distributions are slightly right-skewed, except for the cases M1 with $D = [-10, 10]^2$ and $D = [-20, 20]^2$, which are left-skewed. It is intriguing that, within the same window size, the summary statistics for the selected bandwidth for M2 and M3 are close to each others, while the bandwidth for M1 is larger than those for M2 and M3. This indicates that the sign of the inter-specific interaction may have less effect on the choice of the bandwidth.

Next, to compare the values of b_{opt} and b_{CV} , we note that the cross-validation method selects a larger bandwidth compared to that of the optimal MSE criterion. Specifically, for the smallest window ($D = [-5, 5]^2$), b_{CV} is more than twice as large as b_{opt} . However, as the window size increases, the ratio $b_{\text{CV}}/b_{\text{opt}}$ approaches one. This may indicate that b_{CV} also attains the same asymptotic rate as b_{opt} , which is proportional to $|D_n|^{-1/(d+4)}$. Currently, we do not have a theoretical justification for this, which is a good avenue for future research.

7.3.2 Estimation accuracy

Moving on, we compare the accuracy of the three pseudo-spectrum estimators. To check for the effect of bias and variance separately, we compute the two metrics that are widely used to assess the global performance of the estimator. The first metric is the integrated squared bias (IBIAS²)

over the prespecified domain W_o :

$$\text{IBIAS}^2 = \frac{1}{\#\{\boldsymbol{\omega}_{t,\Omega} \in W_o\}} \sum_{\boldsymbol{\omega}_{t,\Omega} \in W_o} \left(\frac{\frac{1}{500} \sum_{r=1}^{500} \widehat{F}_r^{(i,j)}(\boldsymbol{\omega}_{t,\Omega})}{F_h^{(i,j)}(\boldsymbol{\omega}_{t,\Omega})} - 1 \right)^2. \quad (7.1)$$

Here, $\widehat{F}_r^{(i,j)}$ denotes the r th replication of one of the three estimators of $F_h^{(i,j)}$. We note that since $F_h^{(i,j)}$ is real-valued for all three models under consideration, we only use the real part of the estimator $\widehat{F}_r^{(i,j)}$ when computing the IBIAS^2 . Moreover, in (7.1), we choose the domain of interest $W_o = \{\boldsymbol{\omega} : 0.1\pi \leq \|\boldsymbol{\omega}\|_\infty \leq 1.5\pi\}$ and the computational grid $\boldsymbol{\omega}_{t,\Omega} = \left(\frac{1.5\pi t_1}{A}, \frac{1.5\pi t_2}{A}\right)^\top$, $\mathbf{t} = (t_1, t_2)^\top \in \mathbb{Z}^2$. Here, the upper bound of W_o and the computational grid $\boldsymbol{\omega}_{t,\Omega}$ are chosen in the same spirit as determining the prespecified domain and the computational grid of the cross-validated spectral divergence $L(b)$ (see, Section 7.2). Moreover, since the bias of the feasible periodogram $\widehat{I}_{h,n}(\boldsymbol{\omega}_n)$ does not converge to zero for $\boldsymbol{\omega}_n$ close to the origin (see, Theorem 4.1), we exclude the frequencies such that $\|\boldsymbol{\omega}\|_\infty < 0.1\pi$ when evaluating the IBIAS^2 .

Another metric is the integrated MSE (IMSE), which is defined similarly to IBIAS^2 , but replacing the summand of (7.1) with the MSE, $\frac{1}{500} \sum_{r=1}^{500} (\widehat{F}_r^{(i,j)}(\boldsymbol{\omega}_{t,\Omega})/F_h^{(i,j)}(\boldsymbol{\omega}_{t,\Omega}) - 1)^2$.

The estimation results are presented in Table 2 below. Firstly, we observe that the IBIAS^2 of all three estimators converges to zero as $|D|$ increases. This verifies the asymptotic unbiasedness of the periodogram as stated in Theorem 4.1. The magnitudes of the IBIAS^2 are comparable between the three estimators, while within the same model and the same window, the IBIAS^2 for the cross pseudo-spectrum is larger than those of the marginal pseudo-spectrum. This is because for large $\|\boldsymbol{\omega}\|$ values, $F_h^{(1,2)}(\boldsymbol{\omega})$ converges to zero, thus inflating the numerical error when calculating the (relative) bias as in (7.1).

Secondly, we compare the IMSE. Unlike the IBIAS^2 , we observe a stark distinction between the IMSE of the raw periodogram and those of the other two kernel-smoothed periodograms. The IMSE of the raw periodogram is still significantly present even for the largest domain size, whereas the IMSE of both kernel spectrum estimators converges to zero as the window size increases. This solidifies our theoretical results in Theorems 4.1 and 5.1. Within the same model and the same window, the IMSE of the cross pseudo-spectrum tends to be larger than that of the marginal pseudo-spectrum, which is also due to numerical issues. Moreover, it is intriguing that the IMSE of $\widehat{F}^{(1,2)}$ for the negative inter-specific interaction model (M3) is larger than that of the positive inter-specific interaction model (M2). However, we do not have any theoretical reasoning for this.

Lastly, we compare the estimation performance of the two different bandwidth selection methods. First, we observe that within the same model and the same window, the IBIAS^2 of \widehat{F}_{CV} tends to be smaller than that of \widehat{F}_{opt} . This is because the bias due to the estimation of the first-order intensity has an order of $O(|D_n|^{-1}b^{-d})$ (see Theorem E.4 in the Appendix), yielding larger bias for \widehat{F}_{opt} , provided that b_{CV} is larger than b_{opt} (see Table 1). Next, we see that the

Model	Spectrum	Window	$\widehat{I}_{h,n}$		\widehat{F}_{opt}		\widehat{F}_{CV}	
			IBIAS ²	IMSE	IBIAS ²	IMSE	IBIAS ²	IMSE
M1	$F_h^{(1,1)}$	$[-5, 5]^2$	0.00	1.15	0.00	0.84	0.00	0.24
		$[-10, 10]^2$	0.00	1.07	0.00	0.29	0.00	0.14
		$[-20, 20]^2$	0.00	1.02	0.00	0.12	0.00	0.09
	$F_h^{(2,2)}$	$[-5, 5]^2$	0.02	1.21	0.03	0.92	0.03	0.38
		$[-10, 10]^2$	0.01	1.06	0.01	0.27	0.02	0.15
		$[-20, 20]^2$	0.00	1.01	0.00	0.12	0.01	0.09
	$F_h^{(1,2)}$	$[-5, 5]^2$	0.42	146.13	0.31	101.73	0.10	18.16
		$[-10, 10]^2$	0.20	117.83	0.05	28.31	0.05	11.10
		$[-20, 20]^2$	0.22	102.54	0.03	10.98	0.03	7.80
M2	$F_h^{(1,1)}$	$[-5, 5]^2$	0.03	1.49	0.02	1.14	0.02	0.49
		$[-10, 10]^2$	0.01	1.09	0.00	0.32	0.00	0.17
		$[-20, 20]^2$	0.00	1.02	0.00	0.14	0.00	0.13
	$F_h^{(2,2)}$	$[-5, 5]^2$	0.00	1.06	0.00	0.76	0.00	0.18
		$[-10, 10]^2$	0.00	1.02	0.00	0.26	0.00	0.12
		$[-20, 20]^2$	0.00	0.99	0.00	0.11	0.00	0.11
	$F_h^{(1,2)}$	$[-5, 5]^2$	0.06	28.14	0.04	19.86	0.01	3.76
		$[-10, 10]^2$	0.05	22.61	0.02	5.71	0.01	2.45
		$[-20, 20]^2$	0.05	20.18	0.01	2.29	0.01	2.11
M3	$F_h^{(1,1)}$	$[-5, 5]^2$	0.03	1.57	0.03	1.20	0.02	0.53
		$[-10, 10]^2$	0.01	1.11	0.00	0.32	0.00	0.16
		$[-20, 20]^2$	0.00	1.01	0.00	0.13	0.00	0.13
	$F_h^{(2,2)}$	$[-5, 5]^2$	0.01	1.12	0.00	0.80	0.00	0.18
		$[-10, 10]^2$	0.00	1.02	0.00	0.25	0.00	0.11
		$[-20, 20]^2$	0.00	1.00	0.00	0.11	0.00	0.11
	$F_h^{(1,2)}$	$[-5, 5]^2$	0.45	290.13	0.32	199.28	0.11	27.94
		$[-10, 10]^2$	0.50	209.24	0.12	49.74	0.05	19.43
		$[-20, 20]^2$	0.35	174.96	0.04	19.11	0.03	17.94

Table 2: IBIAS² and IMSE for the three pseudo-spectrum estimators.

IMSE of \widehat{F}_{CV} is uniformly smaller than that of \widehat{F}_{opt} , with the difference being more pronounced when considering small and moderate window sizes ($D = [-5, 5]^2$ and $[-10, 10]^2$). This suggests that, at least for the small and moderate windows, the gains from the data-driven cross-validation method to select the bandwidth outweigh the additional computational costs needed to calculate b_{CV} . Note that, by its construction, the IMSE of \widehat{F}_{opt} has the fastest order of convergence to zero. Therefore, the results in Table 2 for large observational windows may indicate that b_{CV} is also asymptotically optimal in the sense of the MSE criterion.

8 Real data application

In this section, we apply our methods to the tree species data in the tropical forest of Barro Colorado Island (BCI). The dataset contains spatial locations (within the $1000 \times 500 \text{ m}^2$ rectangular window) of trees and shrubs with stem diameters larger than 10 mm (Condit et al. (2019)). The point process modeling of these tree species data has also been considered in Jalilian et al. (2015); Waagepetersen et al. (2016) (fitting parametric multivariate inhomogeneous point process models in the spatial domain) and Grainger et al. (2023) (analyzing frequency domain features assuming stationarity of the data).

For the dataset, we consider five specific tree species, namely *Capparis frondosa* (Cappfr, X_1), *Hirtella triandra* (Hirttr, X_2), *Protium panamense* (Protpa, X_3), *Protium tenuifolium* (Protte, X_4), and *Tetragastris panamensis* (Tet2pa, X_5) from the seventh census, which are also considered in Jalilian et al. (2015). The spatial point distribution of these five species can be found in Figure 2(a) below. Since the point patterns clearly reveal inhomogeneity in the first-order intensities (see also the estimated intensity plots in Figure F.2 in the Appendix), we use a five-variate SOIRS process to explain these point patterns.

To investigate the frequency domain features, we compute the pseudo-spectrum estimator. Note that given relatively large window size, the true first-order intensities are on a scale of 10^{-3} . Thus, computing the feasible periodogram may be sensitive to numerical errors (also problematic for the condition $\inf_{\mathbf{x}} \lambda(\mathbf{x}) > 0$ in Assumption 4.1). Therefore, we rescale the window size to $50 \times 25 \text{ unit}^2$, where one unit is equivalent to 20 m, ensuring that the fitted first-order intensities have a scale between 1 and 10. When calculating the feasible periodogram, we use the log-linear first-order intensity model using ten environmental and geolocational covariates, as provided in Jalilian et al. (2015). Moreover, when computing $\widehat{F}_{n,b}$, we use the cross-validation bandwidth selection method on a computational grid $\{(\frac{1.5\pi t_1}{A_1}, \frac{1.5\pi t_2}{A_2})^\top\}$ for $(A_1, A_2) = (50, 25)$ and $t_i \in \{-A_i, \dots, A_i\}$. Consequently, we select the bandwidth $b = 0.62$.

The lower diagonal part of Figure 2(b) shows the real part of the radial average of $\widehat{F}_{n,b}^{(i,j)}(\boldsymbol{\omega})$. The horizontal dotted line indicates the asymptote of $\widehat{F}_{n,b}^{(i,j)}(\boldsymbol{\omega})$, which equals $(2\pi)^{-2} H_{h^2\lambda^{(i)},1} \delta_{i,j}$. To compare our approach with spatial domain methods, the upper diagonal part of Figure 2(b) displays the shifted pair correlation function (PCF) estimators, which correspond to $\ell^{(i,j)}(\cdot)$ in our context (the asymptote lines are zero).

First, we focus on the marginal estimators. For all five species, the values of $\widehat{F}^{(i,i)}(\boldsymbol{\omega})$ lie above their respective asymptote lines, indicating that all five tree species exhibit marginal clustering (see, Section 3.2 for an interpretation). Additionally, the pseudo-spectrum of X_4 (Protte) shows a peak around $\|\boldsymbol{\omega}\| \approx 1$, while the pseudo-spectra of the other four species seem to monotonically decreasing. Since a nonzero peak in the frequency domain corresponds to oscillatory behavior in the spatial domain, this observation suggests that $g^{(4,4)}(r) - 1$ may behave like a damping function (such as $g^{(4,4)}(r) - 1 = Ae^{-ar} \cos(2\pi r)$ for some $A, a > 0$). However, this oscillatory behavior of X_4 is not as pronounced in the PCF plot.

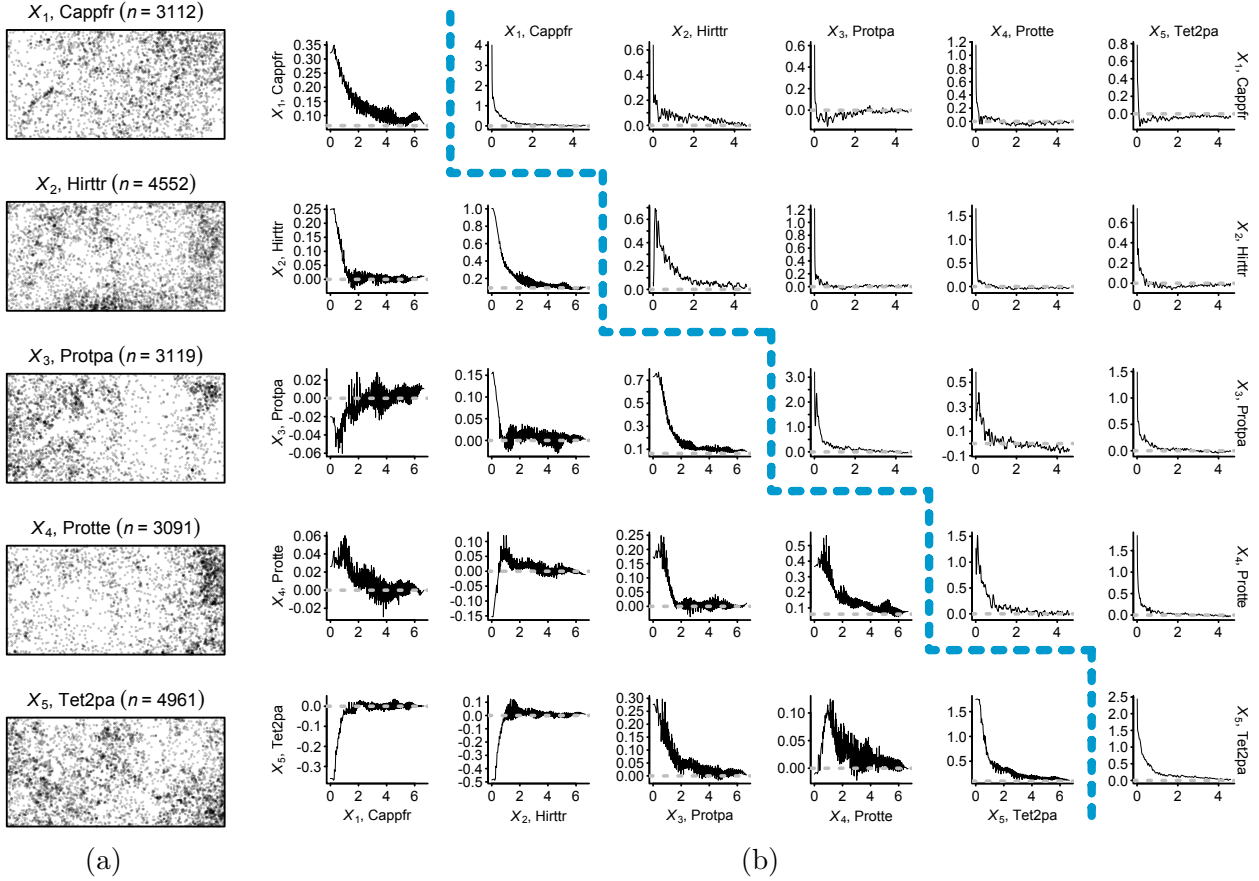


Figure 2: (a) Point patterns of five tree species from the BCI dataset. The number in parentheses indicates the total number of observations. (b) Radial average of the real part of $\widehat{F}^{(i,j)}(\omega)$ (lower diagonal) and the shifted PCF estimators $\widehat{g}^{(i,j)}(r) - 1$ (upper diagonal).

Next, we examine the cross estimators. The cross pseudo-spectrum $\widehat{F}^{(i,j)}(\omega)$ also provides insights into the interaction between the two SOIRS processes in the frequency domain. For example, the real part of $\widehat{F}^{(1,2)}$ is positive, indicating interspecies clustering between X_1 (Cappfr) and X_2 (Hirtrr). This observation is corroborated by $\widehat{g}^{(1,2)}(r) - 1 > 0$ in the PCF plot. Similarly, the negative values of the real part of $\widehat{F}^{(1,5)}$ indicate that X_1 (Cappfr) and X_5 (Tet2pa) repel each other. However, this repulsion is not as evident in the PCF plots, as $\widehat{g}^{(1,5)}(r) - 1$ exhibits a large peak near the origin. Furthermore, the cross estimators involving X_4 have peaks around $\|\omega\| \approx 1$, confirming the earlier observation from $\widehat{F}^{(4,4)}$ that X_4 has a periodic behavior.

Lastly, the cross estimators also provide information about the asymptotic uncorrelatedness of two point processes. For example, the values of $|\widehat{F}^{(1,3)}(\omega)|$ are close to zero, suggesting that the correlation structure between X_1 (Cappfr) and X_3 (Protpa) is weaker compared to other species pairs. Indeed, in Appendix F.3, we quantify the coherence of the multivariate inhomogeneous point processes and find that the maximum coherence value of the intensity reweighted processes of X_1 and X_3 is the smallest among all possible combinations. Please see Appendix F.3 for details on the coherence (and partial coherence) analysis.

Acknowledgments

QWD and JY acknowledge the support of the Taiwan’s National Science and Technology Council (grant 113-2118-M-001-012). QWD’s research assistantship was partly supported by Academia Sinica’s Career Development Award Grant (AS-CDA-114-M03). The authors thank Yongtao Guan for fruitful discussions and suggestions and Abdollah Jalilian for kindly share the BCI data used in Section 8 and Appendix F.

References

- A. J. Baddeley, J. Møller, and R. Waagepetersen. Non- and semi-parametric estimation of interaction in inhomogeneous point patterns. *Stat. Neerl.*, 54(3):329–350, 2000.
- M. S. Bartlett. The spectral analysis of two-dimensional point processes. *Biometrika*, 51(3/4): 299–311, 1964.
- K. I. Beltrão and P. Bloomfield. Determining the bandwidth of a kernel spectrum estimate. *J. Time Series Anal.*, 8(1):21–38, 1987.
- D. R. Brillinger. *Time series: Data Analysis and Theory*. Holden-Day, INC., San Francisco, CA, 1981. Expanded edition.
- R. Condit, R. Pérez, S. Aguilar, S. Lao, R. Foster, and S. Hubbell. Complete data from the barro colorado 50-ha plot: 423617 trees, 35 years, 2019.
- Noel Cressie. *Statistics for spatial data*. John Wiley & Sons, Hoboken, NJ, 2015.
- R. Dahlhaus. Fitting time series models to nonstationary processes. *Ann. Statist.*, 25(1):1–37, 1997.
- R. Dahlhaus. Graphical interaction models for multivariate time series. *Metrika*, 51:157–172, 2000.
- D. J. Daley and D. Vere-Jones. *An Introduction to the Theory of Point Processes: Volume I: Elementary Theory and Methods*. Springer, New York City, NY., 2003. second edition.
- M. Eckardt. Graphical modelling of multivariate spatial point processes. *arXiv preprint arXiv:1607.07083*, 2016.
- M. Eichler. Graphical modelling of multivariate time series. *Probab. Theory Related Fields*, 153: 233–268, 2012.
- J. P. Grainger, T. A. Rajala, D. J. Murrell, and S. C. Olhede. Spectral estimation for spatial point processes and random fields. *arXiv preprint arXiv:2312.10176*, 2023.

- Y. Guan and J. M. Loh. A thinned block bootstrap variance estimation procedure for inhomogeneous spatial point patterns. *J. Amer. Statist. Assoc.*, 102(480):1377–1386, 2007.
- A. Jalilian, Y. Guan, J. Mateu, and R. Waagepetersen. Multivariate product-shot-noise cox point process models. *Biometrics*, 71:1022–1033, 2015.
- Y. Matsuda and Y. Yajima. Fourier analysis of irregularly spaced data on R^d . *J. R. Stat. Soc. Ser. B. Stat. Methodol.*, 71(1):191–217, 2009.
- T. A. Rajala, S. C. Olhede, J. P. Grainger, and D. J. Murrell. What is the Fourier transform of a spatial point process? *IEEE Trans. Inform. Theory*, 2023.
- R. Waagepetersen, A. Guan, Y. and Jalilian, and J. Mateu. Analysis of multispecies point patterns by using multivariate log-Gaussian Cox processes. *J. R. Stat. Soc. Ser. C. Appl. Stat.*, 65(1):77–96, 2016.
- R. P. Waagepetersen. An estimating function approach to inference for inhomogeneous Neyman–Scott processes. *Biometrics*, 63(1):252–258, 2007.
- J. Yang and Y. Guan. Fourier analysis of spatial point processes. *To appear at Bernoulli*, 2024.
- L. Zhu, J. Yang, M. Jun, and S. Cook. On minimum contrast method for multivariate spatial point processes. *arXiv preprint arXiv:2208.07044*, 2023.

A Higher-order intensity reweighted processes

In this section, we define the k th-order intensity-reweighted process (IRS) through the mean of the weighted process of an m -variate process $\underline{X} = (X_1, \dots, X_m)$. Here, the SOIRS process can be viewed as a special case of the k th-order IRS by setting $k = 2$. To do so, we first define the joint intensity and joint cumulant intensity functions of \underline{X} as in Zhu et al. (2023).

Let $\boldsymbol{\alpha} = (\alpha_1, \dots, \alpha_m) \in \{0, 1, \dots\}^m$ be a vector of orders, and let $\underline{\mathbf{x}} = (\underline{\mathbf{x}}_1^\top, \dots, \underline{\mathbf{x}}_m^\top)^\top$, where $\underline{\mathbf{x}}_i = (\mathbf{x}_{i,1}, \dots, \mathbf{x}_{i,\alpha_i})^\top \in \mathbb{R}^{\alpha_i d}$ for $i \in \{1, \dots, m\}$. Then, the $\boldsymbol{\alpha}$ th-order joint intensity function of \underline{X} , denoted as $\lambda^\alpha : \mathbb{R}^{|\boldsymbol{\alpha}|d} \rightarrow \mathbb{R}$, satisfies the following integral equation:

$$\mathbb{E} \left[\sum_{\mathbf{x}_1 \in X_1 \cap (\mathbb{R}^d)^{\alpha_1 \neq}} \cdots \sum_{\mathbf{x}_m \in X_m \cap (\mathbb{R}^d)^{\alpha_m \neq}} f(\underline{\mathbf{x}}_1, \dots, \underline{\mathbf{x}}_m) \right] = \int_{\mathbb{R}^{|\boldsymbol{\alpha}|d}} f(\underline{\mathbf{x}}) \lambda^\alpha(\underline{\mathbf{x}}) d\underline{\mathbf{x}} \quad (\text{A.1})$$

for any positive measurable function $f : \mathbb{R}^{|\boldsymbol{\alpha}|d} \rightarrow \mathbb{R}$. The above identity is often referred to as Campbell's formula.

Next, we define the joint cumulant intensity function using a combinatorial argument (cf. Brillinger (1981), Chapter 2.3). For $i \in \{1, \dots, m\}$, let $B_i \subset \{1, \dots, \alpha_i\}$ and let $(\underline{\mathbf{x}}_i)_{B_i} = (\mathbf{x}_{i,j} : j \in B_i) \in \mathbb{R}^{n(B_i)d}$. Here, $n(A)$ denotes the number of (finite) elements in a set A . Similarly, for $B = (B_1, \dots, B_m)$, let $\underline{\mathbf{x}}_B = ((\underline{\mathbf{x}}_1)_{B_1}, \dots, (\underline{\mathbf{x}}_m)_{B_m}) \in \mathbb{R}^{n(B)d}$. Using this notation, the $\boldsymbol{\alpha}$ th-order cumulant intensity function of \underline{X} is defined as

$$\gamma^\alpha(\underline{\mathbf{x}}) = \sum_{\pi} (n(\pi) - 1)! (-1)^{n(\pi)-1} \prod_{B \in \pi} \lambda^{(n(B_1), \dots, n(B_m))}(\underline{\mathbf{x}}_B), \quad \underline{\mathbf{x}} \in \mathbb{R}^{|\boldsymbol{\alpha}|d}. \quad (\text{A.2})$$

Here, the first summation is taken over all sets of the form $\cup_j (B_{1,j}, \dots, B_{m,j})$, where $\{B_{i,j}\}_j$ is a partition of $\{1, \dots, \alpha_i\}$.

Using the above notation, for $k \in \mathbb{N}$, we first define k th-order stationary processes. We say that \underline{X} is k th-order stationary if, for any $\boldsymbol{\alpha} = (\alpha_1, \dots, \alpha_m) \in \{0, 1, \dots\}^m$ with $1 \leq |\boldsymbol{\alpha}| \leq k$, there exists a function $\gamma_{\text{red}}^\alpha : \mathbb{R}^{(|\boldsymbol{\alpha}|-1)d} \rightarrow \mathbb{R}$ such that

$$\gamma^\alpha(\underline{\mathbf{x}}) = \gamma_{\text{red}}^\alpha(\mathbf{x}_{i,1} - \mathbf{x}_{j,\alpha_j}, \mathbf{x}_{i,2} - \mathbf{x}_{j,\alpha_j}, \dots, \mathbf{x}_{j,\alpha_j-1} - \mathbf{x}_{j,\alpha_j}), \quad \underline{\mathbf{x}} \in \mathbb{R}^{|\boldsymbol{\alpha}|d}. \quad (\text{A.3})$$

Here, $1 \leq i \leq j \leq m$ denote the smallest and largest indices, respectively, where α_i and α_j are both nonzero.

Using the above concept, we define the k th-order IRS process. To properly define the k th-order IRS process, we first introduce the concept of a weighted point process, which incorporates both superposition and thinning operators.

Definition A.1 (Weighted spatial point process). *Let X be a univariate point process on $D \subset \mathbb{R}^d$ and let $w(\cdot)$ be a bounded, non-negative function on D . Let $k \in \mathbb{N}$ be chosen such that $k \geq \sup_{\mathbf{x} \in D} f(\mathbf{x})$. Therefore, $p(\mathbf{x}) = w(\mathbf{x})/k$ is a probability. Let $X^{(1)}, \dots, X^{(k)}$ be independent*

copies of X . Then, the weighted point process of X with respect to the weight function $w(\cdot)$ is defined as a thinned process of the superposition of $X^{(1)}, \dots, X^{(k)}$ with independent thinning probability $p(\cdot)$.

For a multivariate point process $\underline{X} = (X_1, \dots, X_m)$ and a non-negative, bounded vector-valued function $\underline{w}(\mathbf{x}) = (w_1(\mathbf{x}), \dots, w_m(\mathbf{x}))$, a weighted point process of \underline{X} is defined as an m -variate point process where the i th element is the weighted process of X_i with respect to the weight function $w_i(\cdot)$.

Recall $\underline{\lambda}_1(\mathbf{x})$ in (2.1). Using the above concept, we now define the k th-order IRS process.

Definition A.2 (k th-order intensity reweighted stationary point process). \underline{X} is called an m -variate k th-order intensity reweighted (IRS) process on $D \subset \mathbb{R}^d$ if $\tilde{\underline{X}}$, the weighted process of \underline{X} with weights $(1/\lambda_1^{(1)}(\mathbf{x}), \dots, 1/\lambda_1^{(m)}(\mathbf{x}))$, is a k th-order stationary process on D . We refer to $\tilde{\underline{X}}$ as the intensity reweighted process of \underline{X} .

B Properties of the pseudo-spectrum and its estimator

Let $F_h(\boldsymbol{\omega})$ be the pseudo-spectrum defined as in (2.11). Below, we list three mathematical properties of F_h .

Proposition B.1. Let \underline{X}_{D_n} ($n \in \mathbb{N}$) be a sequence of m -variate SOIRS processes that satisfies Assumption 2.1. Suppose further that $L_2(\cdot)$ in Assumption 2.1(i) belongs to $L_1^{m \times m}(\mathbb{R}^d)$. Then, the pseudo-spectrum F_h of $\{\underline{X}_{D_n}\}$ with data taper h satisfies the following assertions.

- (i) If $\{\underline{X}_{D_n}\}$ is an SOS process, then F_h equals the spectrum of the corresponding SOS process.
- (ii) For any $\boldsymbol{\omega} \in \mathbb{R}^d$, $F_h(\boldsymbol{\omega})$ is a positive definite matrix and satisfies $F_h(-\boldsymbol{\omega}) = F_h(\boldsymbol{\omega})^*$.
- (iii) If \underline{X}_{D_n} corresponds to a sequence of m -variate inhomogeneous Poisson point processes, then the pseudo-spectrum is given by

$$F_h(\boldsymbol{\omega}) = (2\pi)^{-d} \text{diag} \left(\frac{\int_{[-1/2, 1/2]^d} (h^2 \lambda^{(1)})(\mathbf{x}) d\mathbf{x}}{\int_{[-1/2, 1/2]^d} h^2(\mathbf{x}) d\mathbf{x}}, \dots, \frac{\int_{[-1/2, 1/2]^d} (h^2 \lambda^{(m)})(\mathbf{x}) d\mathbf{x}}{\int_{[-1/2, 1/2]^d} h^2(\mathbf{x}) d\mathbf{x}} \right).$$

This indicates that the pseudo-spectrum of an inhomogeneous Poisson point process is a constant diagonal matrix, which is analogous to the constant spectrum of the homogeneous Poisson process.

Proof. By substituting the constant first-order intensity $\underline{\lambda}$ in the expression (2.11), it is easily seen that for any h ,

$$F_h(\boldsymbol{\omega}) = (2\pi)^{-d} \text{diag}(\underline{\lambda}) + (\underline{\lambda} \underline{\lambda}^\top) \odot \mathcal{F}^{-1}(L_2)(\boldsymbol{\omega}), \quad \boldsymbol{\omega} \in \mathbb{R}^d.$$

Therefore, F_h is equivalent to the spectrum of the SOS process, proving (i).

To show (ii), we use the integral representation of $F_h(\boldsymbol{\omega})$ as in Theorem 3.2. Since the local spectrum $F^u(\cdot)$ is conjugate symmetric and positive definite, so is F_h .

Lastly, (iii) follows immediately from the fact that $L_2(\boldsymbol{x})$ is a zero matrix for an inhomogeneous Poisson process. \square

Now, we derive the asymptotic behavior of the periodograms, a raw estimator of the pseudo-spectrum. To establish the asymptotic property, we introduce the α -mixing coefficient of \underline{X} .

For compact and convex subsets $E_i, E_j \subset \mathbb{R}^d$, let $d(E_i, E_j) = \inf_{\boldsymbol{x}_i \in E_i, \boldsymbol{x}_j \in E_j} \|\boldsymbol{x}_i - \boldsymbol{x}_j\|_\infty$. Then, the α -mixing coefficient of \underline{X} is defined as

$$\alpha_p(k) = \sup_{A_i, A_j, E_i, E_j} \left\{ |P(A_i \cap A_j) - P(A_i)P(A_j)| : \right. \\ \left. A_i \in \mathcal{F}(E_i), A_j \in \mathcal{F}(E_j), |E_i| = |E_j| \leq p, d(E_i, E_j) \geq k \right\}.$$

Here, $\mathcal{F}(E)$ denotes the σ -field generated by the superposition of \underline{X} in $E \subset \mathbb{R}^d$, and the supremum is taken over all compact and convex subsets E_i and E_j . Using this notion, we show the central limit theorem for the DFTs and periodograms.

Theorem B.1. *Suppose that Assumptions 4.1, 4.2(i), 4.3, 4.4(for $k = 2$), and 4.5 hold. Moreover, there exists $\varepsilon > 0$ such that*

$$\sup_{p \in (0, \infty)} \alpha_p(k) / \max(p, 1) = O(k^{-d-\varepsilon}), \quad k \rightarrow \infty.$$

For fixed $r \in \mathbb{N}$, let $\{\boldsymbol{\omega}_{1,n}\}, \dots, \{\boldsymbol{\omega}_{r,n}\}$ be r sequences of frequencies that satisfy (i) $\lim_{n \rightarrow \infty} \boldsymbol{\omega}_{i,n} = \boldsymbol{\omega}_i \in \mathbb{R}^d$; (ii) $\{\boldsymbol{\omega}_{i,n}\}$ is asymptotically distant from $\{\mathbf{0}\}$; and (iii) $\{\boldsymbol{\omega}_{i,n} + \boldsymbol{\omega}_{j,n}\}$ and $\{\boldsymbol{\omega}_{i,n} - \boldsymbol{\omega}_{j,n}\}$ are asymptotically distant from $\{\mathbf{0}\}$ for $i \neq j$. Then, we have

$$(\widehat{\underline{J}}_{h,n}(\boldsymbol{\omega}_{1,n}), \dots, \widehat{\underline{J}}_{h,n}(\boldsymbol{\omega}_{r,n})) \xrightarrow{\mathcal{D}} (Z_1^c, \dots, Z_r^c),$$

where Z_1^c, \dots, Z_r^c are independent m -variate complex normal random variables with mean zero and variance matrices $F_h(\boldsymbol{\omega}_1), \dots, F_h(\boldsymbol{\omega}_r)$.

If we further assume Assumption 4.4 for $k = 4$, then,

$$(\widehat{\underline{I}}_{h,n}(\boldsymbol{\omega}_{1,n}), \dots, \widehat{\underline{I}}_{h,n}(\boldsymbol{\omega}_{r,n})) \xrightarrow{\mathcal{D}} (W_1^c, \dots, W_r^c),$$

where W_1^c, \dots, W_r^c are independent m -variate complex Wishart random variables with one degree of freedom and variance matrices $F_h(\boldsymbol{\omega}_1), \dots, F_h(\boldsymbol{\omega}_r)$ (see Brillinger (1981), Section 4.2, for the details on the complex normal and complex Wishart distributions).

Proof. Let $\Re \underline{J}_{h,n}(\boldsymbol{\omega})$ and $\Im \underline{J}_{h,n}(\boldsymbol{\omega})$ be the real and imaginary parts of $\underline{J}_{h,n} = (J_{h,n}^{(1)}(\cdot), \dots, J_{h,n}^{(m)}(\cdot))^\top$,

respectively. Then, due to Theorem E.1 below, it is enough to show

$$\begin{aligned} & (\Re \underline{J}_{h,n}(\boldsymbol{\omega}_{1,n})^\top, \Im \underline{J}_{h,n}(\boldsymbol{\omega}_{1,n})^\top, \dots, \Im \underline{J}_{h,n}(\boldsymbol{\omega}_{r,n})^\top)^\top \xrightarrow{\mathcal{D}} \left(\{(F_h(\boldsymbol{\omega}_1)/2)^{1/2} Z_1\}^\top, \right. \\ & \left. \{(F_h(\boldsymbol{\omega}_1)/2)^{1/2} Z_2\}^\top, \dots, \{(F_h(\boldsymbol{\omega}_r)/2)^{1/2} Z_{2r-1}\}^\top, \{(F_h(\boldsymbol{\omega}_r)/2)^{1/2} Z_{2r}\}^\top \right)^\top, \quad n \rightarrow \infty, \end{aligned}$$

where $\{Z_j : j = 1, \dots, 2r\}$ are i.i.d. standard normal random variables on \mathbb{R}^m , and for a positive definite matrix A , $A^{1/2}$ denotes the (unique) positive square root of A . Showing the above is almost identical to that of the proof of Yang and Guan (2024) (YG24, hereafter), Theorem 3.2 (see, Appendix B.2 of the same reference), so we omit the details. \square

C Proof of the main results

C.1 Proof of Theorem 3.1

From 2.1(i), there exists an SOS process $\tilde{\underline{X}}$ on \mathbb{R}^d where the first-order intensity function and covariance intensity function of $\tilde{\underline{X}}$ are $(1, \dots, 1)^\top$ and $L_2(\cdot)$, respectively. Let $\mathbf{u} \in [-1/2, 1/2]^d$ be fixed, and let $\underline{X}^{\mathbf{u}}$ be the weighted process of $\tilde{\underline{X}}$ with respect to the constant weight $\underline{\lambda}(\mathbf{u}) = (\lambda^{(1)}(\mathbf{u}), \dots, \lambda^{(m)}(\mathbf{u}))^\top$, which is defined as in Definition A.1. Then, it is easily seen that $\underline{X}^{\mathbf{u}}$ is also an SOS process with the first-order intensity $\underline{\lambda}(\mathbf{u})$ and reduced covariance $(\underline{\lambda}(\mathbf{u})\underline{\lambda}(\mathbf{u})^\top) \odot L_2(\cdot)$. Therefore, the complete covariance intensity of $\underline{X}^{\mathbf{u}}$ is $C^{\mathbf{u}}$, and in turn, the spectrum of $\underline{X}^{\mathbf{u}}$ is $F^{\mathbf{u}}(\boldsymbol{\omega})$ as in (3.2). This proves the theorem. \square

C.2 Proof of Theorem 3.2

To show the identity, we first substitute (3.2) into the right-hand side. Then, the first integral term is

$$\frac{(2\pi)^{-d}}{H_{h,2}} \int_{[-1/2, 1/2]^d} \text{diag}(h(\mathbf{u})^2 \lambda^{(1)}(\mathbf{u}), \dots, h(\mathbf{u})^2 \lambda^{(m)}(\mathbf{u})) d\mathbf{u} = \frac{(2\pi)^{-d}}{H_{h,2}} \text{diag}(H_{h^2 \underline{\lambda}}).$$

The (i, j) th $(i, j \in \{1, \dots, m\})$ element of the second integral is

$$\frac{1}{H_{h,2}} \mathcal{F}^{-1}(\ell_2^{(i,j)})(\boldsymbol{\omega}) \int_{[-1/2, 1/2]^d} h(\mathbf{u})^2 \lambda^{(i)}(\mathbf{u}) \lambda^{(j)}(\mathbf{u}) d\mathbf{u} = \frac{1}{H_{h,2}} \mathcal{F}^{-1}(\ell_2^{(i,j)})(\boldsymbol{\omega}) H_{h^2 \lambda^{(i)} \lambda^{(j)}, 1}.$$

Therefore, the second integral term is $H_{h,2}^{-1} (H_{h^2 \underline{\lambda}} \odot \mathcal{F}^{-1}(L_2)(\boldsymbol{\omega}))$. Comparing these expressions with (2.11), we get the desired result. \square

C.3 Proof of Theorem 4.1

To prove the theorem, we require the following representation of the covariance of the DFT. Recall $H_{h,k}^{(n)}$ in (4.1). For two functions h and g with support $[-1/2, 1/2]^d$, let

$$R_{h,g}^{(n)}(\mathbf{u}, \boldsymbol{\omega}) = \int_{\mathbb{R}^d} h\left(\frac{\mathbf{x}}{\mathbf{A}}\right) \left\{ g\left(\frac{\mathbf{x} + \mathbf{u}}{\mathbf{A}}\right) - g\left(\frac{\mathbf{x}}{\mathbf{A}}\right) \right\} \exp(-i\mathbf{x}^\top \boldsymbol{\omega}) d\mathbf{x}, \quad \mathbf{u}, \boldsymbol{\omega} \in \mathbb{R}^d.$$

In the lemma below, we provide an expression for $\text{cov}(\underline{J}_{h,n}(\boldsymbol{\omega}_1), \underline{J}_{h,n}(\boldsymbol{\omega}_2))$ using $H_{h,k}^{(n)}(\cdot)$ and $R_{h,g}^{(n)}(\cdot, \cdot)$.

Lemma C.1. *Let \underline{X}_{D_n} ($n \in \mathbb{N}$) be a sequence of m -variate point processes that satisfies Assumptions 2.1 and 4.4 (for $k = 2$). Furthermore, we assume h and the first-order intensities $\lambda^{(i)}$ are bounded on $[-1/2, 1/2]^d$. Then, for $i, j \in \{1, \dots, m\}$ and $\boldsymbol{\omega}_1, \boldsymbol{\omega}_2 \in \mathbb{R}^d$,*

$$\begin{aligned} \text{cov}(J_{h,n}^{(i)}(\boldsymbol{\omega}_1), J_{h,n}^{(j)}(\boldsymbol{\omega}_2)) &= (2\pi)^{-d} H_{h,2}^{-1} |D_n|^{-1} \left(\delta_{i,j} \cdot H_{h^2\lambda^{(i)},1}^{(n)}(\boldsymbol{\omega}_1 - \boldsymbol{\omega}_2) \right. \\ &\quad + H_{h^2\lambda^{(i)}\lambda^{(j)},1}^{(n)}(\boldsymbol{\omega}_1 - \boldsymbol{\omega}_2) \int_{\mathbb{R}^d} e^{-i\mathbf{u}^\top \boldsymbol{\omega}_1} \ell_2^{(i,j)}(\mathbf{u}) d\mathbf{u} \\ &\quad \left. + \int_{\mathbb{R}^d} e^{-i\mathbf{u}^\top \boldsymbol{\omega}_1} \ell_2^{(i,j)}(\mathbf{u}) R_{h\lambda^{(j)},h\lambda^{(i)}}^{(n)}(\mathbf{u}, \boldsymbol{\omega}_1 - \boldsymbol{\omega}_2) d\mathbf{u} \right), \end{aligned} \quad (\text{C.1})$$

where $\delta_{i,j} = 1$ if $i = j$ and zero otherwise.

Proof. By using (A.1) and applying similar techniques as in YG24, Theorem D.1, we have

$$\begin{aligned} \text{cov}(J_{h,n}^{(i)}(\boldsymbol{\omega}_1), J_{h,n}^{(j)}(\boldsymbol{\omega}_2)) &= (2\pi)^{-d} H_{h,2}^{-1} |D_n|^{-1} \left(\delta_{i,j} \int_{D_n} (h^2\lambda^{(i)})(\mathbf{x}/\mathbf{A}) e^{-i\mathbf{x}^\top (\boldsymbol{\omega}_1 - \boldsymbol{\omega}_2)} d\mathbf{x} \right. \\ &\quad \left. + \int_{D_n^2} (h\lambda^{(i)})(\mathbf{x}/\mathbf{A}) (h\lambda^{(j)})(\mathbf{y}/\mathbf{A}) \ell_2^{(i,j)}(\mathbf{x} - \mathbf{y}) e^{-i(\mathbf{x}^\top \boldsymbol{\omega}_1 - \mathbf{y}^\top \boldsymbol{\omega}_2)} d\mathbf{x} d\mathbf{y} \right). \end{aligned} \quad (\text{C.2})$$

The first term in the parentheses above is $\delta_{i,j} H_{h^2\lambda^{(i)},1}^{(n)}(\boldsymbol{\omega}_1 - \boldsymbol{\omega}_2)$. Observe that $(h\lambda^{(i)})(\mathbf{x}/\mathbf{A}) = 0$ on $\mathbf{x} \notin D_n$, and the second term can be written as an integral on \mathbb{R}^{2d} . Therefore, by performing a change of variables $(\mathbf{u}, \mathbf{v}) = (\mathbf{x} - \mathbf{y}, \mathbf{y})$ and using similar techniques as in YG24, Lemma D.1, the second term above equals

$$(2\pi)^{-d} H_{h,2}^{-1} |D_n|^{-1} \int_{\mathbb{R}^d} d\mathbf{u} e^{-i\mathbf{u}^\top \boldsymbol{\omega}_1} \ell_2^{(i,j)}(\mathbf{u}) \left(H_{h^2\lambda^{(i)}\lambda^{(j)},1}^{(n)}(\boldsymbol{\omega}_1 - \boldsymbol{\omega}_2) + R_{h\lambda^{(j)},h\lambda^{(i)}}^{(n)}(\mathbf{u}, \boldsymbol{\omega}_1 - \boldsymbol{\omega}_2) \right).$$

Substitute the above into (C.2), we get the desired result. \square

Now we are ready to prove Theorem 4.1.

Proof of Theorem 4.1. Let $\underline{J}_{h,n}(\cdot)$ and $I_{h,n}(\cdot)$ be the theoretical DFT and periodogram, respectively, defined as in (4.3). Then, thanks to Theorem E.2 below, it is enough to prove the statements for $\underline{J}_{h,n}(\cdot)$ and $I_{h,n}(\cdot)$ replacing $\widehat{\underline{J}}_{h,n}(\cdot)$ and $\widehat{I}_{h,n}(\cdot)$, respectively.

We first show (4.4) and (4.5). By using a similar argument as in YG24, Theorem D.2 (see also, Theorem C.1 of the same reference),

$$\lim_{n \rightarrow \infty} \sup_{\boldsymbol{\omega}_1, \boldsymbol{\omega}_2 \in \mathbb{R}^d} (2\pi)^{-d} H_{h,2}^{-1} |D_n|^{-1} \int_{\mathbb{R}^d} |\ell_2^{(i,j)}(\mathbf{u})| |R_{h\lambda^{(j)}, h\lambda^{(i)}}^{(n)}(\mathbf{u}, \boldsymbol{\omega}_1 - \boldsymbol{\omega}_2)| d\mathbf{u} = 0. \quad (\text{C.3})$$

Therefore, substitute (C.3) into (C.1), we have

$$\begin{aligned} \text{cov}(J_{h,n}^{(i)}(\boldsymbol{\omega}_1), J_{h,n}^{(j)}(\boldsymbol{\omega}_2)) &= (2\pi)^{-d} H_{h,2}^{-1} |D_n|^{-1} \left(\delta_{i,j} H_{h^2\lambda^{(i)},1}^{(n)}(\boldsymbol{\omega}_1 - \boldsymbol{\omega}_2) \right. \\ &\quad \left. + H_{h^2\lambda^{(i)}\lambda^{(j)},1}^{(n)}(\boldsymbol{\omega}_1 - \boldsymbol{\omega}_2) \int_{\mathbb{R}^d} e^{-i\mathbf{u}^\top \boldsymbol{\omega}_1} \ell_2^{(i,j)}(\mathbf{u}) d\mathbf{u} \right) + o(1), \quad n \rightarrow \infty, \end{aligned} \quad (\text{C.4})$$

where the $o(1)$ bound above is uniform over $\boldsymbol{\omega}_1, \boldsymbol{\omega}_2 \in \mathbb{R}^d$.

Next, by using YG24, Lemma C.2,

$$\lim_{n \rightarrow \infty} |D_n|^{-1} |H_{h^2\lambda^{(i)},1}^{(n)}(\boldsymbol{\omega}_{1,n} - \boldsymbol{\omega}_{2,n})| = 0. \quad (\text{C.5})$$

The same argument holds when replacing $h^2\lambda^{(i)}$ with $h^2\lambda^{(i)}\lambda^{(j)}$ above. Therefore, since $\ell_2^{(i,j)} \in L_1(\mathbb{R}^d)$ due to Assumption 4.4 ($k = 2$), substitute (C.5) into (C.4), we show (4.4).

To show (4.5), by using (C.4), we have

$$\begin{aligned} \text{cov}(J_{h,n}^{(i)}(\boldsymbol{\omega}_{1,n}), J_{h,n}^{(j)}(\boldsymbol{\omega}_{1,n})) &= (2\pi)^{-d} H_{h,2}^{-1} |D_n|^{-1} \left(\delta_{i,j} H_{h^2\lambda^{(i)},1}^{(n)}(\mathbf{0}) + H_{h^2\lambda^{(i)}\lambda^{(j)},1}^{(n)}(\mathbf{0}) \int_{\mathbb{R}^d} e^{-i\mathbf{u}^\top \boldsymbol{\omega}_{1,n}} \ell_2^{(i,j)}(\mathbf{u}) d\mathbf{u} \right) + o(1) \\ &= (2\pi)^{-d} H_{h,2}^{-1} H_{h^2\lambda^{(i)},1} \delta_{i,j} + H_{h,2}^{-1} \mathcal{F}^{-1}(\ell^{(i,j)})(\boldsymbol{\omega}_{1,n}) + o(1) \\ &= (2\pi)^{-d} H_{h,2}^{-1} H_{h^2\lambda^{(i)},1} \delta_{i,j} + H_{h,2}^{-1} \mathcal{F}^{-1}(\ell^{(i,j)})(\boldsymbol{\omega}) + o(1), \quad n \rightarrow \infty, \end{aligned} \quad (\text{C.6})$$

where the $o(1)$ bound above is uniform over $\boldsymbol{\omega}_{1,n}$. Here, the last inequality is due to the (uniform) continuity of $\mathcal{F}^{-1}(\ell^{(i,j)})(\cdot)$, provided Assumption 4.4 (for $k = 2$). Therefore, in a matrix form, we have

$$\begin{aligned} \lim_{n \rightarrow \infty} \text{var}(\underline{J}_{h,n}(\boldsymbol{\omega}_{1,n})) &= (2\pi)^{-d} H_{h,2}^{-1} \text{diag}(H_{h^2\lambda}) + H_{h,2}^{-1} (H_{h^2\lambda, \lambda} \odot \mathcal{F}^{-1}(L_2)(\boldsymbol{\omega})) = F_h(\boldsymbol{\omega}). \end{aligned} \quad (\text{C.7})$$

This proves (4.5).

Now, we will show (4.6) and (4.7). By using cumulant decomposition, for $i_1, j_1, i_2, j_2 \in$

$\{1, \dots, m\}$, we have

$$\begin{aligned}
& \text{cov}(I_{h,n}^{(i_1,j_1)}(\boldsymbol{\omega}_1), I_{h,n}^{(i_2,j_2)}(\boldsymbol{\omega}_2)) \\
&= \text{cum}(J_{h,n}^{(i_1)}(\boldsymbol{\omega}_1), J_{h,n}^{(i_2)}(-\boldsymbol{\omega}_2)) \text{cum}(J_{h,n}^{(j_1)}(-\boldsymbol{\omega}_1), J_{h,n}^{(j_2)}(\boldsymbol{\omega}_2)) \\
&\quad + \text{cum}(J_{h,n}^{(i_1)}(\boldsymbol{\omega}_1), J_{h,n}^{(j_2)}(\boldsymbol{\omega}_2)) \text{cum}(J_{h,n}^{(j_1)}(-\boldsymbol{\omega}_1), J_{h,n}^{(i_2)}(-\boldsymbol{\omega}_2)) \\
&\quad + \text{cum}(J_{h,n}^{(i_1)}(\boldsymbol{\omega}_1), J_{h,n}^{(j_1)}(-\boldsymbol{\omega}_1), J_{h,n}^{(i_2)}(-\boldsymbol{\omega}_2), J_{h,n}^{(j_2)}(\boldsymbol{\omega}_2)) \\
&= \text{cum}(J_{h,n}^{(i_1)}(\boldsymbol{\omega}_1), J_{h,n}^{(i_2)}(-\boldsymbol{\omega}_2)) \text{cum}(J_{h,n}^{(j_1)}(-\boldsymbol{\omega}_1), J_{h,n}^{(j_2)}(\boldsymbol{\omega}_2)) \\
&\quad + \text{cum}(J_{h,n}^{(i_1)}(\boldsymbol{\omega}_1), J_{h,n}^{(j_2)}(\boldsymbol{\omega}_2)) \text{cum}(J_{h,n}^{(j_1)}(-\boldsymbol{\omega}_1), J_{h,n}^{(i_2)}(-\boldsymbol{\omega}_2)) + O(|D_n|^{-1}) \\
&=: S_1 + S_2 + O(|D_n|^{-1}), \quad n \rightarrow \infty,
\end{aligned} \tag{C.8}$$

where the $O(|D_n|^{-1})$ bound above is uniform over $\boldsymbol{\omega}_1, \boldsymbol{\omega}_2 \in \mathbb{R}^d$. Here, the last identity is due to YG24, Lemma D.5.

To show (4.6), since $\{\boldsymbol{\omega}_{1,n}\}$ is asymptotically distant from $\{\boldsymbol{\omega}_{2,n}\}$ and $\{-\boldsymbol{\omega}_{2,n}\}$, by Theorem 4.1, $S_1 = S_1(\boldsymbol{\omega}_{1,n}, \boldsymbol{\omega}_{2,n})$ and $S_2 = S_2(\boldsymbol{\omega}_{1,n}, \boldsymbol{\omega}_{2,n})$ are both $o(1)$ as $n \rightarrow \infty$. This shows (4.6).

To show (4.7), from (C.8), we have

$$\begin{aligned}
& \text{cov}(I_{h,n}^{(i_1,j_1)}(\boldsymbol{\omega}_{1,n}), I_{h,n}^{(i_2,j_2)}(\boldsymbol{\omega}_{1,n})) \\
&= \text{cum}(J_{h,n}^{(i_1)}(\boldsymbol{\omega}_{1,n}), J_{h,n}^{(i_2)}(-\boldsymbol{\omega}_{1,n})) \text{cum}(J_{h,n}^{(j_1)}(-\boldsymbol{\omega}_{1,n}), J_{h,n}^{(j_2)}(\boldsymbol{\omega}_{1,n})) \\
&\quad + \text{cum}(J_{h,n}^{(i_1)}(\boldsymbol{\omega}_{1,n}), J_{h,n}^{(j_2)}(\boldsymbol{\omega}_{1,n})) \text{cum}(J_{h,n}^{(j_1)}(-\boldsymbol{\omega}_{1,n}), J_{h,n}^{(i_2)}(-\boldsymbol{\omega}_{1,n})) + o(1), \quad n \rightarrow \infty.
\end{aligned}$$

Since $\{\boldsymbol{\omega}_{1,n}\}$ is asymptotically distant from $\{\mathbf{0}\}$, by using Theorem 4.1 again, we have

$$\text{cov}(I_{h,n}^{(i_1,j_1)}(\boldsymbol{\omega}_{1,n}), I_{h,n}^{(i_2,j_2)}(\boldsymbol{\omega}_{1,n})) = F_h^{(i_1,i_2)}(\boldsymbol{\omega}) F_h^{(j_1,j_2)}(-\boldsymbol{\omega}) + o(1), \quad n \rightarrow \infty.$$

This shows (4.7). All together, we get the desired results. \square

C.4 Proof of Theorem 5.1

Let

$$F_{n,\mathbf{b}}(\boldsymbol{\omega}) = \int_{\mathbb{R}^d} K_{\mathbf{b}}(\boldsymbol{\omega} - \mathbf{x}) I_{h,n}(\mathbf{x}) d\mathbf{x}, \quad \boldsymbol{\omega} \in \mathbb{R}^d, \tag{C.9}$$

be the theoretical counterpart of $\widehat{F}_{n,\mathbf{b}}$, where $I_{h,n}(\cdot)$ is the theoretical periodogram as in (4.3).

The following theorem, which is key to proving Theorem 5.1, addresses the MSE convergence of $F_{n,\mathbf{b}}(\boldsymbol{\omega})$.

Theorem C.1. *Suppose that Assumptions 4.1, 4.2(i), 4.3, 4.4 (for $k = 4$), and 4.5 hold. Moreover, the bandwidth $\mathbf{b} = \mathbf{b}(n)$ satisfies condition (B). Then, for $\boldsymbol{\omega} \in \mathbb{R}^d$,*

$$\lim_{n \rightarrow \infty} \mathbb{E} |F_{n,\mathbf{b}}(\boldsymbol{\omega}) - F_h(\boldsymbol{\omega})|^2 = 0.$$

Proof. To show the result, we calculate the bias and variance of $F_{n,\mathbf{b}}(\boldsymbol{\omega})$ separately.

First, we compute the bias. By using the triangle inequality, we have

$$\begin{aligned}
& |\mathbb{E}[F_{n,\mathbf{b}}(\boldsymbol{\omega})] - F_h(\boldsymbol{\omega})| \\
& \leq \left| \int_{\mathbb{R}^d} K_{\mathbf{b}}(\boldsymbol{\omega} - \mathbf{x}) F_h(\mathbf{x}) d\mathbf{x} - F_h(\boldsymbol{\omega}) \right| + \left| \mathbb{E}[F_{n,\mathbf{b}}(\boldsymbol{\omega})] - \int_{\mathbb{R}^d} K_{\mathbf{b}}(\boldsymbol{\omega} - \mathbf{x}) F_h(\mathbf{x}) d\mathbf{x} \right| \\
& = \left| \int_{\mathbb{R}^d} K_{\mathbf{b}}(\mathbf{x}) \{F_h(\boldsymbol{\omega} - \mathbf{x}) - F_h(\boldsymbol{\omega})\} d\mathbf{x} \right| + \int_{\mathbb{R}^d} K_{\mathbf{b}}(\boldsymbol{\omega} - \mathbf{x}) |\mathbb{E}[I_{h,n}(\mathbf{x})] - F_h(\mathbf{x})| d\mathbf{x} \\
& = A_1 + A_2.
\end{aligned} \tag{C.10}$$

We first bound A_1 . Since $F_h(\cdot)$ is uniformly continuous due to Assumption 4.4 (for $k = 2$), given $\varepsilon > 0$, there exists $\delta > 0$ such that

$$\sup_{\|\mathbf{x} - \mathbf{y}\| < \delta} |F_h(\mathbf{x}) - F_h(\mathbf{y})| < \varepsilon.$$

Next, we note the support of $K_{\mathbf{b}}$ is $[-b_1, b_1] \times \cdots \times [-b_d, b_d]$, which shrinks in all coordinates as $n \rightarrow \infty$. Therefore, for large enough $n \in \mathbb{N}$, we have $\text{supp}(K_{\mathbf{b}}) \subset B(\mathbf{0}; \delta)$, where $B(\mathbf{0}; \delta)$ is the centered ball in \mathbb{R}^d with radius δ . Combining these two facts, for large enough $n \in \mathbb{N}$, we have

$$A_1 \leq \int_{B(\mathbf{0}; \delta)} K_{\mathbf{b}}(\mathbf{x}) |F_h(\boldsymbol{\omega} - \mathbf{x}) - F_h(\boldsymbol{\omega})| d\mathbf{x} \leq \varepsilon \cdot \sup_{\mathbf{x}} K(\mathbf{x}).$$

Since $\varepsilon > 0$ is chosen arbitrarily, we conclude that

$$\lim_{n \rightarrow \infty} A_1 = 0. \tag{C.11}$$

To bound A_2 , we observe that $\lim_{n \rightarrow \infty} \sup_{\boldsymbol{\omega} \in \mathbb{R}^d} |\mathbb{E}[I_{h,n}(\boldsymbol{\omega})] - F_h(\boldsymbol{\omega})| = 0$ due to (C.6). Therefore, we have

$$A_2 \leq o(1) \int_{\mathbb{R}^d} K_{\mathbf{b}}(\boldsymbol{\omega} - \mathbf{x}) d\mathbf{x} = o(1), \quad n \rightarrow \infty. \tag{C.12}$$

Substituting (C.11) and (C.12) into (C.10), we obtain

$$|\mathbb{E}[F_{n,\mathbf{b}}(\boldsymbol{\omega})] - F_h(\boldsymbol{\omega})| = o(1), \quad n \rightarrow \infty. \tag{C.13}$$

Next, we bound the variance. Let $i, j \in \{1, \dots, m\}$ be fixed. Then,

$$\text{var}(F_{n,\mathbf{b}}^{(i,j)}(\boldsymbol{\omega})) = \int_{\mathbb{R}^d} d\mathbf{y} K_{\mathbf{b}}(\boldsymbol{\omega} - \mathbf{y}) \int_{\mathbb{R}^d} d\mathbf{x} K_{\mathbf{b}}(\boldsymbol{\omega} - \mathbf{x}) \text{cov}(I_{h,n}^{(i,j)}(\mathbf{x}), I_{h,n}^{(i,j)}(\mathbf{y})). \tag{C.14}$$

First, we note that under condition (B), we can choose $r = r(n) \in (0, \infty)$ such that, as $n \rightarrow \infty$,

$$r \rightarrow 0, \quad |D_n| r^d \rightarrow \infty, \quad \text{and} \quad \max_j (r/b_j) \rightarrow 0.$$

For $\mathbf{x} \in \mathbb{R}^d$ and $r \in (0, \infty)$, let $B_\infty(\mathbf{x}; r) = \{\mathbf{y} : \|\mathbf{x} - \mathbf{y}\|_\infty \leq r\}$. For $\mathbf{y} \neq \mathbf{0}$ and sufficiently large $n \in \mathbb{N}$, we can partition \mathbb{R}^d into $B_\infty(\mathbf{y}; r)$, $B_\infty(-\mathbf{y}; r)$, and the remaining set, which we denote by $C(\mathbf{y}; r)$. For $\mathbf{y} = \mathbf{0}$, \mathbb{R}^d can be partitioned into $B_\infty(\mathbf{0}; r)$ and the remaining set $C(\mathbf{0}; r)$.

Now, we bound the integral involving $C(\mathbf{y}; r)$. If $\mathbf{x} \in C(\mathbf{y}; r)$, then

$$|D_n|^{1/d} \|\mathbf{x} - \mathbf{y}\|_\infty > |D_n|^{1/d} r \rightarrow \infty.$$

Therefore, by using (C.4), (C.5), and (C.8), it can be easily seen that

$$\sup_{\mathbf{y} \in \mathbb{R}^d} \sup_{\mathbf{x} \in C(\mathbf{y}; r)} |\text{cov}(I_{h,n}^{(i,j)}(\mathbf{x}), I_{h,n}^{(i,j)}(\mathbf{y}))| = o(1), \quad n \rightarrow \infty.$$

Therefore,

$$\begin{aligned} & \int_{\mathbb{R}^d} d\mathbf{y} K_{\mathbf{b}}(\boldsymbol{\omega} - \mathbf{y}) \int_{C(\mathbf{y}; r)} d\mathbf{x} K_{\mathbf{b}}(\boldsymbol{\omega} - \mathbf{x}) |\text{cov}(I_{h,n}^{(i,j)}(\mathbf{x}), I_{h,n}^{(i,j)}(\mathbf{y}))| \\ & \leq o(1) \left(\int_{\mathbb{R}^d} d\mathbf{y} K_{\mathbf{b}}(\boldsymbol{\omega} - \mathbf{y}) \right)^2 = o(1), \quad n \rightarrow \infty. \end{aligned} \quad (\text{C.15})$$

Next, to bound the integral involving $B_\infty(\mathbf{y}; r)$, we observe that if $\mathbf{x} \in B_\infty(\mathbf{y}; r)$, then

$$\|(\mathbf{x} - \mathbf{y})/\mathbf{b}\|_\infty \leq \max_j r/b_j \rightarrow 0.$$

Therefore, since $K(\cdot)$ is Lipschitz continuous on \mathbb{R}^d , for an arbitrary $\varepsilon \in (0, \infty)$, there exists $N = N(\varepsilon) \in \mathbb{N}$ such that if $n > N$, then

$$\sup_{\boldsymbol{\omega}, \mathbf{y} \in \mathbb{R}^d} \sup_{\mathbf{x} \in B_\infty(\mathbf{y}; r)} |K_{\mathbf{b}}(\boldsymbol{\omega} - \mathbf{x}) - K_{\mathbf{b}}(\boldsymbol{\omega} - \mathbf{y})| \leq \varepsilon (b_1 \cdots b_d)^{-1}.$$

Moreover, by using the Cauchy-Schwarz inequality and YG24, Lemma D.5, we have

$$\sup_{\mathbf{x}, \mathbf{y} \in \mathbb{R}^d} |\text{cov}(I_{h,n}^{(i,j)}(\mathbf{x}), I_{h,n}^{(i,j)}(\mathbf{y}))| \leq \sup_{\mathbf{x} \in \mathbb{R}^d} \text{var}(I_{h,n}^{(i,j)}(\mathbf{x})) = O(1), \quad n \rightarrow \infty.$$

Therefore, combining the above two inequalities, we obtain

$$\begin{aligned} & \int_{\mathbb{R}^d} d\mathbf{y} K_{\mathbf{b}}(\boldsymbol{\omega} - \mathbf{y}) \int_{B_\infty(\mathbf{y}; r)} d\mathbf{x} K_{\mathbf{b}}(\boldsymbol{\omega} - \mathbf{x}) |\text{cov}(I_{h,n}(\mathbf{x}), I_{h,n}(\mathbf{y}))| \\ & \leq O(1) \int_{\mathbb{R}^d} d\mathbf{y} K_{\mathbf{b}}(\boldsymbol{\omega} - \mathbf{y}) \int_{B_\infty(\mathbf{y}; r)} d\mathbf{x} K_{\mathbf{b}}(\boldsymbol{\omega} - \mathbf{x}) \\ & \leq O(1) \int_{\mathbb{R}^d} d\mathbf{y} K_{\mathbf{b}}(\boldsymbol{\omega} - \mathbf{y})^2 \int_{B_\infty(\mathbf{y}; r)} d\mathbf{x} + O(1) \varepsilon (b_1 \cdots b_d)^{-1} \int_{\mathbb{R}^d} d\mathbf{y} K_{\mathbf{b}}(\boldsymbol{\omega} - \mathbf{y}) \int_{B_\infty(\mathbf{y}; r)} d\mathbf{x} \quad (\text{C.16}) \\ & \leq O(1) r^d \int_{\mathbb{R}^d} d\mathbf{y} K_{\mathbf{b}}(\boldsymbol{\omega} - \mathbf{y})^2 + O(1) \varepsilon (b_1 \cdots b_d)^{-1} r^d \int_{\mathbb{R}^d} d\mathbf{y} K_{\mathbf{b}}(\boldsymbol{\omega} - \mathbf{y}) \\ & = O(r^d (b_1 \cdots b_d)^{-1}) + O(\varepsilon r^d (b_1 \cdots b_d)^{-1}) = o(1), \quad n \rightarrow \infty. \end{aligned}$$

Here, we use $\int_{B_\infty(\mathbf{y};r)} d\mathbf{x} = |B_\infty(\mathbf{y};r)| = O(r^d)$ in the third inequality.

Lastly, using similar techniques, we can show that

$$\int_{\mathbb{R}^d} d\mathbf{y} K_b(\boldsymbol{\omega} - \mathbf{y}) \int_{B_\infty(-\mathbf{y};r)} d\mathbf{x} K_b(\boldsymbol{\omega} - \mathbf{x}) |\text{cov}(I_{h,n}(\mathbf{x}), I_{h,n}(\mathbf{y}))| = o(1), \quad n \rightarrow \infty. \quad (\text{C.17})$$

Substituting (C.15)–(C.17) into (C.14) and using the triangle inequality, we conclude that for $i, j \in \{1, \dots, m\}$,

$$\lim_{n \rightarrow \infty} \text{var}(F_{n,\mathbf{b}}^{(i,j)}(\boldsymbol{\omega})) = 0.$$

Summing the above over i, j , together with (C.13), we get the desired result. \square

Now, we are ready to prove Theorem 5.1.

Proof of Theorem 5.1. We first show (5.2). By applying Markov's inequality to Theorem C.1, we obtain $F_{n,\mathbf{b}}(\boldsymbol{\omega}) - F_h(\boldsymbol{\omega}) = o_p(1)$ as $n \rightarrow \infty$. Furthermore, Theorem E.3 below states that $\widehat{F}_{n,\mathbf{b}}(\boldsymbol{\omega}) - F_{n,\mathbf{b}}(\boldsymbol{\omega}) = o_p(1)$. Therefore, combining these two results with the triangle inequality, we show (5.2).

Next, the L_2 -convergence result in (5.3) follows immediately from Theorems C.1 and E.4 below.

Altogether, we get the desired results. \square

D Convergence rate of the MSE of $\widehat{F}_{n,\mathbf{b}}(\boldsymbol{\omega})$

In some situations, it is necessary to quantify the rate at which $\widehat{F}_{n,\mathbf{b}}(\boldsymbol{\omega})$ converges to $F_h(\boldsymbol{\omega})$. For example, the MSE convergence rate of $\widehat{F}_{n,\mathbf{b}}(\boldsymbol{\omega})$ is used to determine the optimal bandwidth in Section 6.1. However, since $\widehat{F}_{n,\mathbf{b}}$ involves estimating the parametric form of the first-order intensity, directly computing its moments is infeasible. Instead, we compute the moments of its theoretical counterpart, denoted as $F_{n,\mathbf{b}}(\boldsymbol{\omega})$ in (C.9).

The theorem below addresses the asymptotic order of the bias and variance of $F_{n,\mathbf{b}}(\boldsymbol{\omega})$.

Theorem D.1. *Suppose that Assumptions 4.1, 4.3, 4.4 (for $k = 4$), 4.5, and 6.1 hold. Moreover, assume that the data taper h is Lipschitz continuous on $[-1/2, 1/2]^d$, the side lengths $\mathbf{A}(n)$ satisfy condition (SL), and the bandwidth $\mathbf{b} = \mathbf{b}(n)$ satisfies condition (B). Then, the following two assertions hold:*

$$(i) \sup_{\boldsymbol{\omega} \in \mathbb{R}^d} |\mathbb{E}[F_{n,\mathbf{b}}(\boldsymbol{\omega})] - F_h(\boldsymbol{\omega})| = O(\|\mathbf{b}\|^2 + |D_n|^{-1/d}), \text{ as } n \rightarrow \infty.$$

$$(ii) \sup_{\boldsymbol{\omega} \in \mathbb{R}^d} \text{var}(F_{n,\mathbf{b}}(\boldsymbol{\omega})) = O(|D_n|^{-1}(b_1 \cdots b_d)^{-1}), \text{ as } n \rightarrow \infty.$$

Proof. See Appendix D.1. \square

Remark D.1. We observe from Theorem D.1(i) that there are two sources of bias in $F_{n,\mathbf{b}}(\boldsymbol{\omega})$. The $O(\|\mathbf{b}\|^2)$ bias arises from the classical nonparametric kernel smoothing method, while the $O(|D_n|^{-1/d})$ bias originates from the bias of the periodogram. Specifically, in (D.5) below, we show that

$$\sup_{\boldsymbol{\omega} \in \mathbb{R}^d} |\mathbb{E}[I_{h,n}(\boldsymbol{\omega})] - F_h(\boldsymbol{\omega})| = O(|D_n|^{-1/d}), \quad n \rightarrow \infty. \quad (\text{D.1})$$

The above $O(|D_n|^{-1/d})$ bias is transferred to the bias of the kernel estimator.

Now, we assume a common bandwidth for all coordinates, i.e., $b_1 = \dots = b_d = b \in (0, \infty)$. Recall MSE(b) in (6.1) is given by

$$\text{MSE}(b) = \sup_{\boldsymbol{\omega} \in \mathbb{R}^d} \mathbb{E}|\widehat{F}_{n,b}(\boldsymbol{\omega}) - F_h(\boldsymbol{\omega})|^2.$$

The following theorem addresses the rate of convergence of MSE(b).

Theorem D.2. Suppose that Assumptions 4.1, 4.2(ii) (for $r = 6$), 4.3, 4.4 (for $k = 4$), 4.5, and 6.1 hold. Moreover, assume that the data taper h is Lipschitz continuous on $[-1/2, 1/2]^d$, the side lengths $\mathbf{A}(n)$ satisfy condition (SL), and the bandwidth $b = b(n)$ satisfies condition (B). Then,

$$\text{MSE}(b) = O(b^4 + |D_n|^{-2/d} + |D_n|^{-1}b^{-d}), \quad n \rightarrow \infty.$$

Proof. By using the inequality $\mathbb{E}|a + b|^2 \leq 2\{\mathbb{E}|a|^2 + \mathbb{E}|b|^2\}$, we have

$$\text{MSE}(b) \leq 2 \sup_{\boldsymbol{\omega} \in \mathbb{R}^d} \mathbb{E}|F_{n,b}(\boldsymbol{\omega}) - F_h(\boldsymbol{\omega})|^2 + 2 \sup_{\boldsymbol{\omega} \in \mathbb{R}^d} \mathbb{E}|\widehat{F}_{n,b}(\boldsymbol{\omega}) - F_{n,b}(\boldsymbol{\omega})|^2.$$

Using Theorem D.1, the first term above is bounded by

$$\begin{aligned} \sup_{\boldsymbol{\omega} \in \mathbb{R}^d} \mathbb{E}|F_{n,b}(\boldsymbol{\omega}) - F_h(\boldsymbol{\omega})|^2 &\leq \sup_{\boldsymbol{\omega} \in \mathbb{R}^d} |\mathbb{E}[F_{n,b}(\boldsymbol{\omega})] - F_h(\boldsymbol{\omega})|^2 + \sup_{\boldsymbol{\omega} \in \mathbb{R}^d} \text{var}(|F_{n,b}(\boldsymbol{\omega})|) \\ &= O(b^4 + |D_n|^{-2/d} + |D_n|^{-1}b^{-d}), \quad n \rightarrow \infty. \end{aligned}$$

Next, Theorem E.4 below shows that the second term is bounded by $O(|D_n|^{-1}b^{-d}) + O(|D_n|^{-1}) = O(|D_n|^{-1}b^{-d})$. Thus, combining these two bounds, we obtain

$$\text{MSE}(b) = O(b^4 + |D_n|^{-2/d} + |D_n|^{-1}b^{-d}), \quad n \rightarrow \infty.$$

Thus, we get the desired result. □

D.1 Proof of Theorem D.1

We first show the order of the bias. Recall (C.10) that the bias term can be decomposed into two terms, namely A_1 and A_2 . To compute the rate of convergence of A_1 , by using the Taylor

expansion of F_h , we have

$$\begin{aligned} \left| F_h(\mathbf{v}) - F_h(\boldsymbol{\omega}) + \sum_{\ell=1}^d \frac{\partial F_h(\boldsymbol{\omega})}{\partial \omega_\ell} (v_\ell - \omega_\ell) \right| &\leq \sup_{\boldsymbol{\omega} \in \mathbb{R}^d, 1 \leq \ell, k \leq d} \left| \frac{\partial^2 F_h(\boldsymbol{\omega})}{\partial \omega_\ell \partial \omega_k} \right| \|\mathbf{v} - \boldsymbol{\omega}\|^2 \\ &\leq C \|\mathbf{v} - \boldsymbol{\omega}\|^2 \end{aligned}$$

for any $\mathbf{v} = (v_1, \dots, v_d)^\top$ and $\boldsymbol{\omega} = (\omega_1, \dots, \omega_d)^\top$ in \mathbb{R}^d . Here, the first inequality follows from the assumption that the second partial derivatives of F_h are continuous and bounded. Using the above bound, we have

$$\begin{aligned} A_1 &= \left| \int_{\mathbb{R}^d} K_{\mathbf{b}}(\mathbf{x}) \{F_h(\boldsymbol{\omega} - \mathbf{x}) - F_h(\boldsymbol{\omega})\} d\mathbf{x} \right| \\ &= \left| \int_{\mathbb{R}^d} K_{\mathbf{b}}(\mathbf{x}) \left\{ F_h(\boldsymbol{\omega} - \mathbf{x}) - F_h(\boldsymbol{\omega}) - \sum_{\ell=1}^d \frac{\partial F_h(\boldsymbol{\omega})}{\partial \omega_\ell} x_\ell \right\} d\mathbf{x} \right| \leq C \int_{\mathbb{R}^d} \|\mathbf{x}\|^2 K_{\mathbf{b}}(\mathbf{x}) d\mathbf{x}. \end{aligned}$$

Here, the second identity is due to the symmetry of $K_{\mathbf{b}}$. Since the support of $K_{\mathbf{b}}$ is $[-b_1, b_1] \times \dots \times [-b_d, b_d]$, we have

$$A_1 \leq C \int_{\mathbb{R}^d} \|\mathbf{x}\|^2 K_{\mathbf{b}}(\mathbf{x}) d\mathbf{x} \leq C' \|\mathbf{b}\|^2 \int_{\mathbb{R}^d} K_{\mathbf{b}}(\mathbf{x}) d\mathbf{x} = O(\|\mathbf{b}\|^2), \quad n \rightarrow \infty. \quad (\text{D.2})$$

Next, we bound A_2 . To do so, we need a rate of convergence for $|\mathbb{E}[I_{h,n}(\boldsymbol{\omega})] - F_h(\boldsymbol{\omega})|$. By using Lemma C.1, we have

$$\mathbb{E}[I_{h,n}^{(i,j)}(\boldsymbol{\omega})] - F_h^{(i,j)}(\boldsymbol{\omega}) = (2\pi)^{-d} H_{h,2}^{-1} |D_n|^{-1} \int_{\mathbb{R}^d} e^{-i\mathbf{u}^\top \boldsymbol{\omega}} \ell_2^{(i,j)}(\mathbf{u}) R_{h\lambda^{(j)}, h\lambda^{(i)}}^{(n)}(\mathbf{u}, \mathbf{0}) d\mathbf{u}.$$

Next, Theorem C.1 of YG24 states that there exists $C \in (0, \infty)$ that does not depend on $\mathbf{t} \in \mathbb{R}^d$ such that

$$|D_n|^{-1} |R_{h\lambda^{(j)}, h\lambda^{(i)}}^{(n)}(\mathbf{u}, \mathbf{0})| \leq C \min\{\|\mathbf{t}/\mathbf{A}\|, 1\}, \quad \mathbf{t} \in \mathbb{R}^d.$$

Therefore, we have

$$\begin{aligned} |\mathbb{E}[I_{h,n}^{(i,j)}(\boldsymbol{\omega})] - F_h^{(i,j)}(\boldsymbol{\omega})| &\leq C \int_{\mathbb{R}^d} |L_2(\mathbf{u})| \min\{\|\mathbf{u}/\mathbf{A}\|, 1\} d\mathbf{u} \\ &\leq C \int_{\mathbf{u}: \|\mathbf{u}/\mathbf{A}\| \geq 1} |L_2(\mathbf{u})| d\mathbf{u} + C \int_{\mathbf{u}: \|\mathbf{u}/\mathbf{A}\| \leq 1} \|\mathbf{u}/\mathbf{A}\| \cdot |L_2(\mathbf{u})| d\mathbf{u}. \end{aligned}$$

From the condition (SL) on $\mathbf{A} = (A_1, \dots, A_d)$, $\|\mathbf{u}/\mathbf{A}\| \geq 1$ implies that there exists $C_1 \in (0, \infty)$

such that $\|\mathbf{u}\| \geq C_1|D_n|^{1/d}$. Therefore, the first integral term is bounded by

$$\begin{aligned} & C \int_{\mathbf{u}: \|\mathbf{u}\| \geq C_1|D_n|^{1/d}} \{ \|\mathbf{u}\| / (C_1|D_n|^{1/d}) \} |L_2(\mathbf{u})| d\mathbf{u} \\ & \leq C|D_n|^{-1/d} \int_{\mathbb{R}^d} \|\mathbf{u}\| |L_2(\mathbf{u})| d\mathbf{u} = O(|D_n|^{-1/d}), \quad n \rightarrow \infty. \end{aligned} \quad (\text{D.3})$$

Here, we use $\|\mathbf{u}\| |L_2(\mathbf{u})| \in L_1(\mathbb{R}^d)$, provided Assumption 6.1(ii) holds.

To bound the second term, (SL) also implies that there exists $C_2 \in (0, \infty)$ such that $\|\mathbf{u}/\mathbf{A}\| \leq C_2|D_n|^{-1/d} \|\mathbf{u}\|$. Therefore, the second term is bounded by

$$C_2|D_n|^{-1/d} \int_{\mathbf{u}: \|\mathbf{u}/\mathbf{A}\| \leq 1} \|\mathbf{u}\| |L_2(\mathbf{u})| d\mathbf{u} = O(|D_n|^{-1/d}), \quad n \rightarrow \infty. \quad (\text{D.4})$$

Combining (D.3) and (D.4), we get

$$\sup_{\boldsymbol{\omega} \in \mathbb{R}^d} |\mathbb{E}[I_{h,n}(\boldsymbol{\omega})] - F_h(\boldsymbol{\omega})| = O(|D_n|^{-1/d}), \quad n \rightarrow \infty. \quad (\text{D.5})$$

Therefore, A_2 is bounded by

$$\begin{aligned} A_2 &= C \int_{\mathbb{R}^d} K_{\mathbf{b}}(\boldsymbol{\omega} - \mathbf{x}) |\mathbb{E}[I_{h,n}(\mathbf{x})] - F_h(\mathbf{x})| d\mathbf{x} \\ &= O(|D_n|^{-1/d}) \int_{\mathbb{R}^d} K_{\mathbf{b}}(\boldsymbol{\omega} - \mathbf{x}) d\mathbf{x} = O(|D_n|^{-1/d}), \quad n \rightarrow \infty. \end{aligned} \quad (\text{D.6})$$

Finally, combining (D.2) and (D.6), we have

$$\sup_{\boldsymbol{\omega} \in \mathbb{R}^d} |\mathbb{E}[F_{n,\mathbf{b}}(\boldsymbol{\omega})] - F_h(\boldsymbol{\omega})| = O(\|\mathbf{b}\|^2 + |D_n|^{-1/d}), \quad n \rightarrow \infty.$$

This proves (i).

Now, we prove the order of the variance. By using the cumulant decomposition as in (C.8), for $i, j \in \{1, \dots, m\}$, we have

$$\begin{aligned} \text{var}(F_{n,\mathbf{b}}^{(i,j)}(\boldsymbol{\omega})) &= \int_{\mathbb{R}^{2d}} K_{\mathbf{b}}(\boldsymbol{\omega} - \boldsymbol{\omega}_1) K_{\mathbf{b}}(\boldsymbol{\omega} - \boldsymbol{\omega}_2) \left\{ \text{cum}(J_{h,n}^{(i)}(\boldsymbol{\omega}_1), J_{h,n}^{(i)}(-\boldsymbol{\omega}_2)) \text{cum}(J_{h,n}^{(j)}(-\boldsymbol{\omega}_1), J_{h,n}^{(j)}(\boldsymbol{\omega}_2)) \right. \\ &\quad \left. + \text{cum}(J_{h,n}^{(i)}(\boldsymbol{\omega}_1), J_{h,n}^{(j)}(\boldsymbol{\omega}_2)) \text{cum}(J_{h,n}^{(j)}(-\boldsymbol{\omega}_1), J_{h,n}^{(i)}(-\boldsymbol{\omega}_2)) + O(|D_n|^{-1}) \right\} d\boldsymbol{\omega}_1 d\boldsymbol{\omega}_2 \\ &= B_1(\boldsymbol{\omega}) + B_2(\boldsymbol{\omega}) + O(|D_n|^{-1}), \quad n \rightarrow \infty. \end{aligned}$$

We calculate the bound for $B_1(\boldsymbol{\omega})$, and the bound for $B_2(\boldsymbol{\omega})$ can be treated similarly. Let

$$\tilde{F}(\boldsymbol{\omega}) = (\tilde{f}^{(i,j)}(\boldsymbol{\omega}))_{1 \leq i, j \leq m} = \mathcal{F}^{-1}(L_2)(\boldsymbol{\omega}).$$

Then, Assumption 6.1(i) implies that $\tilde{F} \in L_1^{m \times m}(\mathbb{R}^d)$, and in turn,

$$L_2(\mathbf{x}) = \mathcal{F}(\tilde{F})(\mathbf{x}) = \int_{\mathbb{R}^d} \tilde{F}(\boldsymbol{\omega}) e^{i\mathbf{x}^\top \boldsymbol{\omega}} d\boldsymbol{\omega}.$$

Substitute the above into the cumulant expression in (C.2), we get

$$\begin{aligned} (2\pi)^d H_{h,2} |D_n| \text{cum}(J_{h,n}^{(i)}(\boldsymbol{\omega}_1), J_{h,n}^{(j)}(\boldsymbol{\omega}_2)) &= \delta_{i,j} H_{h^2\lambda^{(i)}}^{(n)}(\boldsymbol{\omega}_1 + \boldsymbol{\omega}_2) \\ &\quad + \int_{\mathbb{R}^d} \tilde{f}^{(i,j)}(\boldsymbol{\xi}) H_{h\lambda^{(i),1}}^{(n)}(\boldsymbol{\omega}_1 - \boldsymbol{\xi}) H_{h\lambda^{(j),1}}^{(n)}(\boldsymbol{\omega}_2 + \boldsymbol{\xi}) d\boldsymbol{\xi}. \end{aligned}$$

For the notational convenience, we write $H_{h^2\lambda^{(i),1}}^{(n)} = H_{h^2\lambda^{(i)}}$, $H_{h\lambda^{(i),1}}^{(n)} = H_{h\lambda^{(i)}}$, \dots . Then, we have $B_1(\boldsymbol{\omega}) = (2\pi)^{-2d} H_{h,2}^{-2} \{B_{11}(\boldsymbol{\omega}) + B_{12}(\boldsymbol{\omega}) + B_{13}(\boldsymbol{\omega}) + B_{14}(\boldsymbol{\omega})\}$, where

$$\begin{aligned} B_{11}(\boldsymbol{\omega}) &= |D_n|^{-2} \iint_{\mathbb{R}^{2d}} K_{\mathbf{b}}(\boldsymbol{\omega} - \boldsymbol{\omega}_1) K_{\mathbf{b}}(\boldsymbol{\omega} - \boldsymbol{\omega}_2) H_{h^2\lambda^{(i)}}(\boldsymbol{\omega}_1 - \boldsymbol{\omega}_2) H_{h^2\lambda^{(j)}}(-\boldsymbol{\omega}_1 + \boldsymbol{\omega}_2) d\boldsymbol{\omega}_1 d\boldsymbol{\omega}_2, \\ B_{12}(\boldsymbol{\omega}) &= |D_n|^{-2} \iint_{\mathbb{R}^{2d}} d\boldsymbol{\omega}_1 d\boldsymbol{\omega}_2 K_{\mathbf{b}}(\boldsymbol{\omega} - \boldsymbol{\omega}_1) K_{\mathbf{b}}(\boldsymbol{\omega} - \boldsymbol{\omega}_2) H_{h^2\lambda^{(i)}}(\boldsymbol{\omega}_1 - \boldsymbol{\omega}_2), \\ &\quad \times \int_{\mathbb{R}^d} \tilde{f}^{(j,j)}(\boldsymbol{\xi}) H_{h\lambda^{(j)}}(-\boldsymbol{\omega}_1 - \boldsymbol{\xi}) H_{h\lambda^{(j)}}(\boldsymbol{\omega}_2 + \boldsymbol{\xi}) d\boldsymbol{\xi}, \\ B_{13}(\boldsymbol{\omega}) &= |D_n|^{-2} \iint_{\mathbb{R}^{2d}} d\boldsymbol{\omega}_1 d\boldsymbol{\omega}_2 K_{\mathbf{b}}(\boldsymbol{\omega} - \boldsymbol{\omega}_1) K_{\mathbf{b}}(\boldsymbol{\omega} - \boldsymbol{\omega}_2) H_{h^2\lambda^{(j)}}(-\boldsymbol{\omega}_1 + \boldsymbol{\omega}_2), \\ &\quad \times \int_{\mathbb{R}^d} \tilde{f}^{(i,i)}(\boldsymbol{\xi}) H_{h\lambda^{(i)}}(\boldsymbol{\omega}_1 - \boldsymbol{\xi}) H_{h\lambda^{(i)}}(-\boldsymbol{\omega}_2 + \boldsymbol{\xi}) d\boldsymbol{\xi}, \\ B_{14}(\boldsymbol{\omega}) &= |D_n|^{-2} \iint_{\mathbb{R}^{2d}} K_{\mathbf{b}}(\boldsymbol{\omega} - \boldsymbol{\omega}_1) K_{\mathbf{b}}(\boldsymbol{\omega} - \boldsymbol{\omega}_2) \int_{\mathbb{R}^d} \tilde{f}^{(i,i)}(\boldsymbol{\xi}_1) H_{h\lambda^{(i)}}(\boldsymbol{\omega}_1 - \boldsymbol{\xi}_1) H_{h\lambda^{(i)}}(-\boldsymbol{\omega}_2 + \boldsymbol{\xi}_1) d\boldsymbol{\xi}_1 \\ &\quad \times \int_{\mathbb{R}^d} \tilde{f}^{(j,j)}(\boldsymbol{\xi}_2) H_{h\lambda^{(j)}}(-\boldsymbol{\omega}_1 - \boldsymbol{\xi}_2) H_{h\lambda^{(j)}}(\boldsymbol{\omega}_2 + \boldsymbol{\xi}_2) d\boldsymbol{\xi}_2 d\boldsymbol{\omega}_1 d\boldsymbol{\omega}_2. \end{aligned}$$

Since $K_{\mathbf{b}}$ is bounded and has finite support, we can define $\widehat{K}_{\mathbf{b}}(\boldsymbol{\omega}) = \mathcal{F}^{-1}(K_{\mathbf{b}})(\boldsymbol{\omega})$. Then, by substituting the expressions for $H_{h^2\lambda^{(i)}}(\cdot)$ and $H_{h^2\lambda^{(j)}}(\cdot)$ into $B_{11}(\boldsymbol{\omega})$ and using Fubini's theorem, we have

$$\begin{aligned} B_{11}(\boldsymbol{\omega}) &= (2\pi)^{2d} |D_n|^{-2} \iint_{D_n^2} |\widehat{K}_{\mathbf{b}}(\mathbf{x} - \mathbf{y})|^2 \left(h^2\lambda^{(i)} \left(\frac{\mathbf{x}}{\mathbf{A}} \right) \right) \left(h^2\lambda^{(j)} \left(\frac{\mathbf{y}}{\mathbf{A}} \right) \right) d\mathbf{x} d\mathbf{y} \\ &\leq C |D_n|^{-2} \int_{D_n} \int_{\mathbb{R}^d} |\widehat{K}_{\mathbf{b}}(\mathbf{x} - \mathbf{y})|^2 d\mathbf{x} d\mathbf{y} \\ &\leq C |D_n|^{-1} \int_{\mathbb{R}^d} |\widehat{K}_{\mathbf{b}}(\mathbf{x})|^2 d\mathbf{x} \\ &= C |D_n|^{-1} \int_{\mathbb{R}^d} |K_{\mathbf{b}}(\boldsymbol{\omega})|^2 d\boldsymbol{\omega} = O(|D_n|^{-1} (b_1 \cdots b_d)^{-1}), \quad n \rightarrow \infty. \end{aligned} \tag{D.7}$$

Here, we use Parseval's theorem in the second-to-last identity.

Next, we bound $B_{12}(\boldsymbol{\omega})$. By substituting the expression of $H_{h^2\lambda^{(i)}}$, ..., and using Fubini's theorem, we have

$$\begin{aligned}
B_{12}(\boldsymbol{\omega}) &= (2\pi)^{2d}|D_n|^{-2} \int_{\mathbb{R}^d} d\xi \tilde{f}^{(j,j)}(\xi) \iiint_{D_n^3} \widehat{K}_b(\mathbf{x} - \mathbf{y}) \widehat{K}_b(\mathbf{z} - \mathbf{x}) (h^2\lambda^{(i)}) \left(\frac{\mathbf{x}}{\mathbf{A}}\right) (h\lambda^{(j)}) \left(\frac{\mathbf{y}}{\mathbf{A}}\right) \\
&\quad \times (h\lambda^{(j)}) \left(\frac{\mathbf{z}}{\mathbf{A}}\right) e^{i(\mathbf{y}-\mathbf{z})^\top \xi} d\mathbf{x} d\mathbf{y} d\mathbf{z} \\
&= (2\pi)^{2d}|D_n|^{-2} \int_{\mathbb{R}^d} d\xi \tilde{f}^{(j,j)}(\xi) \int_{D_n} d\mathbf{x} (h^2\lambda^{(i)}) \left(\frac{\mathbf{x}}{\mathbf{A}}\right) \left\{ \int_{D_n} \widehat{K}_b(\mathbf{x} - \mathbf{y}) (h\lambda^{(j)}) \left(\frac{\mathbf{y}}{\mathbf{A}}\right) e^{i\mathbf{y}^\top \xi} d\mathbf{y} \right\} \\
&\quad \times \left\{ \int_{D_n} \widehat{K}_b(\mathbf{z} - \mathbf{x}) (h\lambda^{(j)}) \left(\frac{\mathbf{z}}{\mathbf{A}}\right) e^{-i\mathbf{z}^\top \xi} d\mathbf{z} \right\} d\xi \\
&= (2\pi)^{2d}|D_n|^{-2} \int_{\mathbb{R}^d} d\xi \tilde{f}^{(j,j)}(\xi) \int_{D_n} (h^2\lambda^{(i)}) \left(\frac{\mathbf{x}}{\mathbf{A}}\right) |g_j(\mathbf{x}, \xi)|^2 d\mathbf{x},
\end{aligned}$$

where

$$g_j(\mathbf{x}, \xi) := \int_{\mathbb{R}^d} \widehat{K}_b(\mathbf{x} - \mathbf{y}) (h\lambda^{(j)}) \left(\frac{\mathbf{y}}{\mathbf{A}}\right) e^{i\mathbf{y}^\top \xi} d\mathbf{y}.$$

Since $\sup_{\xi} |f^{(j,j)}(\xi)| \leq (2\pi)^{-d} \int_{\mathbb{R}^d} |\ell_2^{(j,j)}(\mathbf{x})| d\mathbf{x} < \infty$ and $|h^2\lambda^{(i)}|$ is bounded, B_{12} is bounded by

$$\begin{aligned}
B_{12}(\boldsymbol{\omega}) &\leq O(|D_n|^{-2}) \int_{D_n} d\mathbf{x} \int_{\mathbb{R}^d} |g_j(\mathbf{x}, \xi)|^2 d\xi \\
&= O(|D_n|^{-2}) \int_{D_n} d\mathbf{x} \int_{\mathbb{R}^d} \left| \widehat{K}_b(\mathbf{x} - \mathbf{y}) (h\lambda^{(j)}) \left(\frac{\mathbf{y}}{\mathbf{A}}\right) \right|^2 d\mathbf{y} \\
&\leq O(|D_n|^{-1}) \int_{\mathbb{R}^d} |\widehat{K}(\mathbf{u})|^2 d\mathbf{u} = O(|D_n|^{-1} (b_1 \cdots b_d)^{-1}), \quad n \rightarrow \infty.
\end{aligned} \tag{D.8}$$

Here, the first identity is due to Parseval's theorem for $g_j(\mathbf{x}, \cdot)$ and the second identity is due to Parseval's theorem for \widehat{K}_b . By using similar techniques, it can be seen that

$$B_{13}(\boldsymbol{\omega}), B_{14}(\boldsymbol{\omega}) = O(|D_n|^{-1} (b_1 \cdots b_d)^{-1}), \quad n \rightarrow \infty. \tag{D.9}$$

Combining (D.7)–(D.9), we conclude $B_1(\boldsymbol{\omega}) = O(|D_n|^{-1} (b_1 \cdots b_d)^{-1})$ as $n \rightarrow \infty$. Similarly, $B_2(\boldsymbol{\omega}) = O(|D_n|^{-1} (b_1 \cdots b_d)^{-1})$ as $n \rightarrow \infty$. This shows that

$$\text{var}(F_{n,\mathbf{b}}^{(i,j)}(\boldsymbol{\omega})) = B_1(\boldsymbol{\omega}) + B_2(\boldsymbol{\omega}) + O(|D_n|^{-1}) = O(|D_n|^{-1} (b_1 \cdots b_d)^{-1}), \quad n \rightarrow \infty.$$

Summing the above over $i, j \in \{1, \dots, m\}$, we show (ii).

All together, we get the desired results. □

E Asymptotic equivalence between the feasible and theoretical quantities

In this section, we show the asymptotic equivalence between the feasible and theoretical quantities.

E.1 Bounds for the DFTs and periodograms

Recall $\underline{J}_{h,n}(\boldsymbol{\omega})$ as in (4.3) and let $\widehat{\underline{J}}_{h,n}(\boldsymbol{\omega})$ be its estimated version. For $\boldsymbol{\alpha} = (\alpha_1, \dots, \alpha_p) \in \{0, 1, \dots\}^p$, let $\nabla^{\boldsymbol{\alpha}} \lambda^{(j)} = \left(\frac{\partial^{|\boldsymbol{\alpha}|}}{\partial \beta_1^{\alpha_1} \dots \partial \beta_p^{\alpha_p}} \right) \lambda^{(j)}$ be the $\boldsymbol{\alpha}$ th-order partial derivative of the j th component of $\underline{\lambda}$ with respect to $\boldsymbol{\beta}$. For $t \in \mathbb{N}$, let

$$|H_{h\nabla^{(t)}\underline{\lambda}}^{(n)}(\boldsymbol{\omega})| = \sum_{j=1}^m \sum_{|\boldsymbol{\alpha}|=t} |H_{h\nabla^{\boldsymbol{\alpha}}\lambda^{(j)},1}^{(n)}(\boldsymbol{\omega})|.$$

Below is the key lemma which provides the upper bound of $|\widehat{\underline{J}}_{h,n}(\boldsymbol{\omega}) - \underline{J}_{h,n}(\boldsymbol{\omega})|$.

Lemma E.1. *Suppose that Assumption 4.1 holds. Let $s \in [1, \infty)$ and $k \in \mathbb{N}$ be given. Then, there exists a constant $C \in (0, \infty)$ such that*

$$\begin{aligned} & |\widehat{\underline{J}}_{h,n}(\boldsymbol{\omega}) - \underline{J}_{h,n}(\boldsymbol{\omega})|^s \\ & \leq C \left\{ |D_n|^{1/2} |\widehat{\boldsymbol{\beta}}_n - \boldsymbol{\beta}_0| \right\}^s \sum_{t=1}^{k-1} \left\{ |D_n|^{-1} \left| H_{h\nabla^t \underline{\lambda}}^{(n)}(\boldsymbol{\omega}) \right| \right\}^s + C \left\{ |D_n|^{1/2} \cdot |\widehat{\boldsymbol{\beta}}_n - \boldsymbol{\beta}_0|^k \right\}^s. \end{aligned} \quad (\text{E.1})$$

Proof. For simplicity, we will only show the lemma for $m = p = 1$ and $k = 3$. The general case can be treated similarly. Here, we use $C \in (0, \infty)$ to indicate a generic constant that varies from line to line. The difference between the feasible and infeasible DFT is

$$|\widehat{\underline{J}}_{h,n}(\boldsymbol{\omega}) - \underline{J}_{h,n}(\boldsymbol{\omega})| = (2\pi)^{-d/2} H_{h,2}^{-1/2} |D_n|^{-1/2} |\widehat{H}_{h\lambda,1}^{(n)}(\boldsymbol{\omega}) - H_{h\lambda,1}^{(n)}(\boldsymbol{\omega})|. \quad (\text{E.2})$$

Here, $\widehat{H}_{h\lambda,1}^{(n)}(\boldsymbol{\omega}) = H_{h\widehat{\lambda}_n,1}^{(n)}(\boldsymbol{\omega})$. By using the Taylor expansion of $\lambda(\boldsymbol{x}; \boldsymbol{\beta})$ with respect to $\boldsymbol{\beta}$, for each $\boldsymbol{x} \in [-1/2, 1/2]^d$, there exists $\widetilde{\boldsymbol{\beta}}_n = \widetilde{\boldsymbol{\beta}}_n(\boldsymbol{x})$, a convex combination of $\widehat{\boldsymbol{\beta}}_n$ and $\boldsymbol{\beta}_0$, such that

$$\begin{aligned} \widehat{\lambda}(\boldsymbol{x}) - \lambda(\boldsymbol{x}) &= (\widehat{\boldsymbol{\beta}}_n - \boldsymbol{\beta}_0) \nabla \lambda(\boldsymbol{x}; \boldsymbol{\beta}_0) \\ &\quad + \frac{1}{2} (\widehat{\boldsymbol{\beta}}_n - \boldsymbol{\beta}_0)^2 \nabla^{(2)} \lambda(\boldsymbol{x}; \boldsymbol{\beta}_0) + \frac{1}{6} (\widehat{\boldsymbol{\beta}}_n - \boldsymbol{\beta}_0)^3 \nabla^{(3)} \lambda(\boldsymbol{x}; \widetilde{\boldsymbol{\beta}}_n). \end{aligned}$$

Substitute the above into $\widehat{H}_{h\lambda,1}^{(n)}(\boldsymbol{\omega}) - H_{h\lambda,1}^{(n)}(\boldsymbol{\omega})$, and by using the triangle inequality, we have

$$\begin{aligned} |\widehat{H}_{h\lambda,1}^{(n)}(\boldsymbol{\omega}) - H_{h\lambda,1}^{(n)}(\boldsymbol{\omega})| &\leq |\widehat{\boldsymbol{\beta}}_n - \boldsymbol{\beta}_0| |H_{h\nabla\lambda,1}^{(n)}(\boldsymbol{\omega})| \\ &+ \frac{1}{2} |\widehat{\boldsymbol{\beta}}_n - \boldsymbol{\beta}_0|^2 |H_{h\nabla^{(2)}\lambda,1}^{(n)}(\boldsymbol{\omega})| + \frac{1}{6} |\widehat{\boldsymbol{\beta}}_n - \boldsymbol{\beta}_0|^3 \int_{D_n} h(\mathbf{x}/\mathbf{A}) |\nabla^{(3)}\lambda(\mathbf{x}/\mathbf{A}; \widetilde{\boldsymbol{\beta}}_n)| d\mathbf{x}. \end{aligned}$$

Since both $\widehat{\boldsymbol{\beta}}_n$ and $\boldsymbol{\beta}_0$ belong to Θ , which is compact, we have $|\widehat{\boldsymbol{\beta}}_n - \boldsymbol{\beta}_0| \leq \text{diam}(\Theta) < \infty$. Moreover, $|\nabla^{(3)}\lambda(\cdot; \boldsymbol{\beta})|$ is uniformly bounded due to Assumption 4.1. Therefore, $|\widehat{H}_{h\lambda,1}^{(n)}(\boldsymbol{\omega}) - H_{h\lambda,1}^{(n)}(\boldsymbol{\omega})|$ is bounded by

$$C|\widehat{\boldsymbol{\beta}}_n - \boldsymbol{\beta}_0| \left\{ |H_{h\nabla\lambda,1}^{(n)}(\boldsymbol{\omega})| + |H_{h\nabla^{(2)}\lambda,1}^{(n)}(\boldsymbol{\omega})| \right\} + C|D_n| \cdot |\widehat{\boldsymbol{\beta}}_n - \boldsymbol{\beta}_0|^3.$$

Substituting the above into (E.2) and using the inequality $(a + b + c)^s \leq 3^{s-1}(a^s + b^s + c^s)$ for all $a, b, c > 0$, we obtain (E.1). Thus, we get the desired result. \square

Now, we show that $\widehat{\underline{J}}_{h,n}(\boldsymbol{\omega}) - \underline{J}_{h,n}(\boldsymbol{\omega})$ and $\widehat{\underline{I}}_{h,n}(\boldsymbol{\omega}) - \underline{I}_{h,n}(\boldsymbol{\omega})$ are asymptotically negligible.

Theorem E.1. *Suppose that Assumptions 4.1, 4.2(i), 4.3, and 4.5 hold. Then, for a sequence $\{\boldsymbol{\omega}_n\}$ on \mathbb{R}^d that is asymptotically distant from $\{\mathbf{0}\}$, we have*

$$|\widehat{\underline{J}}_{h,n}(\boldsymbol{\omega}_n) - \underline{J}_{h,n}(\boldsymbol{\omega}_n)| \xrightarrow{\mathcal{P}} 0 \quad \text{and} \quad |\widehat{\underline{I}}_{h,n}(\boldsymbol{\omega}_n) - \underline{I}_{h,n}(\boldsymbol{\omega}_n)| \xrightarrow{\mathcal{P}} 0.$$

Proof. By applying Lemma E.1 for $s = 1$ and $k = 2$ together with Assumption 4.1(i), we have

$$|\widehat{\underline{J}}_{h,n}(\boldsymbol{\omega}_n) - \underline{J}_{h,n}(\boldsymbol{\omega}_n)| \leq O_p(|D_n|^{-1} |H_{h\nabla\lambda}^{(n)}(\boldsymbol{\omega}_n)|) + O_p(|D_n|^{-1/2}).$$

To bound the first term above, by using YG24, Lemma C.2, we have $|D_n|^{-1} |H_{h\nabla\lambda}^{(n)}(\boldsymbol{\omega}_n)| = o(1)$ as $n \rightarrow \infty$. Thus, the first term above is $o_p(1)$. Combining this, we have $|\widehat{\underline{J}}_{h,n}(\boldsymbol{\omega}_n) - \underline{J}_{h,n}(\boldsymbol{\omega}_n)| \xrightarrow{\mathcal{P}} 0$. In turn, $|\widehat{\underline{I}}_{h,n}(\boldsymbol{\omega}_n) - \underline{I}_{h,n}(\boldsymbol{\omega}_n)| \xrightarrow{\mathcal{P}} 0$ due to the continuous mapping theorem. Thus, we get the desired results. \square

Next, we bound the L_2 -norm differences of the DFTs and periodograms. The following corollary is useful for obtaining the bounds.

Corollary E.1. *Suppose that Assumptions 4.1, 4.2(ii) (for some $r \in (1, \infty)$), 4.3, and 4.5 hold. Then, for a sequence $\{\boldsymbol{\omega}_n\}$ on \mathbb{R}^d that is asymptotically distant from $\{\mathbf{0}\}$, and for any $s \in [1, r)$, we have $\mathbb{E}|\widehat{\underline{J}}_{h,n}(\boldsymbol{\omega}_n) - \underline{J}_{h,n}(\boldsymbol{\omega}_n)|^s = o(1)$ as $n \rightarrow \infty$.*

Proof. Let $k \in \mathbb{N}$ be chosen such that $ks > r$. Then, by Lemma E.1, we have $\mathbb{E}|\widehat{\underline{J}}_{h,n}(\boldsymbol{\omega}_n) - \underline{J}_{h,n}(\boldsymbol{\omega}_n)|^s$ bounded by

$$C\mathbb{E} \left\{ |D_n|^{1/2} |\widehat{\boldsymbol{\beta}}_n - \boldsymbol{\beta}_0| \right\}^s \times \sum_{t=1}^{k-1} \left\{ |D_n|^{-1} |H_{h\nabla^t\lambda}^{(n)}(\boldsymbol{\omega}_n)| \right\}^s + C|D_n|^{s/2} \mathbb{E}|\widehat{\boldsymbol{\beta}}_n - \boldsymbol{\beta}_0|^{ks}. \quad (\text{E.3})$$

Since $|D_n|^{-1}|H_{h\nabla t_\lambda}^{(n)}(\boldsymbol{\omega}_n)| = o(1)$ due to YG24, Lemma C.2, and $\mathbb{E}\left\{|D_n|^{1/2}|\widehat{\boldsymbol{\beta}}_n - \boldsymbol{\beta}_0|\right\}^s = O(1)$ due to Assumption 4.2(ii) (for $r > s$), the first term is $o(1)$. Moreover, since $ks > r$, the second term is bounded by $C|D_n|^{s/2}\mathbb{E}|\widehat{\boldsymbol{\beta}}_n - \boldsymbol{\beta}_0|^r \leq O(1)|D_n|^{s/2-r/2} = o(1)$. Altogether, we get the desired result. \square

Theorem E.2. *Suppose that Assumptions 4.1, 4.2(ii) (for $r > 2$), 4.3, and 4.5 hold. Then, for a sequence $\{\boldsymbol{\omega}_n\}$ on \mathbb{R}^d that is asymptotically distant from $\{\mathbf{0}\}$, we have*

$$\lim_{n \rightarrow \infty} \mathbb{E}|\widehat{\mathcal{J}}_{h,n}(\boldsymbol{\omega}_n) - \underline{\mathcal{J}}_{h,n}(\boldsymbol{\omega}_n)|^2 = 0. \quad (\text{E.4})$$

If we further assume Assumptions 4.2(ii) for $r > 4$ and 4.4 for $k = 4$, then

$$\lim_{n \rightarrow \infty} \mathbb{E}|\widehat{I}_{h,n}(\boldsymbol{\omega}_n) - I_{h,n}(\boldsymbol{\omega}_n)|^2 = 0. \quad (\text{E.5})$$

Proof. (E.4) is immediate from Corollary E.1 for $s = 2$ and $r > 2$. To show (E.5), we first note that

$$\begin{aligned} |\widehat{I}_{h,n}(\boldsymbol{\omega}_n) - I_{h,n}(\boldsymbol{\omega}_n)| &= |\widehat{\mathcal{J}}_{h,n}(\boldsymbol{\omega}_n)\widehat{\mathcal{J}}_{h,n}^*(\boldsymbol{\omega}_n) - \underline{\mathcal{J}}_{h,n}(\boldsymbol{\omega}_n)\underline{\mathcal{J}}_{h,n}^*(\boldsymbol{\omega}_n)| \\ &\leq |\widehat{\mathcal{J}}_{h,n}(\boldsymbol{\omega}_n)\{\widehat{\mathcal{J}}_{h,n}^*(\boldsymbol{\omega}_n) - \underline{\mathcal{J}}_{h,n}^*(\boldsymbol{\omega}_n)\}| + |\{\widehat{\mathcal{J}}_{h,n}(\boldsymbol{\omega}_n) - \underline{\mathcal{J}}_{h,n}(\boldsymbol{\omega}_n)\}\underline{\mathcal{J}}_{h,n}^*(\boldsymbol{\omega}_n)| \\ &\leq |\widehat{\mathcal{J}}_{h,n}(\boldsymbol{\omega}_n) - \underline{\mathcal{J}}_{h,n}(\boldsymbol{\omega}_n)|\{|\widehat{\mathcal{J}}_{h,n}(\boldsymbol{\omega}_n)| + |\underline{\mathcal{J}}_{h,n}(\boldsymbol{\omega}_n)|\} \\ &\leq |\widehat{\mathcal{J}}_{h,n}(\boldsymbol{\omega}_n) - \underline{\mathcal{J}}_{h,n}(\boldsymbol{\omega}_n)|\{|\widehat{\mathcal{J}}_{h,n}(\boldsymbol{\omega}_n) - \underline{\mathcal{J}}_{h,n}(\boldsymbol{\omega}_n)| + 2|\underline{\mathcal{J}}_{h,n}(\boldsymbol{\omega}_n)|\} \end{aligned} \quad (\text{E.6})$$

Here, we use the triangle inequality in the first and third inequalities, and $|\boldsymbol{x}\boldsymbol{y}^*| = |\boldsymbol{x}||\boldsymbol{y}^*|$ and $|\boldsymbol{x}^*| = |\boldsymbol{x}|$ in the second inequality. Taking the square on both sides above and by iteratively applying the Cauchy-Schwarz inequality, $\mathbb{E}|\widehat{I}_{h,n}(\boldsymbol{\omega}_n) - I_{h,n}(\boldsymbol{\omega}_n)|^2$ is bounded by

$$C \left\{ \mathbb{E}|\widehat{\mathcal{J}}_{h,n}(\boldsymbol{\omega}_n) - \underline{\mathcal{J}}_{h,n}(\boldsymbol{\omega}_n)|^4 \right\}^{1/2} \left\{ \mathbb{E}|\widehat{\mathcal{J}}_{h,n}(\boldsymbol{\omega}_n) - \underline{\mathcal{J}}_{h,n}(\boldsymbol{\omega}_n)|^4 + \mathbb{E}|\underline{\mathcal{J}}_{h,n}(\boldsymbol{\omega}_n)|^4 \right\}^{1/2}. \quad (\text{E.7})$$

The first term above is $o(1)$ due to Corollary E.1. To bound the second term, we note that

$$\begin{aligned} \mathbb{E}|\underline{\mathcal{J}}_{h,n}(\boldsymbol{\omega}_n)|^4 &= \mathbb{E}|I_{h,n}(\boldsymbol{\omega}_n)|^2 \leq \sum_{i_1, j_1, i_2, j_2=1}^m \mathbb{E}|I_{h,n}^{(i_1, j_1)}(\boldsymbol{\omega}_n)||I_{h,n}^{(i_2, j_2)}(\boldsymbol{\omega}_n)| \\ &\leq \sum_{i_1, j_1, i_2, j_2=1}^m \sqrt{\text{var}(I_{h,n}^{(i_1, j_1)}(\boldsymbol{\omega}_n)) + |\mathbb{E}I_{h,n}^{(i_1, j_1)}(\boldsymbol{\omega}_n)|^2} \sqrt{\text{var}(I_{h,n}^{(i_2, j_2)}(\boldsymbol{\omega}_n)) + |\mathbb{E}I_{h,n}^{(i_2, j_2)}(\boldsymbol{\omega}_n)|^2}. \end{aligned}$$

Here, we use the Cauchy-Schwarz inequality together with $\mathbb{E}|X|^2 = \text{var}(X) + |\mathbb{E}X|^2$ in the last inequality. Since $\sup_{n \in \mathbb{N}} \text{var}(I_{h,n}^{(i_1, j_1)}(\boldsymbol{\omega}_n)) < \infty$ and $\sup_{n \in \mathbb{N}} |\mathbb{E}I_{h,n}^{(i_1, j_1)}(\boldsymbol{\omega}_n)| = O(1)$, provided Assumption 4.4($k = 4$) holds, we conclude that $\mathbb{E}|\underline{\mathcal{J}}_{h,n}(\boldsymbol{\omega}_n)|^4 = O(1)$ as $n \rightarrow \infty$. Therefore, the second term in (E.7) is $O(1)$.

Altogether, we have $\mathbb{E}|\widehat{I}_{h,n}(\boldsymbol{\omega}_n) - I_{h,n}(\boldsymbol{\omega}_n)|^2 = o(1)$ as $n \rightarrow \infty$, thus getting the desired

result. □

E.2 Bounds for the kernel spectral density estimator

In this section, we derive the bounds between the theoretical and feasible kernel spectral density estimators. Recall that $\widehat{F}_{n,b}(\boldsymbol{\omega})$ is defined as in (5.1) and its theoretical counterpart $F_{n,b}(\boldsymbol{\omega})$ is as in (C.9).

In the two theorems below, we first show that $F_{n,b}(\boldsymbol{\omega})$ and $\widehat{F}_{n,b}(\boldsymbol{\omega})$ are asymptotically negligible, then calculate the rate of convergence.

Theorem E.3. *Suppose that the Assumptions 4.1, 4.2(i), 4.3, 4.4 (for $k = 4$), and 4.5 hold. Moreover, assume that the bandwidth $b = b(n)$ satisfies condition (B). Then,*

$$\sup_{\boldsymbol{\omega} \in \mathbb{R}^d} |\widehat{F}_{n,b}(\boldsymbol{\omega}) - F_{n,b}(\boldsymbol{\omega})| = o_p(1), \quad n \rightarrow \infty.$$

Proof. Recall (5.1) and (C.9). We have

$$\begin{aligned} |\widehat{F}_{n,b}(\boldsymbol{\omega}) - F_{n,b}(\boldsymbol{\omega})| &\leq \int_{\mathbb{R}^d} K_b(\boldsymbol{\omega} - \mathbf{x}) |\widehat{I}_{h,n}(\mathbf{x}) - I_{h,n}(\mathbf{x})| d\mathbf{x} \\ &\leq \int_{\mathbb{R}^d} K_b(\boldsymbol{\omega} - \mathbf{x}) |\widehat{J}_{h,n}(\mathbf{x}) - \underline{J}_{h,n}(\mathbf{x})| \{|\widehat{J}_{h,n}(\mathbf{x})| + |\underline{J}_{h,n}(\mathbf{x})|\} d\mathbf{x} \\ &\leq \left\{ \int_{\mathbb{R}^d} K_b(\boldsymbol{\omega} - \mathbf{x}) |\widehat{J}_{h,n}(\mathbf{x}) - \underline{J}_{h,n}(\mathbf{x})|^2 d\mathbf{x} \right\}^{1/2} \\ &\quad \times \left\{ 2 \int_{\mathbb{R}^d} K_b(\boldsymbol{\omega} - \mathbf{x}) \{|\widehat{J}_{h,n}(\mathbf{x})|^2 + |\underline{J}_{h,n}(\mathbf{x})|^2\} d\mathbf{x} \right\}^{1/2}. \end{aligned} \tag{E.8}$$

Here, the second inequality follows from the proof of Theorem E.2, and the third inequality is due to the Cauchy-Schwarz inequality.

To bound the first term above, we apply Lemma E.1 for $(s, k) = (2, 2)$ and obtain

$$\begin{aligned} &\int_{\mathbb{R}^d} K_b(\boldsymbol{\omega} - \mathbf{x}) |\widehat{J}_{h,n}(\mathbf{x}) - \underline{J}_{h,n}(\mathbf{x})|^2 d\mathbf{x} \\ &\leq C \{ |D_n|^{1/2} |\widehat{\boldsymbol{\beta}}_n - \boldsymbol{\beta}_0| \}^2 \int_{\mathbb{R}^d} K_b(\boldsymbol{\omega} - \mathbf{x}) \left\{ |D_n|^{-1} |H_{h\nabla\Delta}^{(n)}(\mathbf{x})| \right\}^2 d\mathbf{x} \\ &\quad + C \left\{ |D_n|^{1/2} \cdot |\widehat{\boldsymbol{\beta}}_n - \boldsymbol{\beta}_0|^2 \right\}^2 \int_{\mathbb{R}^d} K_b(\boldsymbol{\omega} - \mathbf{x}) d\mathbf{x} \\ &\leq O_p(1) \int_{\mathbb{R}^d} K_b(\boldsymbol{\omega} - \mathbf{x}) \left\{ |D_n|^{-1} |H_{h\nabla\Delta}^{(n)}(\mathbf{x})| \right\}^2 d\mathbf{x} + O_p(|D_n|^{-1}). \end{aligned}$$

Here, the second inequality follows from Assumption 4.2(i) and the identity $\int_{\mathbb{R}^d} K_b(\boldsymbol{\omega} - \mathbf{x}) d\mathbf{x} = 1$.

Moreover, since $\sup_{\boldsymbol{\omega}} K_{\mathbf{b}}(\boldsymbol{\omega}) < C(b_1 \cdots b_d)^{-1}$, this, together with YG24, Lemma C.3(a), yields

$$\begin{aligned} & \int_{\mathbb{R}^d} K_{\mathbf{b}}(\boldsymbol{\omega} - \mathbf{x}) \left\{ |D_n|^{-1} |H_{h\nabla_{\Delta}}^{(n)}(\mathbf{x})| \right\}^2 d\mathbf{x} \\ & \leq C |D_n|^{-1} (b_1 \cdots b_d)^{-1} \int_{\mathbb{R}^d} \left\{ |D_n|^{-1/2} |H_{h\nabla_{\Delta}}^{(n)}(\mathbf{x})| \right\}^2 d\mathbf{x} \\ & = O(|D_n|^{-1} (b_1 \cdots b_d)^{-1}). \end{aligned} \tag{E.9}$$

Therefore, the first term in (E.8) is $O_p(|D_n|^{-1/2} (b_1 \cdots b_d)^{-1/2}) + O_p(|D_n|^{-1/2})$, which is $o_p(1)$ due to the condition (B) on the bandwidth.

Next, we bound the second term. By using the triangle inequality and the Cauchy-Schwarz inequality, we have

$$|\widehat{J}_{h,n}(\mathbf{x})|^2 \leq 2|\underline{J}_{h,n}(\mathbf{x}) - \underline{J}_{h,n}(\mathbf{x})|^2 + 2|\underline{J}_{h,n}(\mathbf{x})|^2.$$

Therefore, we have

$$\begin{aligned} & \int_{\mathbb{R}^d} K_{\mathbf{b}}(\boldsymbol{\omega} - \mathbf{x}) |\widehat{J}_{h,n}(\mathbf{x})|^2 d\mathbf{x} \\ & \leq 2 \int_{\mathbb{R}^d} K_{\mathbf{b}}(\boldsymbol{\omega} - \mathbf{x}) |\underline{J}_{h,n}(\mathbf{x}) - \underline{J}_{h,n}(\mathbf{x})|^2 d\mathbf{x} \\ & \quad + 2 \int_{\mathbb{R}^d} K_{\mathbf{b}}(\boldsymbol{\omega} - \mathbf{x}) |\underline{J}_{h,n}(\mathbf{x})|^2 d\mathbf{x} = o_p(1) + 2 \int_{\mathbb{R}^d} K_{\mathbf{b}}(\boldsymbol{\omega} - \mathbf{x}) |\underline{J}_{h,n}(\mathbf{x})|^2 d\mathbf{x}. \end{aligned}$$

To bound the second term above, we note from the arguments in Appendix C.3 that $|\underline{J}_{h,n}(\mathbf{x})|^2 = |\underline{J}_{h,n}(\mathbf{x})| = O_p(1)$ uniformly over $\mathbf{x} \in \mathbb{R}^d$. Therefore, the second term in (E.8) is bounded by

$$\begin{aligned} & 2 \int_{\mathbb{R}^d} K_{\mathbf{b}}(\boldsymbol{\omega} - \mathbf{x}) \left\{ |\widehat{J}_{h,n}(\mathbf{x})|^2 + |\underline{J}_{h,n}(\mathbf{x})|^2 \right\} d\mathbf{x} \\ & \leq o_p(1) + 3 \int_{\mathbb{R}^d} K_{\mathbf{b}}(\boldsymbol{\omega} - \mathbf{x}) |\underline{J}_{h,n}(\mathbf{x})|^2 d\mathbf{x} = o_p(1) + 3O_p(1) \int_{\mathbb{R}^d} K_{\mathbf{b}}(\boldsymbol{\omega} - \mathbf{x}) d\mathbf{x} = O_p(1). \end{aligned}$$

Altogether, we show that $|\widehat{F}_{n,\mathbf{b}}(\boldsymbol{\omega}) - F_{n,\mathbf{b}}(\boldsymbol{\omega})| = o_p(1)$, and the $o_p(1)$ bound is uniform over $\boldsymbol{\omega} \in \mathbb{R}^d$. Thus, we get the desired result. \square

Theorem E.4. *Suppose that Assumptions 4.1, 4.2(ii) (for $r > 4$), 4.3, 4.4 (for $k = 4$), and 4.5 hold. Moreover, assume that the bandwidth $b = b(n)$ satisfies condition (B). Then,*

$$\sup_{\boldsymbol{\omega} \in \mathbb{R}^d} \mathbb{E} |\widehat{F}_{n,\mathbf{b}}(\boldsymbol{\omega}) - F_{n,\mathbf{b}}(\boldsymbol{\omega})|^2 = O(|D_n|^{-1} (b_1 \cdots b_d)^{-1}) + O(|D_n|^{2-r/2}), \quad n \rightarrow \infty.$$

Proof. By using (E.8), we have

$$\begin{aligned} |\widehat{F}_{n,\mathbf{b}}(\boldsymbol{\omega}) - F_{n,\mathbf{b}}(\boldsymbol{\omega})|^2 &\leq \left(\int_{\mathbb{R}^d} K_{\mathbf{b}}(\boldsymbol{\omega} - \mathbf{x}) |\widehat{I}_{h,n}(\mathbf{x}) - I_{h,n}(\mathbf{x})| d\mathbf{x} \right)^2 \\ &\leq \int_{\mathbb{R}^d} K_{\mathbf{b}}(\boldsymbol{\omega} - \mathbf{x}) |\widehat{I}_{h,n}(\mathbf{x}) - I_{h,n}(\mathbf{x})|^2 d\mathbf{x}. \end{aligned}$$

Here, the second inequality follows from Jensen's inequality, provided that $\int_{\mathbb{R}^d} K_{\mathbf{b}}(\boldsymbol{\omega} - \mathbf{x}) d\mathbf{x} = 1$.

Next, by using (E.6) together with the Cauchy-Schwarz inequality, $|\widehat{F}_{n,\mathbf{b}}(\boldsymbol{\omega}) - F_{n,\mathbf{b}}(\boldsymbol{\omega})|^2$ is bounded by

$$2 \int_{\mathbb{R}^d} K_{\mathbf{b}}(\boldsymbol{\omega} - \mathbf{x}) |\widehat{J}_{h,n}(\mathbf{x}) - \underline{J}_{h,n}(\mathbf{x})|^4 d\mathbf{x} + 8 \int_{\mathbb{R}^d} K_{\mathbf{b}}(\boldsymbol{\omega} - \mathbf{x}) |\widehat{J}_{h,n}(\mathbf{x}) - \underline{J}_{h,n}(\mathbf{x})|^2 |\underline{J}_{h,n}(\mathbf{x})|^2 d\mathbf{x}.$$

By using (E.3) for $s = 4$ and $k \in \mathbb{N}$ such that $4k > r$, the expectation of the first term above is bounded by

$$\begin{aligned} &C \mathbb{E} \{ |D_n|^{1/2} |\widehat{\boldsymbol{\beta}}_n - \boldsymbol{\beta}_0| \}^4 \sum_{t=1}^{k-1} \int_{\mathbb{R}^d} K_{\mathbf{b}}(\boldsymbol{\omega} - \mathbf{x}) \left\{ |D_n|^{-1} |H_{h\nabla^t \underline{\lambda}}^{(n)}(\mathbf{x})| \right\}^4 d\mathbf{x} \\ &\quad + C |D_n|^2 \mathbb{E} |\widehat{\boldsymbol{\beta}}_n - \boldsymbol{\beta}_0|^r \int_{\mathbb{R}^d} K_{\mathbf{b}}(\boldsymbol{\omega} - \mathbf{x}) d\mathbf{x} \\ &\leq C \sum_{t=1}^{k-1} \int_{\mathbb{R}^d} K_{\mathbf{b}}(\boldsymbol{\omega} - \mathbf{x}) \left\{ |D_n|^{-1} |H_{h\nabla^t \underline{\lambda}}^{(n)}(\mathbf{x})| \right\}^4 d\mathbf{x} + O(|D_n|^{2-r/2}) \\ &\leq C \sum_{t=1}^{k-1} \int_{\mathbb{R}^d} K_{\mathbf{b}}(\boldsymbol{\omega} - \mathbf{x}) \left\{ |D_n|^{-1} |H_{h\nabla^t \underline{\lambda}}^{(n)}(\mathbf{x})| \right\}^2 d\mathbf{x} + O(|D_n|^{2-r/2}) \\ &= O(|D_n|^{-1} (b_1 \cdots b_d)^{-1}) + O(|D_n|^{2-r/2}). \end{aligned}$$

Here, the first inequality is due to Assumption 4.2(ii) (for $r > 4$), the second inequality is due to $\sup_{\mathbf{x}} |D_n|^{-1} |H_{h\nabla^t \underline{\lambda}}^{(n)}(\mathbf{x})| < \infty$, and the last inequality is due to (E.9).

To bound the expectation of the second term, using the Cauchy-Schwarz inequality together with $\sup_{\mathbf{x}} \mathbb{E} \left[|\underline{J}_{h,n}(\mathbf{x})|^4 \right] = O(1)$, the expectation of the second term is bounded by

$$8 \int_{\mathbb{R}^d} K_{\mathbf{b}}(\boldsymbol{\omega} - \mathbf{x}) \left\{ \mathbb{E} |\widehat{J}_{h,n}(\mathbf{x}) - \underline{J}_{h,n}(\mathbf{x})|^4 \right\}^{1/2} d\mathbf{x}.$$

Using similar techniques, the above term is bounded by

$$\begin{aligned}
& C\mathbb{E} \left\{ |D_n|^{1/2} |\widehat{\beta}_n - \beta_0| \right\}^2 \sum_{t=1}^{k-1} \int_{\mathbb{R}^d} K_b(\boldsymbol{\omega} - \mathbf{x}) \left\{ |D_n|^{-1} |H_{h\nabla^t \underline{\lambda}}^{(n)}(\mathbf{x})| \right\}^2 d\mathbf{x} \\
& + C|D_n| \mathbb{E} |\widehat{\beta}_n - \beta_0|^r \int_{\mathbb{R}^d} K_b(\boldsymbol{\omega} - \mathbf{x}) d\mathbf{x} \\
& = O(|D_n|^{-1} (b_1 \cdots b_d)^{-1}) + O(|D_n|^{1-r/2}).
\end{aligned}$$

Combining the above two bounds, and since these bounds are uniform over $\boldsymbol{\omega} \in \mathbb{R}^d$, we have

$$\sup_{\boldsymbol{\omega} \in \mathbb{R}^d} \mathbb{E} |\widehat{F}_{n,b}(\boldsymbol{\omega}) - F_{n,b}(\boldsymbol{\omega})|^2 = O(|D_n|^{-1} (b_1 \cdots b_d)^{-1}) + O(|D_n|^{2-r/2}), \quad n \rightarrow \infty.$$

This proves the theorem. □

F Supplement on the simulations and real-data analysis

F.1 Details on the simulation settings

Recall the bivariate Cox process $\underline{X} = (X_1, X_2)$ in Section 7.1. The corresponding latent intensity field $(\Lambda_1(\mathbf{x}), \Lambda_2(\mathbf{x}))^\top$ of \underline{X} is given by

$$\Lambda_i(\mathbf{x}) = \lambda^{(i)}(\mathbf{x}/A) S_i(\mathbf{x}) Y_i(\mathbf{x}), \quad \mathbf{x} \in D = [-A/2, A/2]^2.$$

Let Φ_1, Φ_2, Φ_3 be independent homogeneous Poisson point processes on \mathbb{R}^2 with intensities κ_1, κ_2 , and κ_3 . Then, the shot-noise fields are given by

$$S_i(\cdot) = \kappa_i^{-1} \sum_{\mathbf{v} \in \Phi_i} \phi_i(\|\cdot - \mathbf{v}\|), \quad i \in \{1, 2\},$$

where $\phi_i(u)$ denotes the Gaussian kernel with variance parameter $\sigma_i^2 \in (0, \infty)$ of the form

$$\phi_i(r) = (2\pi\sigma_i^2)^{-1/2} \exp\{-r^2/(2\sigma_i^2)\}, \quad r \in (0, \infty). \tag{F.1}$$

Here, S_i captures the intra-specific clustering induced by Φ_i .

Next, the compound fields Y_1 and Y_2 are given by

$$Y_i(\cdot) = \exp\left(-\sum_{j=1}^3 \frac{\kappa_j \xi_{j \rightarrow i}}{\phi_j(0)}\right) \prod_{j=1}^3 \prod_{\mathbf{v} \in \Phi_j} \left\{ 1 + \xi_{j \rightarrow i} \frac{\phi_j(\|\cdot - \mathbf{v}\|)}{\phi_j(0)} \right\}, \quad i \in \{1, 2\}.$$

Here, $\phi_3(\cdot)$ denotes the Gaussian kernel as in (F.1) with the variance parameter $\sigma_3^2 \in (0, \infty)$ that is distinct from σ_1^2 and σ_2^2 . The interaction parameter $\xi_{j \rightarrow i} \in (-1, \infty)$ above indicates whether

the offspring process X_i is repelled by ($\xi_{j \rightarrow i} < 0$) or clustered around ($\xi_{j \rightarrow i} > 0$) the parent process Φ_j . Here, we set $\xi_{i \rightarrow i} = 0$ since Φ_i affects X_i through the shot-noise field. Therefore, $Y_i(\cdot)$ combines the effects of all other parent processes on the i th offspring.

For simulations, we consider the following three parameter combinations, namely M1–M3.

M1: Homogeneous isotropic process that exhibits inter-species clustering. We set the constant first-order intensities $(\lambda^{(1)}, \lambda^{(2)}) = (0.5, 1.5)$, thus the model is homogeneous. For the shot-noise fields, we set $(\kappa_1, \kappa_2, \kappa_3) = (0.25, 0.75, 0.2)$ and $(\sigma_1, \sigma_2, \sigma_3) = (0.6, 0.3, 1)$. For the compound fields, we set $(\xi_{1 \rightarrow 2}, \xi_{2 \rightarrow 1}, \xi_{3 \rightarrow 1}, \xi_{3 \rightarrow 2}) = (0.7, 0.9, 0.3, 0.1)$. Since both $\xi_{1 \rightarrow 2}$ and $\xi_{2 \rightarrow 1}$ are positive, the model exhibits clustering between X_1 and X_2 .

M2: Inhomogeneous isotropic process that exhibits inter-species clustering. We use the same parameters for the shot-noise and compound fields as in M1, but the first-order intensities of X_1 and X_2 are given by

$$\lambda^{(1)}(\mathbf{x}) = 3 \exp \{-2(x_1^2 + x_2^2)\} \quad \text{and} \quad \lambda^{(2)}(\mathbf{x}) = 2 \exp \{-2(x_1^2 - x_2^2)\}$$

for $\mathbf{x} = (x_1, x_2)^\top \in [-1/2, 1/2]^2$. Therefore, the model is inhomogeneous and exhibits clustering between the two processes.

M3: Inhomogeneous isotropic process that exhibits inter-species repulsion. The first-order intensities and the shot-noise fields are the same as those of M2, but the interaction parameters of the compound fields are set at $(\xi_{1 \rightarrow 2}, \xi_{2 \rightarrow 1}, \xi_{3 \rightarrow 1}, \xi_{3 \rightarrow 2}) = (-0.7, -0.9, 0.3, 0.1)$. Since $\xi_{1 \rightarrow 2}, \xi_{2 \rightarrow 1} < 0$, this model exhibits repulsive behavior between X_1 and X_2 .

A single realization of M1–M3 can be found in Figure F.1 below.

In Section 7.2, we discuss the practical guidelines for evaluating the periodogram and kernel spectral density estimators. When computing the DFT $\mathcal{J}_{h,n}(\boldsymbol{\omega})$, we use the separable data taper $h(\mathbf{x}) = h_a(x_1)h_a(x_2)$ with $a = 0.025$, where for $a \in (0, 1/2)$,

$$h_a(x) = \begin{cases} (x + \frac{1}{2})/a - \frac{1}{2\pi} \sin(2\pi(x + \frac{1}{2})/a), & -\frac{1}{2} \leq x \leq -\frac{1}{2} + a. \\ 1, & -\frac{1}{2} + a < x < \frac{1}{2} - a. \\ h_a(-x), & \frac{1}{2} - a < x \leq \frac{1}{2}. \end{cases} \quad (\text{F.2})$$

The same data taper function is also considered in the simulation studies of YG24. Next, when calculating $\widehat{I}_{h,n}$, the first-order intensities $\lambda^{(i)}$ ($i \in \{1, 2\}$) of Models M2 and M3 are estimated by fitting the log-linear model $\lambda(\mathbf{x}; \boldsymbol{\beta}) = \exp(\beta_0 + \beta_1 x_1^2 + \beta_2 x_2^2)$ (thus, referring to the correctly specified model), where the estimation of $\boldsymbol{\beta}$ is computed using the method in Waagepetersen (2007). For M1, since the model is homogeneous, we fit the intercept-only model by setting $\beta_1 = \beta_2 = 0$.

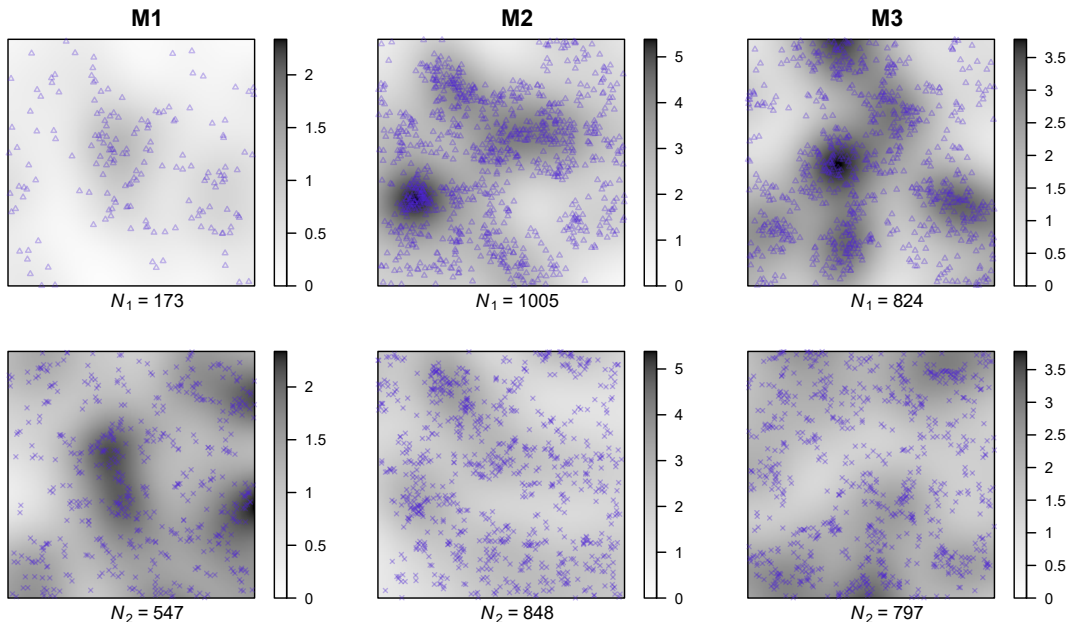


Figure F.1: A single realization of M1 (left)–M3 (right) on the domain $[-10, 10]^2$. The triangle (top) indicates the first process and the cross (bottom) indicates the second process. N_1 and N_2 denote the number of points in the first and second processes, respectively, and the grayscale surface shows the kernel estimate of the intensity function for each process.

F.2 Details on the real data analysis

In Section 8, we analyze five tree species in the tropical forest of Barro Colorado Island (BCI), namely *Capparis frondosa* (Cappfr, X_1), *Hirtella triandra* (Hirtr, X_2), *Protium panamense* (Protpa, X_3), *Protium tenuifolium* (Protte, X_4), and *Tetragastris panamensis* (Tet2pa, X_5). The original window size of the BCI dataset is 1000×500 m², but for numerical purposes, we rescale the window size to 50×25 unit², where one unit is equivalent to 20 m. This ensures that the fitted first-order intensities have a scale between 1 and 10.

When calculating the periodogram, we need to estimate the first-order intensity of each point process. For each first-order intensity, we use the log-linear model: $\lambda(\cdot; \boldsymbol{\beta}) = \exp\{\sum_{j=1}^p \beta_j Z_j(\cdot)\}$, where $\boldsymbol{\beta} = (\beta_1, \dots, \beta_p)^\top$ and $\{Z_j(\cdot)\}$ are covariates. In particular, in our data analysis, we use the three geolocational covariates (x coordinates, y coordinates, and the interaction term) and seven environmental covariates (which include elevation and gradient) that are provided in Jalilian et al. (2015), Supporting Information. As a consequence, Figure F.2 plots the fitted intensities of five tree species. The plot ensures that the ten covariates are sufficient to depict the behaviors of the true first-order intensity functions.

F.3 Coherence and partial coherence analysis

One of the wide applications of the spectrum of the multivariate stationary stochastic process is the coherence and partial coherence analysis. Suppose that $\underline{X} = (X_1, \dots, X_m)$ is an SOS spatial

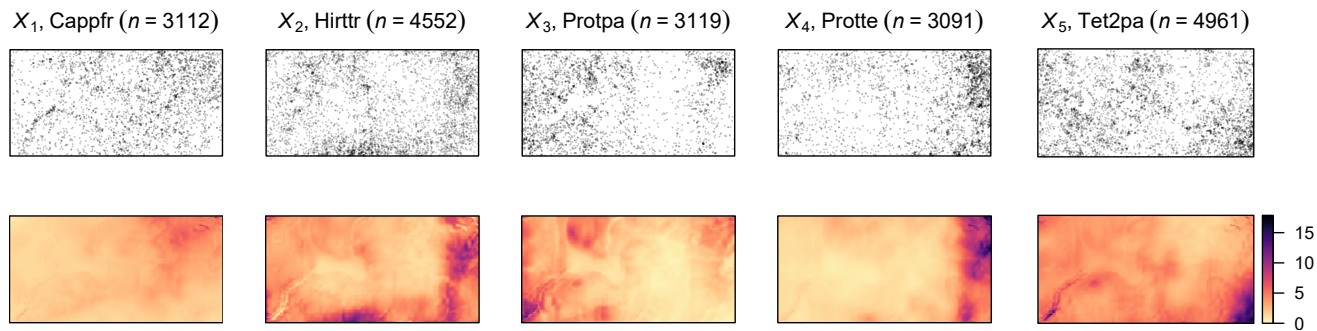


Figure F.2: Point patterns (top) and the heatmap of the estimated first-order intensity functions (bottom) of five tree species from the BCI dataset.

point process on \mathbb{R}^d . For $a \neq b$, we say that X_a and X_b are uncorrelated if $\text{cov}(N_a(A), N_b(B)) = 0$; conditionally uncorrelated if $\text{cov}(N_a(A), N_b(B) | \text{sp}(N_{-(a,b)})) = 0$ for any $A, B \in \mathcal{B}(\mathbb{R}^d)$. Here, $\text{sp}(N_{-(a,b)})$ denotes the linear span of $\{N_i(A) : i \in \{1, \dots, m\} \setminus \{a, b\}, A \in \mathcal{B}(\mathbb{R}^d)\}$. See Dahlhaus (2000); Eichler (2012) in time series literature and Eckardt (2016) for an extension to spatial point processes. In particular, Dahlhaus (2000) showed that the spectrum and its inverse contain information about the uncorrelatedness and conditional uncorrelatedness relationships of multivariate time series. To be specific, let

$$R^{(a,b)}(\boldsymbol{\omega}) = \frac{|F^{(a,b)}(\boldsymbol{\omega})|^2}{F^{(a,a)}(\boldsymbol{\omega})F^{(b,b)}(\boldsymbol{\omega})} \quad \text{and} \quad D^{(a,b)}(\boldsymbol{\omega}) = \frac{|F^{-(a,b)}(\boldsymbol{\omega})|^2}{F^{-(a,a)}(\boldsymbol{\omega})F^{-(b,b)}(\boldsymbol{\omega})} \quad (\text{F.3})$$

be the squared magnitude coherence and partial coherence of two point processes X_a and X_b , respectively, where $F^{-(a,b)}$ is the (a,b)th element of the inverse spectrum $F(\boldsymbol{\omega})^{-1}$. Then, by extending Dahlhaus (2000) to the SOS spatial point process framework, it can be seen that both $R^{(a,b)}(\boldsymbol{\omega})$ and $D^{(a,b)}(\boldsymbol{\omega})$ are less than one, and X_a and X_b are uncorrelated (resp. conditionally uncorrelated) if and only if $R^{(a,b)}(\boldsymbol{\omega}) = 0$ (resp. $D^{(a,b)}(\boldsymbol{\omega}) = 0$) for all $\boldsymbol{\omega} \in \mathbb{R}^d$.

Now, we extend the coherence and partial coherence analysis to inhomogeneous spatial point processes. However, for the SOIRS process, it is unwieldy how the uncorrelatedness and conditional uncorrelatedness relationships are represented in the frequency domain. Therefore, below, we define new types of correlation structures for multivariate inhomogeneous processes. Recall the intensity reweighted process $\tilde{\underline{X}} = (\tilde{X}_1, \dots, \tilde{X}_m)$ of \underline{X} as in Definition A.2.

Definition F.1. *Let $\underline{X} = (X_1, \dots, X_m)$ be an m -variate SOIRS process. Then, for $a \neq b$, we say that X_a and X_b are uncorrelated after reweighting (u.a.r.) if the two SOS processes \tilde{X}_a and \tilde{X}_b are uncorrelated. Moreover, we say that X_a and X_b are conditionally uncorrelated after reweighting (cond. u.a.r.) if \tilde{X}_a and \tilde{X}_b are conditionally uncorrelated.*

To represent the u.a.r. and cond. u.a.r. relationships in the frequency domain, recall that $\tilde{\underline{X}}$ is an SOS process with unit first-order intensity and has $L_2(\cdot)$ (see, (2.8)) as its reduced

covariance intensity function. Therefore, the spectrum of \tilde{X} is given by

$$\tilde{F}(\boldsymbol{\omega}) = (2\pi)^{-d}I_m + \mathcal{F}^{-1}(L_2)(\boldsymbol{\omega}). \quad (\text{F.4})$$

Let $\tilde{R}^{(a,b)}(\boldsymbol{\omega})$ and $\tilde{D}^{(a,b)}(\boldsymbol{\omega})$ be defined similarly as in (F.3), but replacing F with \tilde{F} in the equations. Then, it is straightforward to see that

$$\begin{aligned} X_a \text{ and } X_b \text{ are u.a.r. if and only if } \tilde{R}^{(a,b)}(\boldsymbol{\omega}) &\equiv 0, \text{ and} \\ X_a \text{ and } X_b \text{ are cond. u.a.r. if and only if } \tilde{D}^{(a,b)}(\boldsymbol{\omega}) &\equiv 0. \end{aligned} \quad (\text{F.5})$$

Next, we estimate $\tilde{R}^{(a,b)}(\boldsymbol{\omega})$ and $\tilde{D}^{(a,b)}(\boldsymbol{\omega})$ based on the observed point pattern on D_n that follows an asymptotic framework as in Assumption 2.1. To do so, we first estimate the inverse Fourier transform of L_2 . Recall the pseudo-spectrum F_h in (2.11). By simple algebra, we have

$$\mathcal{F}^{-1}(L_2)(\boldsymbol{\omega}) = H_{h,2} (F_h(\boldsymbol{\omega}) - (2\pi)^{-d}H_{h,2}^{-1}\text{diag}(H_{h^2\hat{\lambda}})) \oslash H_{h^2\hat{\lambda}\cdot\hat{\lambda}^\top},$$

where $A \oslash B = (A^{(i,j)} / B^{(i,j)})_{1 \leq i,j \leq m}$. Therefore, a natural estimator of $\mathcal{F}^{-1}(L_2)(\boldsymbol{\omega})$ is given by

$$\widehat{\mathcal{F}^{-1}(L_2)}(\boldsymbol{\omega}) = H_{h,2} \left(\widehat{F}_{n,b}(\boldsymbol{\omega}) - (2\pi)^{-d}H_{h,2}^{-1}\text{diag}(H_{h^2\hat{\lambda}}) \right) \oslash H_{h^2\hat{\lambda}\cdot\hat{\lambda}^\top},$$

where $\widehat{F}_{n,b}(\boldsymbol{\omega})$ is the kernel spectral density estimator and $\hat{\lambda}$ is the parametric estimator. By substituting $\widehat{\mathcal{F}^{-1}(L_2)}(\boldsymbol{\omega})$ into (F.4) and using the relationship in (F.3), we obtain the estimated criterion for $\tilde{R}^{(a,b)}(\boldsymbol{\omega})$ and $\tilde{D}^{(a,b)}(\boldsymbol{\omega})$, which we denote as $\widehat{R}^{(a,b)}(\boldsymbol{\omega})$ and $\widehat{D}^{(a,b)}(\boldsymbol{\omega})$, respectively.

For the BCI dataset considered in Section 8, we evaluate $\widehat{R}^{(a,b)}(\boldsymbol{\omega})$ and $\widehat{D}^{(a,b)}(\boldsymbol{\omega})$ on a regular grid in $[-1.5\pi, 1.5\pi]^2$, where the grid size is greater than twice the bandwidth, $b_{CV} = 0.62$. As a result, we evaluate $\widehat{R}^{(a,b)}(\boldsymbol{\omega})$ and $\widehat{D}^{(a,b)}(\boldsymbol{\omega})$ at 49 different frequencies. For each pair (a, b) , let

$$\widehat{R}^{(a,b)} = \max \widehat{R}^{(a,b)}(\boldsymbol{\omega}) \quad \text{and} \quad \widehat{D}^{(a,b)} = \max \widehat{D}^{(a,b)}(\boldsymbol{\omega}) \quad (\text{F.6})$$

be the maximum coherence and partial coherence, where the maximum is taken over the 49 different frequencies explained above. Below, we calculate $\widehat{R}^{(a,b)}$ (upper diagonal) and $\widehat{D}^{(a,b)}$ (lower diagonal) for the five-variate BCI dataset.

$$\begin{pmatrix} \text{Cappfr} & .164 & .028 & .038 & .228 \\ .099 & \text{Hirttr} & .032 & .044 & .118 \\ .024 & .177 & \text{Protpa} & .133 & .126 \\ .041 & .168 & .235 & \text{Protte} & .111 \\ .109 & .100 & .141 & .069 & \text{Tet2pa} \end{pmatrix},$$

See also Figure F.3 below for the plot of $\widehat{R}^{(a,b)}(\boldsymbol{\omega})$ and $\widehat{D}^{(a,b)}(\boldsymbol{\omega})$ against $\|\boldsymbol{\omega}\|$.

We note from (F.5) that the closer $\widehat{R}^{(a,b)}$ (resp., $\widehat{D}^{(a,b)}$) is to zero, the stronger evidence that X_a and X_b are u.a.r. (resp., cond. u.a.r.). However, deriving the asymptotic behavior of $\widehat{R}^{(a,b)}(\boldsymbol{\omega})$ and $\widehat{D}^{(a,b)}(\boldsymbol{\omega})$ under the SOIRS framework is currently unavailable. Thus, computing the α -level confidence regions for $\widehat{R}^{(a,b)}$ and $\widehat{D}^{(a,b)}$ in (F.6) under the null hypotheses of u.a.r. and cond. u.a.r. is beyond the scope of this article (which is a good revenue for future research).

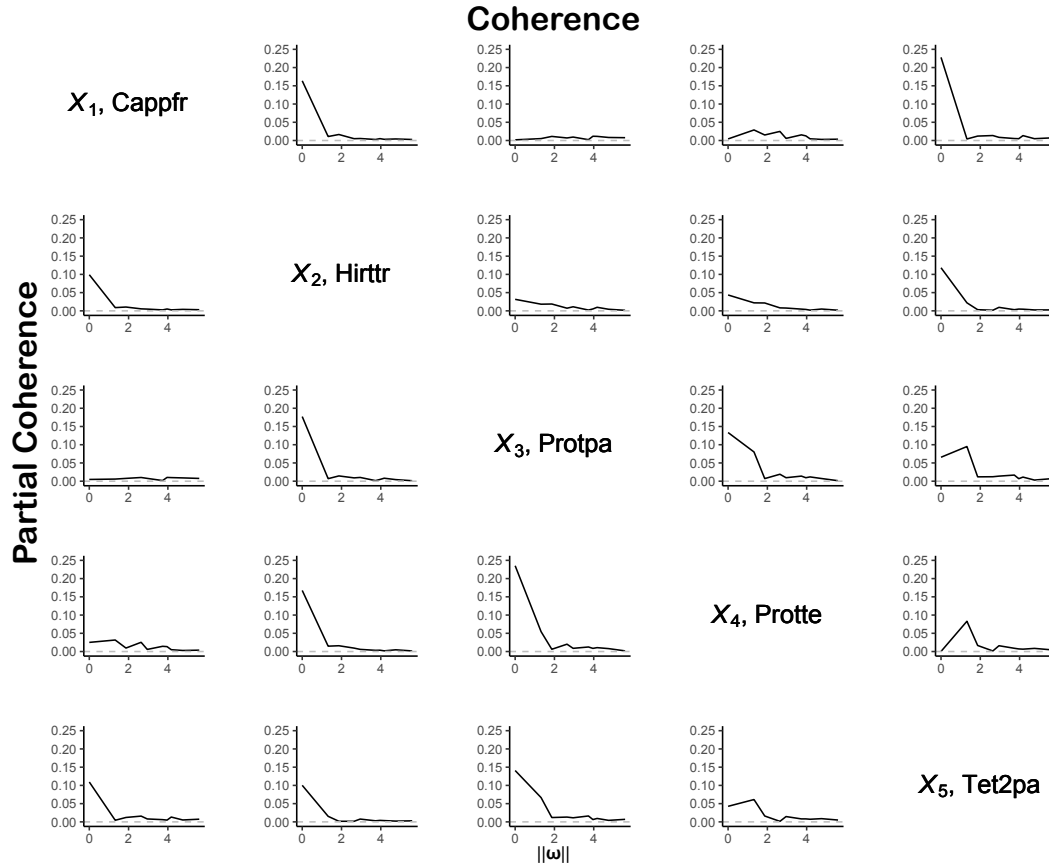


Figure F.3: The coherence $\widehat{R}^{(a,b)}(\boldsymbol{\omega})$ (upper diagonal) and partial coherence $\widehat{D}^{(a,b)}(\boldsymbol{\omega})$ (lower diagonal) of the BCI dataset plotted against $\|\boldsymbol{\omega}\|$.